

**OPTICAL PROPERTIES AND QUANTUM CONFINEMENT OF  
NANOCRYSTALLINE II-VI SEMICONDUCTOR PARTICLES**



Utrecht University

# OPTICAL PROPERTIES AND QUANTUM CONFINEMENT OF NANOCRYSTALLINE II-VI SEMICONDUCTOR PARTICLES

**Optische eigenschappen en kwantum  
opsluitingseffecten van nanokristallijne  
II-VI halfgeleiderdeeltjes**

(met een samenvatting in het Nederlands)

PROEFSCHRIFT

TER VERKRIJGING VAN DE GRAAD VAN DOCTOR AAN DE UNIVERSITEIT UTRECHT  
OP GEZAG VAN DE RECTOR MAGNIFICUS, PROF. DR. H.O. VOORMA, INGEVOLGE  
HET BESLUIT VAN HET COLLEGE VOOR PROMOTIES IN HET OPENBAAR TE  
VERDEDIGEN OP WOENSDAG 6 OKTOBER 1999 DES MIDDAGS TE 12:45 UUR

DOOR

ALBERT VAN DIJKEN

GEBOREN OP 19 AUGUSTUS 1972 TE BENNEKOM

P R O M O T O R : Prof. Dr. A. Meijerink  
C O - P R O M O T O R : Dr. D. Vanmaekelbergh

Faculteit Scheikunde  
Universiteit Utrecht

CIP-GEGEVENS KONINKLIJKE BIBLIOTHEEK, DEN HAAG

Dijken, Albert van

Optical Properties and Quantum Confinement of Nanocrystalline II-VI Semiconductor Particles / Albert van Dijken. - Utrecht : Universiteit Utrecht, Faculteit Scheikunde, Debye Instituut.

Proefschrift Universiteit Utrecht. Met een samenvatting in het Nederlands.

ISBN 90-393-2164-7





The work described in this thesis is supported by the Council for Chemical Science (CW), with financial aid from the Netherlands Organization for Scientific Research (NWO).

*"It has long been an axiom of mine that the little things are infinitely the most important."*

(Sherlock Holmes in "A Case of Identity", from *The Adventures of Sherlock Holmes* by Arthur Conan Doyle).





# CONTENTS

## 1. Introduction

Nanocrystalline II-VI Semiconductor Particles and Quantum Size Effects : Past and Present	1
1.1 Early observations	2
1.2 Of boxes and wells	3
1.3 Reducing the dimensions	3
1.4 Colloidal suspensions of sulphides	4
1.5 Modelling quantum size effects	5
1.6 Recent small particle research	7
1.7 Summary of this thesis	8
References	11

## 2. Size Selective Photoetching

Adjusting the Size of Nanocrystalline II-VI Semiconductor Particles	15
2.1 Introduction	16
2.2 Theory	17
2.3 Experimental methods	20
2.3.1 Sample preparation	20
2.3.2 Photoetching	21
2.3.3 Optical measurements	21
2.3.4 Transmission Electron Microscopy	22
2.3.5 X-ray Powder Diffraction	22
2.4 Results and discussion	22
2.4.1 CdS	22
2.4.2 ZnS	30
2.4.3 PbS	32
2.4.4 ZnO	33
2.5 Conclusion	37
References	38

## 3. Nanocrystalline ZnO Particles

I. Identification of the Transition Responsible for the Visible Emission	41
3.1 Introduction	42
3.2 Theory	43
3.3 Experimental methods	44
3.3.1 Sample preparation	44
3.3.2 Optical measurements	45

3.4	Results and discussion	46
3.4.1	Emission measurements	46
3.4.2	Identification of the visible emission transition	48
3.5	Conclusion	52
	References	53

## 4. Nanocrystalline ZnO Particles

II.	The Kinetics of the Radiative and Non-Radiative Processes upon Photoexcitation	55
4.1	Introduction	56
4.2	Experimental methods	57
4.2.1	Sample preparation	57
4.2.2	Optical measurements	57
4.3	Results	58
4.3.1	Absorption	58
4.3.2	Steady-state luminescence	60
4.3.3	Time-resolved luminescence	60
4.3.4	Temperature-dependent luminescence	62
4.4	Discussion	63
4.4.1	Steady-state luminescence	63
4.4.2	Time-resolved luminescence	65
4.4.3	Temperature-dependent luminescence	66
4.4.4	Nature of the deep hole trap	67
4.4.5	Model	68
4.5	Conclusion	73
	References	74

## 5. Nanocrystalline ZnO Particles

III.	The Influence of Adsorbed Oxygen on the Emission Properties	77
5.1	Introduction	78
5.2	Experimental methods	79
5.2.1	Sample preparation	79
5.2.2	Optical measurements	80
5.3	Results	80
5.4	Discussion	84
5.5	Conclusion	89
	References	90

## **6. Luminescence Quantum Efficiencies**

The Influence of Preparation, Surface Passivation and Particle Size .....	93
6.1 Introduction .....	94
6.2 Experimental methods .....	95
6.2.1 Sample preparation .....	95
6.2.2 Luminescence quantum efficiencies .....	96
6.3.3 Optical measurements .....	97
6.3 Results and discussion .....	97
6.3.1 CdS prepared with H <sub>2</sub> S .....	97
6.3.2 CdS prepared with Na <sub>2</sub> S .....	97
6.3.3 Luminescence quantum efficiencies of CdS .....	99
6.3.4 ZnO .....	101
6.3.5 Luminescence quantum efficiencies of ZnO .....	101
6.4 Conclusion .....	104
References .....	105

<b>Samenvatting</b> .....	107
---------------------------	-----

<b>List of publications</b> .....	113
-----------------------------------	-----

## **Over de inhoud van dit proefschrift**

Een overzicht voor niet-ingewijden .....	115
--	-----

## **Tot besluit**

Een woord van dank .....	121
--------------------------	-----

<b>Curriculum Vitae</b> .....	125
-------------------------------	-----



## CHAPTER

# 1

## INTRODUCTION

---

### **Nanocrystalline II-VI Semiconductor Particles and Quantum Size Effects : Past and Present**

---

#### **ABSTRACT.**

This chapter gives a short historical overview of the development of a new interdisciplinary field in materials science : the study of nanocrystalline semiconductor particles. The overview starts with the observation of anomalous effects, mainly in absorption measurements on small semiconductor particles. Later, these anomalies turned out to be manifestations of so-called quantum size effects which will be the main topic of this chapter and the rest of this thesis. It will be made clear where the work that is described in this thesis fits into the vast amount of experiments being performed in the field of nanocrystalline semiconductor particles today.

## 1.1 EARLY OBSERVATIONS.

In the 1920's it was observed that the onset of absorption as well as the luminescence colour of glasses containing CdS colloids, shifts to longer wavelengths upon heating. This was correlated to the growth of CdS colloids [1] :

*“Die Fluoreszenzfarbe und die Absorptionsgrenze der gelben Cadmium-sulfidgläser verschiebt sich [...] nach den längeren Wellen, was auf ein Wachsen der färbenden Kolloide zurückgeführt wird.”*

In the late 1960's, researchers reported differences between the absorption spectra of colloidal semiconductor particles and the spectra of the corresponding macrocrystalline material [2-4]. In 1967, Berry reported that the absorption onset of suspensions of small crystals of AgBr [2] and AgI [3] was shifted to shorter wavelengths as compared to the macrocrystalline material, and made the following statement :

*“The observed shift of the absorption curve to shorter wavelengths should not be regarded as suggesting a mechanism in which the bandgap is widened, but as either a decreased number of absorbing atoms or a decreased efficiency of the phonon-assisted electronic transitions.”*

In 1968, Stasenko presented experiments on thin films of CdS [5], motivated by the prediction that for very thin semiconductor films the bandgap is inversely proportional to the square of the film thickness [6]. The results were in good agreement with the theoretically predicted shift of the bandgap :

*“Such a forbidden-energy gap increase [...] is connected with quantum effects.”*

As will be shown in the next part of this chapter, it was realised in the early 1980's that these *quantum effects* are not only responsible for the different properties of thin films as compared to the macrocrystalline material, but also for the peculiar behaviour of colloidal semiconductor particles. Some 15 years after the firm statement by Berry, it was shown that the mechanism that he ruled out (widening of the bandgap) is in fact responsible for his observations.

---

## 1.2 OF BOXES AND WELLS.

The theoretical description of the influence of thickness (or size) of a material on its electronic properties is based on an elementary quantum mechanical concept, known as the “*particle-in-a-box*”. When a particle is confined to a limited space, its kinetic energy can only have discrete values that are determined by the mass of the *particle* and the dimensions of the *box*. The larger the box, the smaller the separation between the different allowed energy levels will be. When the box becomes infinitely large, a continuum of energy levels is formed. Based on this model, it can be expected that the properties of charge carriers in solids will show a size-dependency when the dimensions of the solid become sufficiently small. The first time that it was suggested that quantisation of the kinetic energy could possibly be observed in very thin semiconducting films was in 1957 by Schrieffer [7] but it took another ten years before these effects were actually observed. This was achieved in so-called *inversion layers*, which are very narrow layers (~10 nm) at the surface of a semiconductor. They behave as potential energy wells in which electrons (or holes) can be contained. In 1966, energy quantisation was observed for electrons in an inversion layer on a silicon surface [8,9]. From that time on, many experiments have been valuable in demonstrating quantum size effects [5,10].

A major breakthrough took place at the end of the 1960's, when a technique called *Molecular Beam Epitaxy* (MBE) was developed at the Bell Telephone Laboratories [11,12]. This paved the way for the preparation of semiconductor structures that have since been studied very extensively : *quantum wells*. These artificial structures are formed by sandwiching a very thin layer of a semiconductor material with a small bandgap between two layers of a semiconductor with a larger bandgap. Within the small-bandgap layer, the charge carriers are spatially confined in one dimension, while they are free to move in the other two dimensions. A quantum well is an example of a two-dimensional (2D) structure. Soon after the development of MBE, researchers reported the experimental observation of quantised energy levels of confined charge carriers in quantum wells [13].

## 1.3 REDUCING THE DIMENSIONS.

Following the invention and development of MBE, many different 2D-structures have been prepared and investigated. Several interesting physical properties were observed and researchers subsequently tried to reduce the dimensions of these structures even further. This reduction first resulted in the preparation of one-

dimensional *quantum wires*. These 1D-structures can be prepared directly by MBE or indirectly, starting with 2D-structures which are laterally patterned by lithographic or dry-etching techniques. Another approach is the confinement of charge carriers in quantum wells by applying strong magnetic fields. By varying the strength of such a magnetic field, the confinement can be tuned between the 2D and 0D limits, allowing the study of *quantum dots*. An alternative approach to studying 0D-structures is the preparation of quantum dots in the gas phase by laser vaporisation [14,15].

The 2D-, 1D- and 0D-structures mentioned thus far are all *artificial* structures, prepared by physical techniques. Other, more *natural* structures have also received considerable attention. These structures are prepared chemically and include conjugated polymers [16] and small crystalline semiconductor particles prepared in zeolite hosts [17,18], in glasses [19,20], in polymer films [21] or as colloids in suspension. Mainly the latter samples have been subjected to an enormous amount of experiments since the early 1980's. The following paragraphs will present an overview of this research.

## 1.4 COLLOIDAL SUSPENSIONS OF SULPHIDES.

The interest in colloidal suspensions of nanocrystalline semiconductor particles originated from photocatalysis. Particulate semiconductor systems were studied because they are inexpensive, relatively easy to fabricate and have a high surface area [22]. An additional advantage of colloidal systems is that kinetic studies can be performed in more detail. One of the popular semiconductors during the early 1980's was CdS. This material absorbs visible light and the reduction of CO<sub>2</sub> to methanol [23,24] and even the direct splitting of water to O<sub>2</sub> and H<sub>2</sub> upon irradiation of CdS powders [25] was reported.

These early experiments initiated an enormous amount of research into the photocatalytic properties of colloidal suspensions of CdS particles, particularly in the group of Henglein [26-28]. Efforts were directed towards obtaining extremely small CdS particles, which eventually resulted in the preparation of a CdS powder that was white instead of yellow (the colour of macrocrystalline CdS). Also, studies on the photoanodic dissolution of colloidal CdS particles showed that the onset of absorption shifted towards higher energies as the particles dissolved [26]. As was mentioned in the beginning of this chapter, similar size-dependent changes of the absorption characteristics had already been observed for colloidal suspensions of silver halides, but the origin was then still unclear. At first, it was thought that the observed effects were due to an amorphous structure of the colloidal particles [26]. However, Brus was



---

the first to show that these particles had an ordered structure and that the dependence of the optical properties on particle size can be understood in terms of quantum size effects [29,30]. As mentioned in the previous paragraphs, this interpretation had already been used to describe the behaviour of thin semiconducting films. Besides Brus, other groups also reported size effects in small semiconductor particles [31]. Nevertheless, Brus is generally credited for being the first to develop the theoretical framework for the description of quantum size effects in nanocrystalline semiconductor particles.

## 1.5 MODELLING QUANTUM SIZE EFFECTS.

For macrocrystalline semiconductors, the bandgap is defined as the minimum energy needed to excite an electron from the valence band to the conduction band. Through Coulomb interaction, these charge carriers may form a bound state - a so-called Wannier exciton - which has an energy slightly lower than the bandgap. An exciton can be viewed as an electron orbiting a hole at a certain distance in a dielectric medium. In analogy with a hydrogen atom, this distance is called the Bohr radius of the exciton ( $a_{\text{exc}}$ ) [32] :

$$a_{\text{exc}} = \frac{4\pi\epsilon_0\hbar^2}{m_0e^2} \cdot \epsilon_{\infty} \cdot \left( \frac{1}{m_e^*} + \frac{1}{m_h^*} \right) = a_0 \cdot \epsilon_{\infty} \cdot \left( \frac{1}{m_e^*} + \frac{1}{m_h^*} \right) \quad (1.1)$$

In equation (1.1),  $a_0$  is the Bohr radius of a hydrogen atom (0.529 Å),  $\epsilon_{\infty}$  the high-frequency relative dielectric constant of the medium,  $m_e^*$  and  $m_h^*$  the effective masses of the electron and hole respectively (both in units  $m_0$ ). Usually, the effective masses of the charge carriers are only a small fraction of the electron rest mass. This in combination with the fact that the Coulomb interaction between the electron and hole is almost entirely screened ( $\epsilon_{\infty} \sim 5$ ) results in a relatively large Bohr radius of the exciton (for instance,  $a_{\text{exc}}$  is about 30 Å for CdS). As the size of the semiconductor particle approaches the Bohr radius of the exciton, the electron-hole pair gets spatially confined and assumes a state of higher kinetic energy. Therefore, when considering quantum size effects in semiconductor particles, the Bohr radius of the exciton gives an indication of the dimensions at which these effects become apparent.

The first model calculations by Brus were based on the effective mass approximation and used a treatment of bulk states in the limit of small size [33]. The effective mass approximation had been developed for macrocrystalline materials but it had already been shown that it could also be used to quantitatively describe the motion

of excitons in very thin semiconductor layers [34]. Effects that could complicate the calculations, such as structural rearrangements as a function of size or the involvement of surface states, were not considered. The system was approximated by a spherical semiconductor particle with an infinitely high potential energy outside the sphere. For the energy of the lowest excited state (comparable to the value for the bandgap in the case of a macrocrystalline semiconductor) as a function of the particle radius  $R$ , the following formula was derived :

$$E = E_g + \frac{h^2}{8m_0R^2} \cdot \left( \frac{1}{m_e^*} + \frac{1}{m_h^*} \right) - \frac{1.8e^2}{4\pi\epsilon_0\epsilon_\infty R} \quad (1.2)$$

In equation (1.2), next to the bandgap of the macrocrystalline material ( $E_g$ ), two terms are given, both dependent on the particle size. The first term is a confinement term, which increases as  $R^{-2}$  and the second term is the Coulomb attraction, increasing with  $R^{-1}$ . In the limit of large  $R$ , the value for  $E$  approaches that of  $E_g$ . Although the effective mass approximation is not valid for very small particle sizes, equation (1.2) has often been used to describe quantum size effects in nanocrystalline semiconductor particles. The dependency of  $E$  on  $R$  as given by equation (1.2) can be used to describe the results from size-dependent measurements of optical properties fairly well. Since the early calculations by Brus, several papers have appeared presenting models that are based on more realistic boundary conditions, such as a finite barrier height [35,36].

Equation (1.2) implies that when the radius of a semiconductor particle decreases, the energy for the lowest excited state increases. In other words, this means that when a particle becomes smaller, its “bandgap” increases. As a consequence of the spatial confinement of charge carriers, the kinetic energy becomes quantised. Strictly speaking, the word “bandgap” is inappropriate for very small particles. The quantisation of the kinetic energy manifests itself as a gradual transition of continuous energy bands to discrete energy levels. This transition starts at the edges of the energy bands as these states are particularly sensitive to the particle size. Figure 1.1 schematically shows the change of the electronic properties of a semiconductor as its size decreases to values lower than the Bohr radius of the exciton.

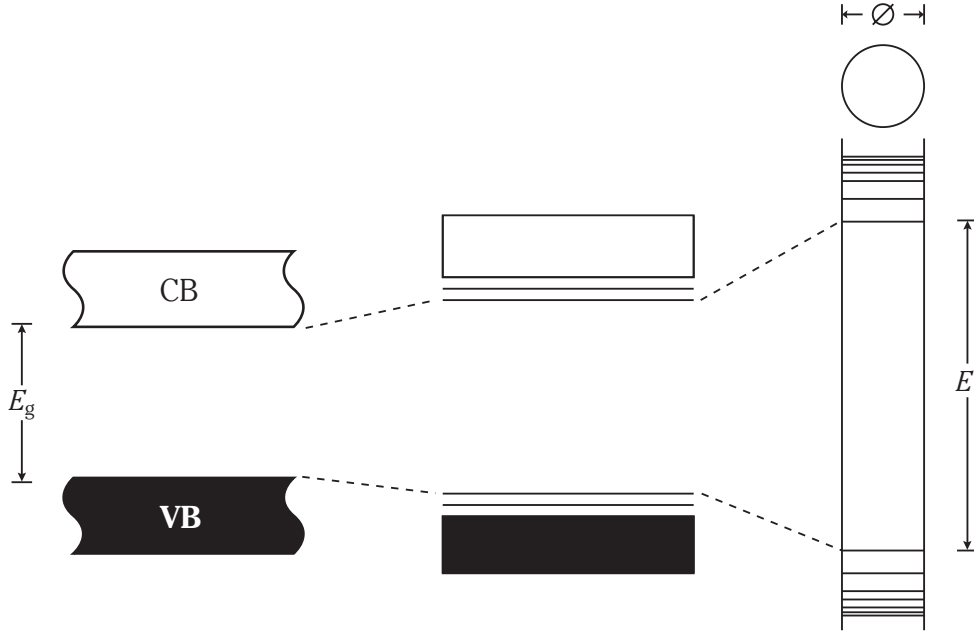


**Figure 1.1** : Schematic representation of the gradual change of the electronic properties when the size of a semiconductor decreases (from left to right). At the left, an energy band diagram for a macrocrystalline semiconductor is shown,  $E_g$  being the bandgap. The valence band (full, black) and conduction band (empty, white) are denoted as VB and CB respectively. In the case of the middle picture, the size of the semiconductor is comparable to the size of the exciton while the picture on the right represents the situation when the dimensions of the semiconductor are smaller than those of the exciton ( $E$  is the energy of the lowest excited state).

Next to these effects, the increase of the relative surface area also results in major changes of the optical properties of very small semiconductor particles. As the number of atoms at the surface becomes comparable to the number of bulk atoms, surface states will play an important role, for instance in providing pathways for non-radiative recombination of photogenerated charge carriers [37]. However, surface states can also be involved in radiative transitions, as will be demonstrated in chapter 4 of this thesis.

## 1.6 RECENT SMALL PARTICLE RESEARCH.

The previous paragraphs described the period in which the foundations were laid for the development of a new area of research. Since the first correct interpretation of the size-dependent optical properties of nanocrystalline semiconductor particles in the early 1980's, a lot of research has been directed towards studying these materials.

The combination of a good theoretical framework and sophisticated preparative techniques has created a new field of materials science that has attracted scientists from many different disciplines. Over the years, several excellent review articles have appeared [38-48]. Especially the possibility to adjust the electronic properties of semiconductor particles by changing their size has stimulated research on these systems.

An interesting accomplishment is the construction of light-emitting diodes (LED's) based on nanocrystalline semiconductor particles [49,50]. In semiconductors, the direct recombination of photogenerated charge carriers gives a narrow emission band at an energy close to the absorption onset. For nanocrystalline semiconductor particles this means that the luminescence is size-tunable. LED's based on these systems can thus be fabricated with a whole range of output colours. Another recent development is the self-organisation of nanocrystalline semiconductor particles into 3D superlattices which makes it possible to study collective electronic phenomena that arise from interactions between the particles [51].

The study of size-dependent optical properties of nanocrystalline semiconductor particles in suspension is complicated by inhomogeneous broadening of the luminescence signals due to a distribution of particle sizes. A very important recent development that eliminates this complication is the possibility to do photoluminescence spectroscopy on single semiconductor particles. In the case of CdSe particles, such measurements have presented interesting results. For the exciton emission, resolution limited spectral linewidths of about 120  $\mu\text{eV}$  at 10 K were reported [52]. Furthermore, it was shown that the emission of a single fluorescing CdSe particle turns on and off under continuous illumination. Both phenomena cannot be observed when studying an ensemble of CdSe particles [53].

## 1.7 SUMMARY OF THIS THESIS.

In this thesis, experiments are described that were performed on suspensions of nanocrystalline II-VI semiconductor particles. The object of this research is to study quantum size effects in relation to the luminescence properties of these particles. A prerequisite for performing studies of size-dependent optical properties is the availability of monodisperse particles with different particle sizes. Chapter 2 will deal with this subject in more detail as it will describe a method called *size-selective photoetching* that provides a way to adjust the particle size in a controlled manner after preparation. In this chapter CdS is used as a model system and it is shown that the initial mean particle radius of 35 Å can be decreased gradually to 7.5 Å using light of different wavelengths.

---

At the same time, the width of the particle size distribution decreased from 40% to 10-15%. The colour of the light that is used for photoetching determines the size of the semiconductor particles. The feasibility of size-selective photoetching as a means to decrease the size of ZnS and ZnO particles is also demonstrated, although the preparation of a large variety of particle sizes could not be accomplished.

With respect to quantum size effects in nanocrystalline II-VI semiconductor particles, the sulphides and selenides are by far the most extensively studied materials. Much less is known about oxidic II-VI semiconductors, of which ZnO is probably the most suitable compound for studies of size-dependent optical properties. This compound is known to luminesce quite strongly and it is relatively easy to prepare a range of particle sizes, small enough to show quantum size effects. The chapters 3-5 of this thesis comprise a variety of luminescence experiments that were performed on nanocrystalline ZnO particles with different sizes. Upon photoexcitation, a ZnO suspension shows two emission bands, one being a UV emission band (exciton emission) and the other a visible emission band (trap emission). The visible emission is well-known and it is the main reason for the use of ZnO as a phosphor in various applications. Both nanocrystalline ZnO particles as well as macrocrystalline ZnO show the visible emission and it probably has the same origin in both systems. Despite numerous studies using macrocrystalline ZnO the exact mechanism of the green emission is still unknown.

In chapter 3, a study of the size-dependence of the two emission bands of ZnO is presented. With increasing particle size, both emissions shift to lower energies due to size quantisation. The experiments show that a linear relationship exists between the energetic positions of the visible emission band and the UV emission band. From the slope of the linear relationship it can be concluded that the visible emission is due to the recombination of an electron from the conduction band with a hole trapped about 2 eV below the conduction band edge. As the energetic position of this trap level is in good agreement with the position of a  $V_O^{\bullet\bullet}$  centre in ZnO, it is assumed that this defect is the recombination centre for the visible emission.

While the conclusion of chapter 3 is valid for ZnO in general, chapters 4 and 5 concern the specific behaviour of nanocrystalline ZnO particles. In chapter 4, results are presented of steady-state and time-resolved luminescence measurements performed on suspensions of nanocrystalline ZnO particles of different sizes and at different temperatures. The temperature- and size-dependence of the ratio of the visible to exciton luminescence and the kinetics are explained based on the identification of the transition responsible for the visible emission (chapter 3). A model is proposed in which the photogenerated hole is transferred from the valence band to a  $V_O^{\bullet}$  level in the bulk of the particle in a two-step process. The first step of this process is an efficient

surface-trapping - probably at an  $O^{2-}$  site - followed by tunneling of the surface-trapped hole back into the particle where it recombines with an electron in an oxygen vacancy ( $V_O^\bullet$ ) resulting in the creation of a  $V_O^{\bullet\bullet}$  centre, the recombination centre for the visible emission.

A remarkable property of ZnO particles is the quenching of the visible emission when an oxygen-free suspension is irradiated with UV radiation. At the same time, the intensity of the UV emission increases. In the past, various models have been proposed to explain this phenomenon. In chapter 5, the quenching behaviour is investigated in detail. Based on the model for the visible emission described in chapters 3 and 4, the quenching of this emission is ascribed to charging of the ZnO particles. In a ZnO particle, a photogenerated electron can be scavenged by an adsorbed oxygen molecule while the photogenerated hole can be used to oxidise an adsorbed solvent molecule. In an oxygen-free suspension, the electron remains on the particle but the hole can still be scavenged. The excess electron can be trapped by a  $V_O^\bullet$  centre which results in the formation of a  $V_O^{\bullet\bullet}$  centre. The  $V_O^\bullet$  centres are involved in the visible emission process and removal of these centres results in quenching of the visible emission.

A detailed analysis of the luminescence quantum efficiencies of nanocrystalline CdS and ZnO particles is presented in chapter 6. For CdS the influence of the preparation method and the nature of the surface on the quantum efficiency is investigated. It is shown that a preparation using  $Na_2S$  yields particles with a higher quantum efficiency than when  $H_2S$  is used. For both preparations, the quantum efficiency can be increased by coating the particles with a cadmium hydroxide layer or by cooling the suspension to below its freezing point. This can be explained by a removal of the non-radiative recombination centres at the surface of the particle. For ZnO, the influence of particle size on the quantum efficiency of the visible emission is studied. The quantum efficiency decreases from 20% to 12% as the size of the particles increases from 7 Å to 10 Å. This result is in agreement with the model that is presented in chapter 4.

---

## REFERENCES .

- [1] G. Jaeckel, *Z. Tech. Phys.* 6 (1926) 301.
- [2] C.R. Berry, *Phys. Rev.* 153 (1967) 989.
- [3] C.R. Berry, *Phys. Rev.* 161 (1967) 848.
- [4] E.J. Meehan, J.K. Miller, *J. Phys. Chem.* 72 (1968) 1523.
- [5] A.G. Stasenko, *Sov. Phys. Sol. State* 10(1) (1968) 186.
- [6] V.B. Sandomirskii, *Sov. Phys. JETP* 16 (1963) 1630.
- [7] J.R. Schrieffer, "Mobility in inversion layers : Theory and experiment", in *Semiconductor Surface Physics*, edited by R.H. Kingston, University of Pennsylvania Press, Philadelphia (1957) p.55-69.
- [8] F.F. Fang, W.E. Howard, *Phys. Rev. Lett.* 16 (1966) 797.
- [9] A.B. Fowler, F.F. Fang, W.E. Howard, P.J. Stiles, *Phys. Rev. Lett.* 16 (1966) 901.
- [10] G. Dorda, "Surface quantization in semiconductors", in *Festkörperprobleme (Advances in solid state physics)*, Vol. XIII, edited by H.J. Queisser, Pergamon-Vieweg, Braunschweig (1973), p. 215-239.
- [11] J.R. Arthur, *J. Appl. Phys.* 39 (1968) 4032.
- [12] A.Y. Cho, *J. Vac. Sci. Technol.* 8(5) (1971) S31.
- [13] R. Dingle, W. Wiegmann, C.H. Henry, *Phys. Rev. Lett.* 33(14) (1974) 827.
- [14] U. Rothlisberger, W. Andreoni, M. Parinello, *Phys. Rev. Lett.* 72 (1994) 665.
- [15] C.C. Arnold, D.M. Neumark, *J. Chem. Phys.* 99 (1993) 3353.
- [16] T. Kobayashi, *IEICE Trans. Fundamentals* E-75A (1992) 38.
- [17] W. Chen, Z. Lin, Z. Wang, L. Lin, *Sol. St. Commun.* 100(2) (1996) 101.
- [18] T. Türk, F. Sabin, A. Vogler, *Mat. Res. Bull.* 27 (1992) 1003.
- [19] D.I. Chepic, A.I. Efros, A.I. Ekimov, M.G. Ivanov, V.A. Kharchenko, I.A. Kudriavtsev, T.V. Yazeva, *J. Lumin.* 47 (1990) 113.
- [20] S. Mochizuki, K. Umezawa, *J. Phys. : Condens. Matter* 8 (1996) 7509.
- [21] K. Misawa, H. Yao, T. Hayashi, T. Kobayashi, *Chem. Phys. Lett.* 183(1,2) (1991) 113.
- [22] A.J. Bard, *J. Phys. Chem.* 86 (1982) 172.
- [23] T. Inoue, A. Fujishima, S. Konishi, K. Honda, *Nature* 277 (1979) 637.
- [24] M. Halmann, *Nature* 275 (1978) 115.
- [25] K. Kalyanasundaram, E. Borgarello, M. Grätzel, *Helv. Chim. Acta* 64 (1981) 362.
- [26] A. Henglein, *Ber. Bunsenges. Phys. Chem.* 86 (1982) 301.
- [27] A. Henglein, *J. Phys. Chem.* 86 (1982) 2291.
- [28] Z. Alfassi, D. Bahnemann, A. Henglein, *J. Phys. Chem.* 86 (1982) 4656.
- [29] R. Rossetti, S. Nakahara, L.E. Brus, *J. Chem. Phys.* 79(2) (1983) 1086.
- [30] R. Rossetti, J.L. Ellison, J.M. Gibson, L.E. Brus, *J. Chem. Phys.* 80(9) (1984) 4464.
- [31] G.C. Papavassiliou, *J. Sol. State Chem.* 40 (1981) 330.
- [32] D.L. Dexter, R.S. Knox, *Excitons*, Interscience Publishers (John Wiley & Sons), New York (1965).
- [33] L.E. Brus, *J. Chem. Phys.* 80(9) (1984) 4403.
- [34] R. Dingle, W. Wiegmann, C.H. Henry, *Phys. Rev. Lett.* 33(14) (1974) 827.
- [35] L. Spanhel, M. Haase, H. Weller, A. Henglein, *J. Am. Chem. Soc.* 109 (1987) 5649.
- [36] Y. Nosaka, *J. Phys. Chem.* 95 (1991) 5054.
- [37] J.I. Pankove, *Optical Processes in Semiconductors*, Dover Publications, New York (1971).
- [38] A.P. Alivisatos, *J. Phys. Chem.* 100 (1996) 13226.

- [39] A.P. Alivisatos, *Science* 271 (1996) 933.
- [40] D.W. Bahnemann, *Israel J. Chem.* 33 (1993) 115.
- [41] L. Brus, *J. Phys. Chem. Solids* 59(4) (1998) 459.
- [42] A. Henglein, *Top. Curr. Chem.* 143 (1988) 113.
- [43] A. Henglein, *Chem. Rev.* 89 (1989) 1861.
- [44] A. Henglein, *Ber. Bunsenges. Phys. Chem.* 101 (1997) 1562.
- [45] Y. Wang, N. Herron, *J. Phys. Chem.* 95 (1991) 525.
- [46] H. Weller, *Adv. Mater.* 5(2) (1993) 89.
- [47] H. Weller, *Angew. Chem. Int. Ed. Engl.* 32 (1993) 41.
- [48] H. Weller, A. Eychmüller, "Preparation and characterization of semiconductor nanoparticles", in *Semiconductor Nanoclusters. Studies in Surface Science and Catalysis*, vol. 103, edited by P.V. Kamat and D. Meisel, Elsevier Science (1996), p. 5-22.
- [49] V.L. Colvin, M.C. Schlamp, A.P. Alivisatos, *Nature* 370 (1994) 354.
- [50] B.O. Dabbousi, M.G. Bawendi, O. Onitsuka, M.F. Rubner, *Appl. Phys. Lett.* 66 (1995) 1316.
- [51] C.B. Murray, C.R. Kagan, M.G. Bawendi, *Science* 270 (1995) 1335.
- [52] S.A. Empedocles, D.J. Norris, M.G. Bawendi, *Phys. Rev. Lett.* 77(18) (1996) 3873.
- [53] M. Nirmal, B.O. Dabbousi, M.G. Bawendi, J.J. Macklin, J.K. Trautman, T.D. Harris, L.E. Brus, *Nature* 383 (1996) 802.



---



**ABSTRACT.**

This chapter presents an overview of size selective photoetching experiments performed on nanocrystalline semiconductor particles in suspension. Four different II-VI compounds (CdS, ZnS, PbS and ZnO) are prepared by standard colloid-chemical synthetic methods. For CdS, the initial mean radius of 35 Å can be gradually decreased to 7.5 Å by size selective photoetching. The adjustment of the particle size can be controlled to a high degree by varying the wavelength of the light that is used. It is also shown that the particle size distribution narrows during the photoetching process from about 40% to 10-15%. For ZnS and ZnO, only the feasibility of the technique can be demonstrated. This is due to the fact that these compounds have a large bandgap which limits the range for photoetching experiments. The initial radius of the ZnO particles is approximately 30-35 Å and can be decreased to about 15 Å, again accompanied by a narrowing of the particle size distribution. For PbS, no concrete evidence is obtained for the feasibility of size selective photoetching.

## 2.1 INTRODUCTION.

As was discussed in the previous chapter, semiconductors exhibit quantum size effects as a result of spatial confinement of charge carriers when the dimensions of the material become smaller than the size of the exciton [1-3]. Two well-known manifestations of these quantum size effects are the shift of the absorption onset to higher energies (due to an increase of the energy of the lowest excited state) and the transition from energy bands to discrete energy levels. These two phenomena are mainly responsible for the increased interest in quantum-confined systems over the last couple of years [2-7].

Several techniques that allow the preparation of semiconductor particles with nanometer sizes are based on sol-gel methods. They have been reported for the preparation of various semiconductor particles, such as CdS [2,8], ZnS [2,4], PbS [2,11], ZnO [2,12-15] and TiO<sub>2</sub> [12,16,17].

To study size-dependent properties it is important to have monodisperse suspensions of different particle sizes. To achieve this one can basically use two different approaches. In the first of these, the preparation method itself determines the particle size and size distribution. These methods are based on preparation inside a limited space, such as a cavity in a zeolite [18-20] or an inverse micelle in solution [21-23]. The second approach starts with a sol-gel preparation followed by treatments to separate different particle sizes from the initial size distribution. These treatments include exclusion chromatography [24], gel electrophoresis [25] and size selective precipitation [26-28]. In general, preparation inside an inverse micelle yields a size distribution of about 10-25% [22] while a preparation followed by size selective precipitation gives a dispersity of 5-10% [28,29].

Recently a novel technique has been described that allows the particle size to be adjusted after preparation by photoetching the semiconductor particles to a size which is determined by the wavelength of the light. The first observations in this direction were made by Henglein et al. who studied the photoanodic dissolution of semiconductor particles and showed that they can be photoetched via an electroless mechanism [5]. The size-selectivity of the technique was first demonstrated for nanocrystalline CdS particles by Matsumoto et al. [30,31]. We have shown that these results can be extended towards much smaller particle size [32]. For other sulphides such as ZnS and PbS, no size selective photoetching experiments have been described before. In this chapter, an overview is presented of the results that are obtained from size selective photoetching experiments that were performed on colloidal suspensions of nanocrystalline II-VI semiconductor particles. It is shown that for CdS the particle

---

radius can be gradually decreased to 7.5 Å. Information about the particle size is obtained by performing TEM and XRD measurements and by analyzing the absorption spectra. From this analysis it is also possible to give an estimation of the particle size distribution. We have also applied the technique of size selective photoetching to ZnS, PbS and ZnO.

## **2.2 THEORY.**

When a semiconductor is illuminated with light that has an energy which exceeds that of the bandgap, absorption can take place and electron-hole pairs are created. The electron can subsequently recombine with the hole, either radiatively or non-radiatively. Radiative recombination can give rise to a relatively sharp emission band centred at approximately the bandgap energy (exciton emission) or a relatively broad emission band at lower energies when (deep) traps are involved in the recombination process (trap emission). In the case of nanocrystalline particles of CdS and ZnO both emission bands can be observed at room temperature. Due to a large surface-to-volume ratio, non-radiative recombination via surface traps is the predominant route.

When the recombination of electron-hole pairs is prohibited by removing the electron (by an interfacial process), the hole can be used to dissolve the semiconductor. This well-known process of electroless photoetching [33-35], in combination with the shift of the absorption onset to higher energies upon a decrease of the particle size, provides the basis for the technique of size selective photoetching.

Removal of the electron from a semiconductor particle can be achieved by using electron scavengers such as oxygen molecules or methylviologen ions ( $MV^{2+}$ ) that are adsorbed on the surface of the particle. Methylviologen shuttles the photogenerated electrons from the semiconductor particle to the adsorbed oxygen molecules. First, the electrons are efficiently scavenged from the conduction band, resulting in the formation of  $MV^{+•}$  radicals, followed by the reduction of oxygen and regeneration of  $MV^{2+}$ . As a result, the use of methylviologen can increase the rate of the photoetching process [31,32].

It was explained in the previous chapter that one can take as a threshold for the occurrence of quantum size effects the value for the Bohr radius of the exciton in the macrocrystalline material.

The value for the Bohr radius of the exciton ( $a_B^{\text{exc}}$ , in Å) is given by :

$$a_B^{\text{exc}} = 0.529 \cdot \epsilon_{\infty} \cdot \left( \frac{1}{m_e^*} + \frac{1}{m_h^*} \right) \quad (2.1)$$

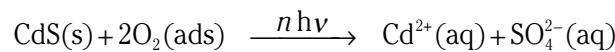
In equation (2.1),  $\epsilon_{\infty}$  is the high-frequency relative dielectric constant while  $m_e^*$  and  $m_h^*$  are the effective masses of the electron and hole respectively (both in units  $m_0$ ).

When the radius of a semiconductor particle has decreased below  $a_B^{\text{exc}}$ , the energy for the lowest electronic transition can be calculated using the following equation, based on the quantum mechanical model of a particle in a spherical box with infinite potential energy barriers [1]:

$$E = E_g + \frac{h^2}{8m_0R^2} \cdot \left( \frac{1}{m_e^*} + \frac{1}{m_h^*} \right) - \frac{1.8e^2}{4\pi\epsilon_0\epsilon_{\infty}R} \quad (2.2)$$

In equation (2.2),  $E_g$  is the bandgap of the macrocrystalline semiconductor and  $R$  is the radius of the semiconductor particle. The  $R^{-2}$ -term is a confinement energy term while the  $R^{-1}$ -term reflects the Coulomb interaction between electrons and holes. In figure 2.1A, the dependence of  $E$  on the particle size as given by equation (2.2) is shown schematically. When semiconductor particles with a size distribution as shown in figure 2.1B are illuminated with light of energy  $h\nu_1$ , only the particles that are 50 Å or bigger will be able to absorb the light. These particles can be photoetched which is accompanied by an increase of their bandgap. Gradually the size of these particles will be such that the bandgap energy is larger than the photon energy. At this particle size - determined by the wavelength of the light - the photoetching will stop. The initial size distribution should now have changed to that shown in figure 2.1C. In the same way one can decrease the particle size further by using light of a higher energy (e.g.  $h\nu_2$ , see figure 2.1D).

To demonstrate the technique of size selective photoetching as shown in figure 2.1, nanocrystalline CdS particles can be used as a model system. This system has been studied extensively in the literature [2,10,36-38]. The overall photodissolution reaction is very well known [9] :



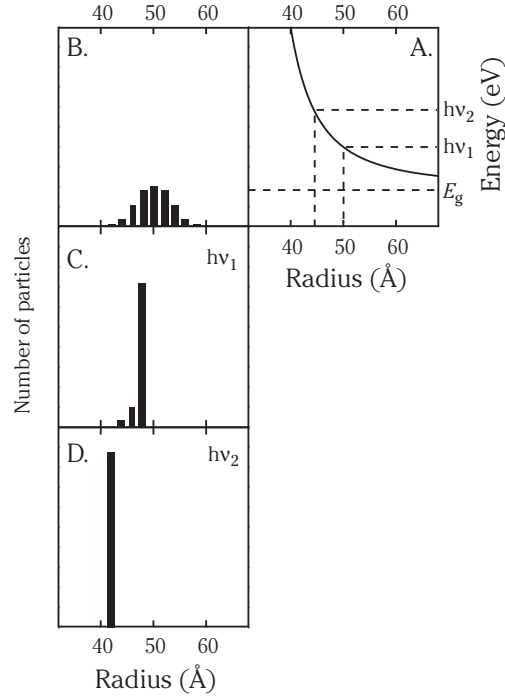


**Figure 2.1** : Schematic picture of the concept of size selective photoetching. A : bandgap energy as a function of particle radius for an arbitrary semiconductor. B : initial size distribution. C : size distribution after photoetching with light of energy  $h\nu_1$ . D : size distribution after photoetching with light of energy  $h\nu_2$ .

Illumination of CdS particles with photons of an energy higher than the bandgap leads to the formation of electron-hole pairs. Adsorbed oxygen can be reduced by electrons from the conduction band while the holes in the valence band lead to a dissolution of CdS. The efficiency of this process is low since the majority of the electron-hole pairs will recombine, either radiatively or non-radiatively.

To determine the particle size after size selective photoetching, techniques such as transmission electron microscopy (TEM) and X-ray diffraction (XRD) can be used. The width of a diffraction peak increases as the size of the crystallites decreases. The Scherrer-formula can be used to determine the size ( $s$ ) of the crystallite, which is equal to the diameter of the semiconductor particle :

$$s = \frac{0.9\lambda}{B \cdot \cos\theta_B} \quad (2.3)$$

In equation (2.3)  $\lambda$  is the wavelength of the X-rays (for Cu-K $\alpha_1$  this is 1.541 Å),  $B$  is the FWHM of the diffraction peak (in radians) and  $\theta_b$  is the maximum of the diffraction peak (in radians). Apart from these experimental techniques, empirical relationships between the mean particle radius and the position of the first absorption maximum can also be used. Such relationships have been established in the literature for CdS [10] and ZnO [14] and they will be used here instead of equation (2.2) although there is a reasonable agreement between the values obtained by both methods.

Finally, to measure the narrowing of the particle size distribution after size selective photoetching the width of the inhomogeneously broadened bands in the absorption and emission spectra can be analyzed.

## 2.3 EXPERIMENTAL METHODS.

### 2.3.1 Sample preparation.

**CdS.** To obtain a colloidal suspension of nanocrystalline CdS particles, 20 ml of an aqueous solution of 0.05 M sodium polyphosphate were added to 40 ml of an aqueous solution of 0.01 M Cd(ClO<sub>4</sub>)<sub>2</sub>·6H<sub>2</sub>O. After diluting this solution to 100 ml, 7.2 ml H<sub>2</sub>S (Aldrich lecture bottle, 99.5+ %) were injected using an airtight syringe. Vigorously shaking the sample for several minutes at room temperature resulted in a transparent suspension with a yellow colour. According to the literature, this preparation of an aqueous CdS suspension should yield particles with a mean radius of about 35 Å [36,37].

**ZnS.** A colloidal suspension of nanocrystalline ZnS particles was obtained by diluting 5 ml of an aqueous solution of 0.01 M Zn(ClO<sub>4</sub>)<sub>2</sub>·6H<sub>2</sub>O to 100 ml before adding 10 ml of an aqueous solution of 0.05 M sodium polyphosphate. After injection of 1 ml H<sub>2</sub>S, the sample was vigorously shaken for several minutes at room temperature and allowed to age for a day [4]. The resulting colloidal suspension was transparent and colourless.

**PbS.** For this suspension a mixture of 2 ml of an aqueous solution of 0.005 M Pb(ClO<sub>4</sub>)<sub>2</sub>·3H<sub>2</sub>O and 2 ml of an aqueous solution of 0.5 M polyvinyl alcohol was diluted to 100 ml before injecting 215 µl H<sub>2</sub>S. This resulted in a transparent colloidal suspension with a dark red colour. According to the literature, the PbS particles have a rod-like shape with a length of 180 Å and a diameter of 15 to 25 Å [11].

**ZnO.** A solution of 0.06 g ( $2.7 \cdot 10^{-4}$  mol) Zn(OAc)<sub>2</sub>·2H<sub>2</sub>O in 80 ml 2-propanol was made at 50 °C. After diluting the solution to 230 ml with 2-propanol it was cooled to



---

0 °C. At this temperature 20 ml of a solution of 0.082 g ( $2.0 \cdot 10^{-3}$  mol) NaOH in 100 ml 2-propanol were added within 1 minute while stirring. After ageing in a water bath at 65 °C for 2 hours a transparent, colourless suspension of ZnO particles was obtained. According to the literature [13], the ZnO particles are almost spherical with a mean radius of 25 Å and a relatively narrow particle size distribution ( $\Delta R=5$  Å).

Since alcohols can act as hole scavengers, photoetching of ZnO could not be performed in the solvent in which ZnO was prepared. Therefore the ZnO particles were transferred to water before photoetching. This was done by first adsorbing the ZnO particles on a silica powder (Aerosil Ox50 Degussa). After centrifuging the suspension and washing the precipitate, the ZnO particles - still adsorbed on silica - were redispersed in water.

### **2.3.2 Photoetching.**

The size selective photoetching experiments were performed with a 450 W xenon lamp (Ushio UXL 450SP). The wavelength of the light was tuned by using a series of cut-off filters: (1) 2.48 eV (Schott A490), (2) 2.73 eV (Schott A440), (3) 2.94 eV (Schott GG420), (4) 3.06 eV (Schott WG395), (5) 3.31 eV (Schott WG375), (6) 3.44 eV (Schott WG360), (7) 3.49 eV (Schott A350-1), (8) 3.54 eV (Schott A330) and (9) 4.08 eV (Schott A280). A cut-off filter absorbs photons of energies higher than the cut-off energy while photons with a lower energy are transmitted. The cut-off energy is defined as the energy at which the transmission is 50% of the maximum transmission.

The suspensions were illuminated in a quartz container under continuous stirring and bubbling with oxygen. To avoid interference from extra absorption bands, methylviologen was not used in the experiments. The aqueous suspension of ZnS particles was illuminated without using a cut-off filter. The suspension of ZnO particles adsorbed on silica was first diluted 1:10 with water before it was illuminated while in a glass container. In this way, the glass acts as a cut-off filter at about 4 eV.

### **2.3.3 Optical characterisation.**

Absorption measurements were performed on a Perkin Elmer Lambda 16 UV/VIS spectrophotometer. The absorbance ( $A$ ) was measured as the logarithm of the transmission ( $T=I/I_0$ ) with water as a reference. Luminescence measurements were performed on a SPEX Fluorolog spectrophotometer model F2002 equipped with two double-grating 0.22 m SPEX 1680 monochromators and a 450 W xenon lamp as the excitation source.

### 2.3.4 Transmission Electron Microscopy.

TEM measurements were performed on a Philips CM30 electron microscope operating at 300 kV. Only non-etched samples were used for these measurements. To perform TEM measurements on samples after photoetching it is necessary to first remove the etch products (e.g.  $\text{Cd}^{2+}$  and  $\text{SO}_4^{2-}$  ions) from the suspension (e.g. by dialysis).

### 2.3.5 X-ray Powder Diffraction.

XRD measurements were done using  $\text{Cu-K}\alpha_1$  radiation on a Philips PW1729 X-Ray Generator equipped with a PW1710 Diffractometer Control.

## 2.4 RESULTS AND DISCUSSION.

### 2.4.1 CdS.

Figure 2.2 shows the results of TEM measurements on CdS particles. It is clear that the particles are crystalline and lattice planes can be observed with interplanar distances of about 3.4 Å. These measurements also show that the particle size distribution is relatively broad. Due to cluster formation, it is difficult to determine a mean particle radius from the TEM measurements but analysis shows many particles with radii between 30 and 40 Å.

XRD spectra show diffraction peaks that are broadened due to small crystal sizes. As a result of this broadening it is difficult to determine the crystal structure of the CdS particles (wurtzite or zincblende). The interplanar distance of 3.4 Å occurs in both modifications. For macrocrystalline CdS the most common modification is wurtzite [39]. For nanocrystalline CdS particles both modifications have been reported although the zincblende structure is generally observed when CdS particles are prepared in solution [27,38]. For the strongest diffraction peak, using equation (2.3) with  $\theta_B=0.23$  rad and  $B=0.02$ , a mean particle radius of 35 Å is obtained which is in good agreement with the values obtained from TEM measurements and the value reported in the literature [37].

For the wurtzite structure ( $m_e^*=0.22$ ,  $m_h^*=0.70$  and  $\epsilon_\infty=5.3$  [39]), the Bohr radius of the exciton in macrocrystalline CdS calculated from equation (2.1) is 17 Å while for the

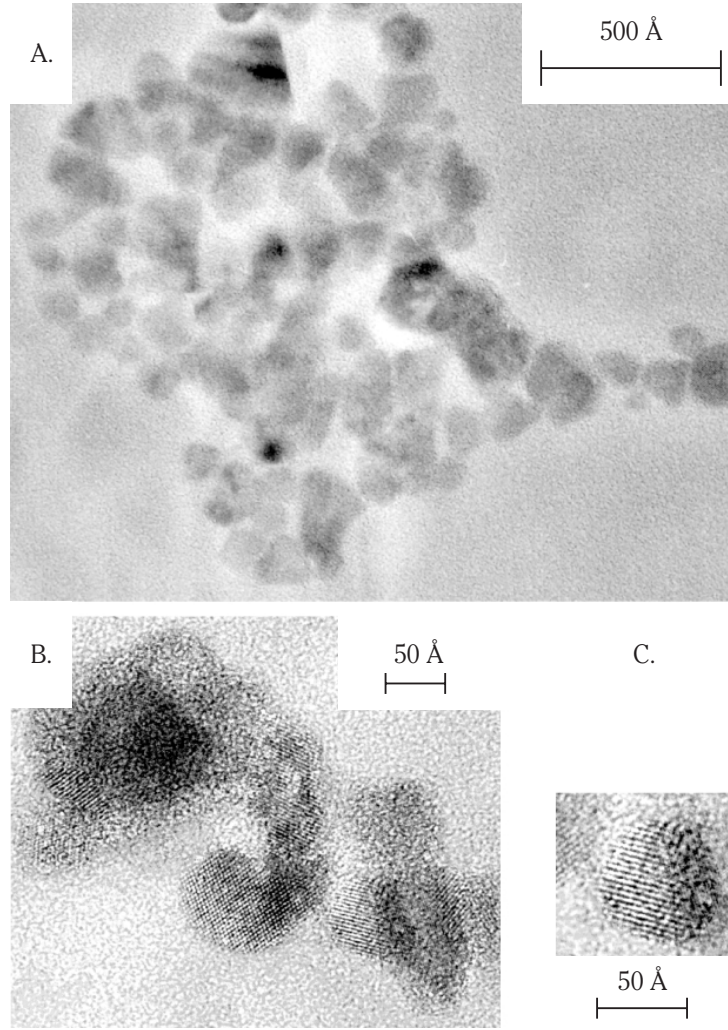


**Figure 2.2** : TEM-micrographs of CdS particles from an aqueous suspension before illumination.

zincblende structure ( $m_e^*=0.14$ ,  $m_h^*=0.51$  and  $\epsilon_\infty=5.3$  [39]) a value of  $26 \text{ \AA}$  is obtained. This means that the initial radius of our particles is close to that of the exciton in macrocrystalline CdS.

This is in agreement with results obtained from absorption and luminescence measurements. Figure 2.3 shows the absorption and emission spectrum of an aqueous suspension of nanocrystalline CdS particles before illumination. The onset of absorption - determined from extrapolation of the steep part of the spectrum - is at about  $2.5 \text{ eV}$ , similar to the value for the bandgap energy of macrocrystalline CdS. The absorption spectrum is also structureless, indicating the presence of continuous energy bands. The emission spectrum shows an exciton emission band centred at  $2.45 \text{ eV}$ .

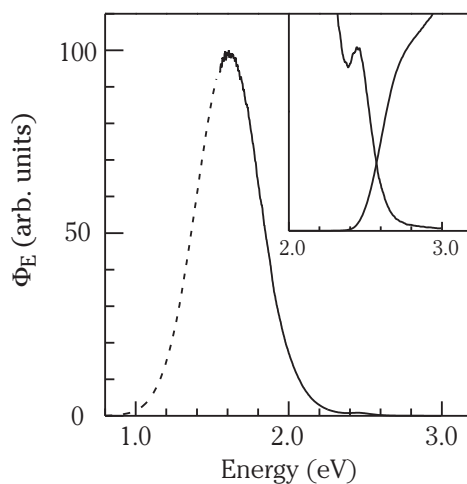


**Figure 2.3** : Emission spectrum of an aqueous suspension of nanocrystalline CdS particles upon excitation with 3.5 eV before photoetching.  $\Phi_E$  denotes the photon flux per constant energy interval. The inset shows the exciton emission band together with the absorption spectrum of the suspension.

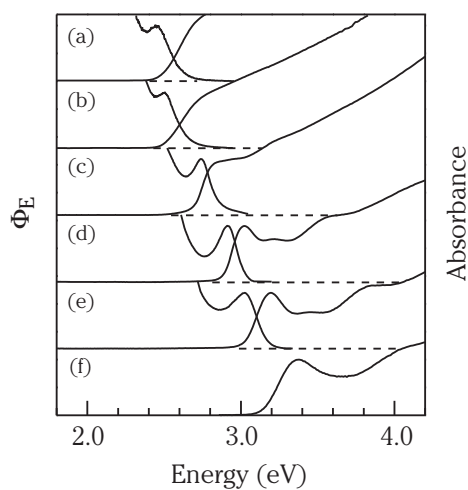


**Figure 2.4** : Absorption and emission spectra of nanocrystalline CdS particles in aqueous suspension. Spectra (a) were recorded before illumination, spectra (b)-(f) after illumination for two hours through filters with cut-off energies of 2.48 eV, 2.73 eV, 2.94 eV, 3.06 eV and 3.31 eV respectively. The intensities of the exciton emission maxima and the first absorption maxima are set to unity. The emission spectra were recorded upon excitation with 4.1 eV radiation.  $\Phi_E$  denotes the photon flux per constant energy interval.

All the spectra shown in figure 2.4 concern the same suspension and each of them is taken after illumination for two hours using filters with increasing cut-off energies. As the absorption spectra did not change upon prolonged illumination, the photoetching process was completed within this time span. Previously, it was reported that the use of methylviologen enhances the rate of the photoetching process [31,32]. The spectra show a gradual shift of the absorption onset and a concomitant development of structure. These are clear indications of a decrease in size of quantum-confined semiconductor particles. The observation of structure is characteristic for a narrow size distribution.

Table 2.1 : Results of size selective photoetching of an aqueous suspension of nanocrystalline CdS particles, using filters with different cut-off energies. The first row contains the data for the CdS suspension before illumination.

filter cut-off energy <sup>a</sup> (eV)	emission maximum (eV)	absorption onset <sup>b</sup> (eV)	absorption maximum (eV)	mean particle radius (Å)
—	2.45	2.47	—	35 <sup>c</sup>
2.48	2.50	2.57	—	—
2.73	2.74	2.68	2.86	24
2.94	2.91	2.87	3.02	18
3.06	3.02	3.01	3.19	14
3.31	—	3.13	3.38	12
3.44	—	3.36	3.64	10
3.49	—	3.41	3.70	9.5
3.54	—	3.45	3.78	9.0
4.08	3.93	—	4.20 <sup>d</sup>	7.5

<sup>a</sup>Defined as the energy where the transmission is half the maximum value.

<sup>b</sup>Determined from extrapolating the steep part of the absorption spectrum.

<sup>c</sup>Determined from TEM and XRD measurements.

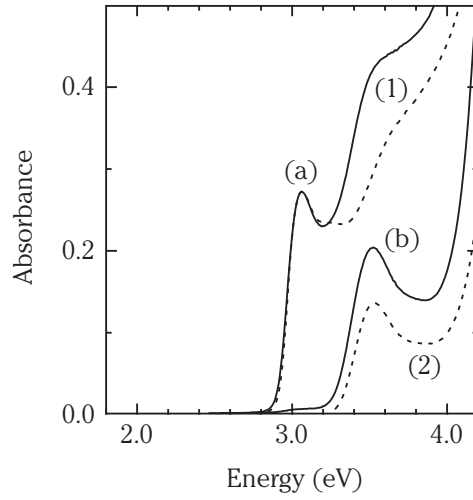
<sup>d</sup>Position of the lowest excitation maximum.

Table 2.1 gives the values for the cut-off energies of the filters that were used, together with the energetic positions of the onset of absorption, first absorption maximum, and the position of the exciton emission band. The column on the right contains the particle size that was estimated from the empirical relationship between the first absorption maximum and mean particle radius [10]. The absorption and emission data from table 2.1 show good agreement with the cut-off energies of the

filters. This indicates that the particle size obtained after size selective photoetching can be controlled by tuning the wavelength of the light.

To illustrate that size selective photoetching can be used to narrow the size distribution of a suspension of nanocrystalline semiconductor particles, absorption measurements were performed on a mixture of two CdS suspensions. These suspensions were obtained by photoetching with light of 2.94 eV and 3.31 eV respectively. Figure 2.5 shows the absorption spectra of the separate suspensions (1 and 2) after a 1:1 dilution with water. Figure 2.5 also shows an absorption spectrum of a 1:1 mixture of the undiluted suspensions 1 and 2 (a). The mixture (a) was again illuminated through a filter with a cut-off energy of 3.31 eV, resulting in spectrum (b). Because spectrum (b) resembles spectrum (2), it is clear that the particle size distribution narrows upon photoetching. Only the bigger particles added to suspension (2) from suspension (1) have been photoetched. The total area of the first absorption peak of spectrum (b) is a factor 1.85 higher than that of the first absorption peak of spectrum (2). This means that the total number of particles has decreased slightly upon photoetching CdS particles from a radius of 18 Å to 12 Å. These results are not in agreement with those obtained by Matsumoto et al. [31]. By analyzing the amount of sulphate ions produced during the photoetching process they have concluded that the number of particles decreased to about 40% of the initial number of particles over the same size range as in our experiment.

At first sight one might think that a broadening of the first absorption band and the exciton emission band indicates a broadening of the particle size distribution after photoetching. In figure 2.6, it can be seen that the first absorption band broadens upon photoetching while the same effect is also visible in the emission spectra. Figure 2.7A contains two exciton emission bands : after photoetching with 2.94 eV (a) and 4.08 eV (b). It is clear that the second emission band, originating from much smaller particles, is broader. The broadening of both absorption and exciton emission bands reflects the increasing dependence of the bandgap energy on the particle size. This means that even particles with a relatively narrow size distribution can exhibit broad absorption and emission bands once they are in the strong confinement regime. The principle of broadening of the exciton emission band as a result of quantum confinement is illustrated in figure 2.7B-D. The dependence of the lowest electronic transition in a semiconductor particle on the particle size is shown in figure 2.7B. In figure 2.7C, three possible particle size distributions are shown differing in mean particle size and/or distribution width. The exciton emission bands, as shown in figure 2.7D, are constructed by plotting, for each particle size, the number of particles versus the energy for the lowest electronic transition (the intensity is taken proportional to the number of



**Figure 2.5** : Absorption spectra of aqueous suspensions of nanocrystalline CdS particles after illumination through filters with cut-off energies 2.94 eV (1) and 3.31 eV (2) respectively. A 1:1 mixture of (1) and (2), shown as (a), was again illuminated through a filter with cut-off energy 3.31 eV to yield (b).

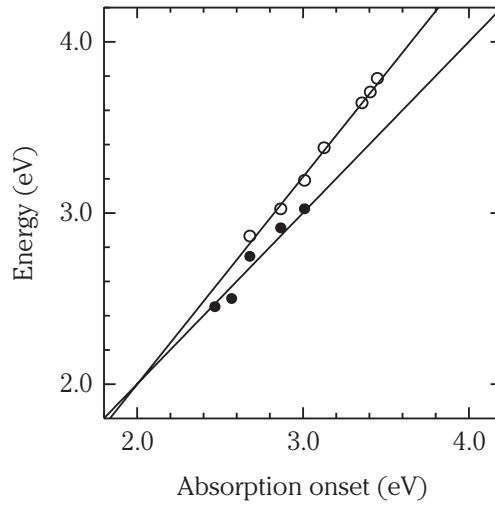


**Figure 2.6** : Energetic positions of the exciton emission maximum (solid circles) and the first absorption maximum (open circles) versus the absorption onset energy of nanocrystalline CdS particles in aqueous suspension.

particles). In this way, only inhomogeneous line broadening is considered. It is clear that the widths of the emission bands originating from the smallest particles, (b) and (c), are much larger than in the case of the bigger particles (a), even when the particle size distribution has narrowed.

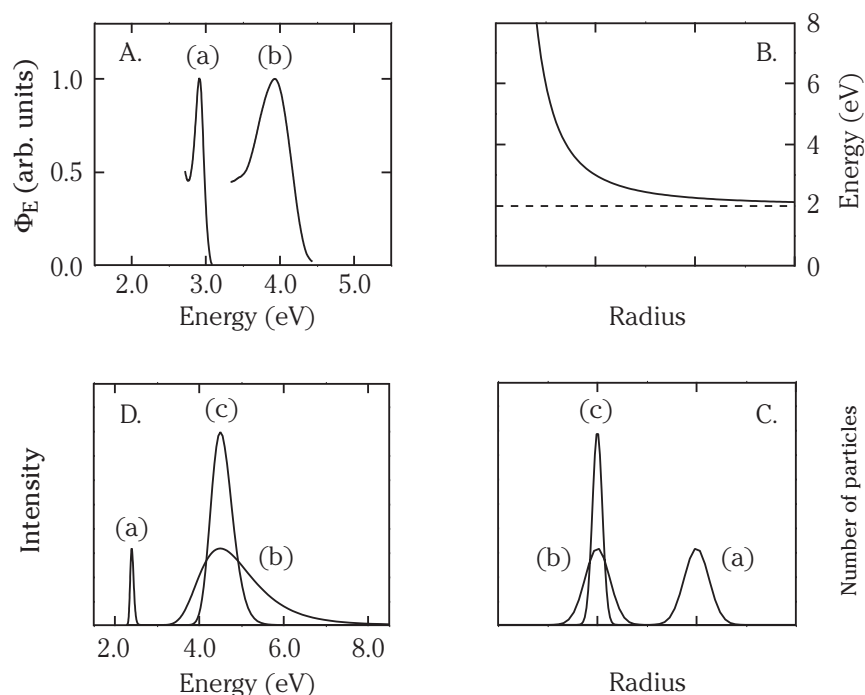


**Figure 2.7** : A : Emission measurements on aqueous suspensions of nanocrystalline CdS particles showing the exciton emission band. Spectrum (a) was taken after photoetching at 2.94 eV (excitation with 4.1 eV) and spectrum (b) after photoetching at 4.08 eV (excitation with 5.2 eV).  $\Phi_E$  denotes the photon flux per constant energy interval. B-D : Illustration of the broadening of excitonic absorption and/or emission bands as a consequence of semiconductor particles becoming more quantum confined. B : The variation of the bandgap energy with particle radius. C : Three possible particle size distributions, differing in mean particle size and monodispersity. D : The corresponding shapes of the excitonic emission bands. The intensity is taken to be proportional to the number of particles. The homogeneous line broadening is considered to be negligible in comparison to the inhomogeneous line broadening.

A quantitative analysis of the change in particle size distribution can be performed by considering the width of the first absorption band. It is assumed that this band is inhomogeneously broadened due to a distribution in particle size. Experimental results obtained by Vossmeier et al. [10] can be used to determine both the mean particle radius ( $\langle R \rangle$ ) from the absorption maximum as well as the dispersion in particle size ( $\Delta R$ ) using the energy at which the absorption is half the maximum value on the low-energy side of the first absorption band. In table 2.2 the values for  $\langle R \rangle$  and  $\Delta R$  are shown. It is clear that not only  $\langle R \rangle$  but also  $\Delta R$  decreases upon photoetching. As a result of size selective photoetching, the dispersion in particle size decreased from 40% to 10-15%, which is comparable to that obtained by other techniques such as inverse micelle preparation and size selective precipitation [22,28,29].



Table 2.2 : Mean particle radii ( $\langle R \rangle$ ) and accompanying  $\Delta R$  (defined as half the FWHM of a gaussian particle size distribution) determined from the energetic positions of the absorption maxima and the half-maxima using [10].

filter cut-off energy (eV)	absorption		$\langle R \rangle$ (Å)	$\Delta R$ (Å)
	maximum (eV)	half-maximum (eV)		
2.73	2.86	2.75	24	9
2.94	3.02	2.93	18	3
3.06	3.19	3.10	14	1.5
3.31	3.38	3.23	12	1.5
4.08	4.20 <sup>a</sup>	3.92 <sup>a</sup>	7.5	1

<sup>a</sup>Determined from the lowest excitation maximum.

Figure 2.6 also shows the increasing energy separation between the exciton emission maximum and the first absorption maximum, reflecting an increase in exciton binding energy with decreasing particle size. This size-dependence of the exciton binding energy has been reported before and was attributed to the enhanced spatial overlap between the electron and hole wave functions [6].

As a result of this enhanced overlap, an increase of the oscillator strength with decreasing particle size is also expected [6] and has been observed [10]. Since the oscillator strength is linearly proportional to the absorption coefficient, absorption spectra can be used to study the size-dependence of the oscillator strength. In our case, all absorption spectra are recorded for the same suspension of nanocrystalline CdS particles and only the particle size is changed by photoetching. In this way the change in oscillator strength due to a change in particle size can be determined accurately. In figure 2.8, some of the absorption spectra from figure 2.4 are plotted without scaling the absorption signal. It is clear that the total absorption signal decreases upon photoetching as a result of a decrease in the amount of absorbing material. The first absorption maximum can be fitted to a gaussian curve and the area of this curve, normalised for the particle volume, gives an indication of the absorption coefficient of the semiconductor particle per CdS unit. As the radius of the CdS particle decreases from 24 Å to 11 Å the absorption coefficient (and therefore the oscillator strength) increases with a factor of 3.5. This is in good agreement with the experimental results obtained by Vossmeier et al. [10] but not with the theoretical  $R^3$ -dependence [6].

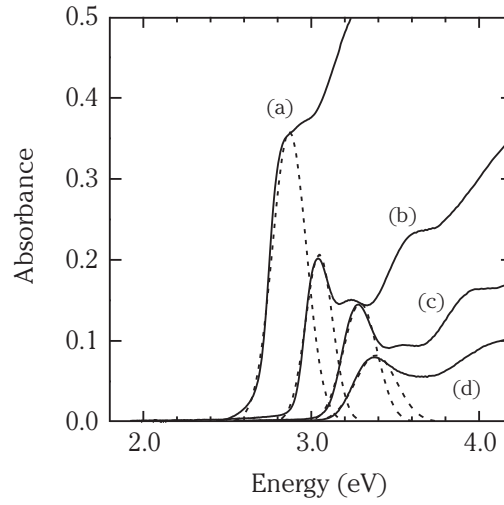


**Figure 2.8** : Absorption spectra of an aqueous suspension of CdS particles after photoetching at 2.73 eV (a), 2.94 eV (b), 3.06 eV (c) and 3.31 eV (d). The dashed curves are gaussian fits to the first absorption maxima.

#### 2.4.2 ZnS.

Only XRD measurements were performed to characterise the ZnS particles. The diffraction pattern indicates that the ZnS particles have the zincblende modification, which is in agreement with the fact that the wurtzite structure is the high-temperature modification of ZnS [39].

From the strongest diffraction peak at  $\theta_B=0.25$  rad ( $B=0.03$  rad) a mean radius of 25 Å is determined for the ZnS particles. For macrocrystalline ZnS (zincblende), using  $m_e^*=0.34$ ,  $m_h^*=0.5$  (both in units  $m_0$ ) and  $\epsilon_\infty=5.4$  [39], equation (2.1) gives a Bohr radius of the exciton of about 15 Å.

Figure 2.9A contains the emission and absorption spectrum of an aqueous suspension of nanocrystalline ZnS particles before illumination. The mean radius of the ZnS particles is larger than that of the exciton and therefore no strong quantum size effects are expected. Indeed, the absorption spectrum shows no structure. However, extrapolation of the steep part of the absorption spectrum yields a value of 3.87 eV while macrocrystalline ZnS (zincblende) has a bandgap of 3.70 eV [39]. Extrapolation of the steep part of the absorption curve gives an approximation of the bandgap, not an accurate value.

The emission spectrum shown in figure 2.9A contains a broad trap emission band centred at 2.90 eV and no detectable exciton emission band at the onset of

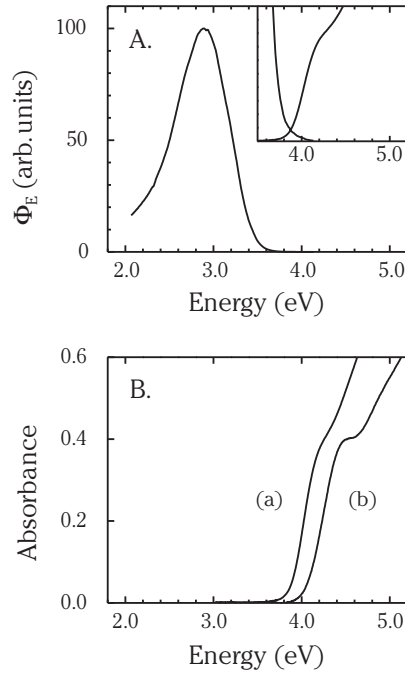


**Figure 2.9** : A : Emission spectrum of an aqueous suspension of nanocrystalline ZnS particles upon excitation with 5 eV.  $\Phi_E$  denotes the photon flux per constant energy interval. The inset shows a part of the emission spectrum together with the absorption spectrum of the suspension. B : Absorption spectra of an aqueous suspension of nanocrystalline ZnS particles before illumination (a) and after illumination for 30 min (b). Absorption spectrum (b) was scaled with respect to spectrum (a).

absorption. An exciton emission band appeared as a weak shoulder on the high energy side of the trap emission band only after the surface of the ZnS particles was passivated with a hydroxide layer. Generally, these surface-passivated semiconductor particles cannot be photoetched [32]. This means that in the case of (non surface-passivated) ZnS only absorption measurements can be used to study photoetching processes. As ZnS is a wide-bandgap semiconductor, photoetching experiments have to be carried out with light of a relatively high energy. A similar photoetching series as for CdS could not be made because few filters with high cut-off energies were available. From figure 2.9B it is clear that by using the xenon lamp without a cut-off filter, nanocrystalline ZnS particles can be photoetched. Upon illumination for 30 min the onset of absorption has shifted to 4.04 eV and the spectrum shows some structure. At about 4.5 eV a maximum of the first absorption band is visible. These results clearly indicate that upon photoetching the ZnS particles have entered the quantum confinement regime.

### 2.4.3 PbS.

An interesting system for size selective photoetching experiments is PbS. The bandgap energy for macrocrystalline PbS is relatively low (0.41 eV) which means that photoetching experiments could be performed over a wide energy range, covering the IR to the UV spectral region. After preparation, absorption and luminescence measurements were performed to characterise the PbS suspensions. In figure 2.10, curve (a) is the absorption spectrum of an aqueous suspension of nanocrystalline PbS particles. The absorption band at about 6 eV is due to the presence of excess  $\text{Pb}^{2+}$  ions in solution. As the absorption starts at energies well above that of the bandgap of macrocrystalline PbS and the spectrum is structured, the PbS particles are clearly quantum-confined. Because of the low effective masses of the charge carriers in PbS ( $m_e^*, m_h^* = 0.09m_0$  [39]), equation (2.2) yields a value for the Bohr radius of the exciton of more than 200 Å. The three absorption maxima at 2.1 eV, 3.3 eV and 4.3 eV probably result from transitions to different discrete energy levels [11]. Similar to ZnS, emission measurements on nanocrystalline PbS particles yielded only a broad trap emission band.

From spectrum (b) in figure 2.10 it is clear that upon illumination through a filter with a cut-off energy of 2.25 eV the total intensity of the absorption signal decreases while at the same time the structure becomes less pronounced. Although no distinct shift in the absorption onset is visible it seems that the positions of the three maxima have shifted slightly towards higher energies. The loss of structure could be due to a broadening of the absorption bands. A possible reason for this broadening has already been addressed before for CdS. However, when illumination is continued for longer periods or with higher energies, the total absorption intensity goes down even further.

Two explanations could account for the above mentioned observations. First, nanocrystalline PbS particles could be very difficult to photoetch due to the insolubility of  $\text{PbSO}_4$  in water. Illumination of nanocrystalline PbS particles would then probably result in the formation of a passivating sulphate layer at the surface of the particles which consequently inhibits further etching. However, this does not account for the observed decrease in absorbance upon prolonged illumination. A second explanation is based on the shape of the PbS particles. According to the literature [11], the particles have a rod-like shape. The length of these rods is about 180 Å, which is fairly close to the value for the Bohr radius of the exciton in macrocrystalline PbS ( $\approx 200$  Å). When illumination of the PbS particles leads to a shortening instead of a narrowing of the rods, photoetching might not influence the positions of the absorption bands but the total absorption signal will decrease as the PbS particles are dissolving. However, from TEM

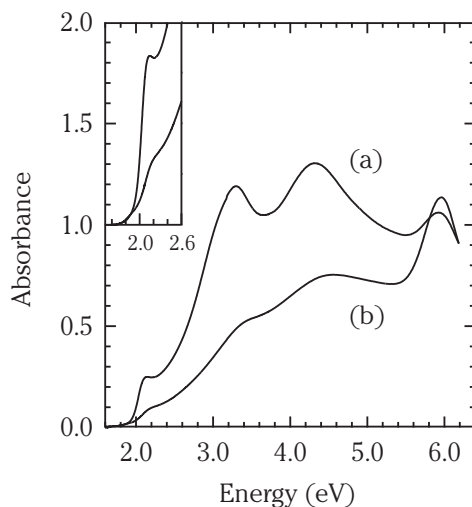


**Figure 2.10** : Absorption spectrum of an aqueous suspension of nanocrystalline PbS particles before illumination (a) and after illumination for 15 min using a filter with a cut-off energy of 2.25 eV (b). The inset is an enlargement of the onset of absorption.

measurements that we performed it was clear that the PbS particles did not have a rod-like shape but were almost spherical.

In contrast to the experimental results on CdS and ZnS, the results on nanocrystalline PbS particles do not provide concrete evidence for the possibility of size selective photoetching for these particles.

#### 2.4.4 ZnO.

TEM measurements were performed to characterise the ZnO particles and shown in figure 2.11. The particles are crystalline with interplanar distances of about 3.3 Å. As in the case of CdS, these measurements only allow a rough estimation of the mean particle radius, which is about 30 Å. According to the literature, the Bohr radius of the exciton for macrocrystalline ZnO is equal to 19 Å [39].

Figure 2.12A shows the emission spectrum of an aqueous suspension of ZnO particles adsorbed on silica. This spectrum contains two bands : a broad trap emission band centred at 2.08 eV and an exciton emission band centred at 3.42 eV. The position of the exciton emission band corresponds to the value reported in the literature for the bandgap of macrocrystalline ZnO (values between 3.2-3.4 eV [2,13,39]). Figure 2.12A also shows the absorption spectrum of the suspension. Extrapolation of the steep part of the absorption spectrum gives an onset of 3.38 eV. Using an experimental relationship between the onset of absorption and the mean particle radius [14], an onset of 3.38 eV

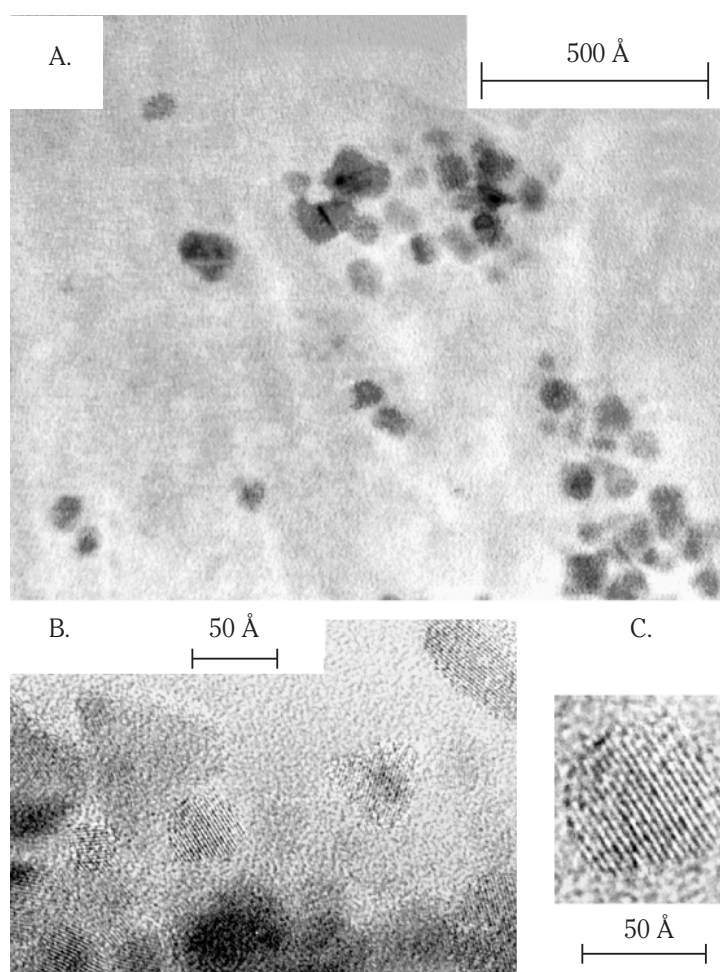


**Figure 2.11** : TEM-micrographs of ZnO particles from a 2-propanol suspension before illumination.

corresponds to a particle radius of 35 Å, which is in good agreement with our TEM measurements but larger than reported in the literature for a similar preparation [13]. For ZnO particles in this size range the energetic position of the onset of absorption varies only very slightly with particle size. Therefore the error in the calculated value for the mean radius of the ZnO particles is relatively large.

Photoetching experiments were performed using glass as a cut-off filter at 4 eV. These experiments show that nanocrystalline ZnO particles can be photoetched in water. Figure 2.12B shows the shift of the exciton emission band from 3.42 eV to 3.55 eV upon illumination for 16 hours. This shift indicates that the ZnO particles have become smaller and have entered the quantum confinement regime. After photoetching, the ZnO particles were very instable as the exciton emission band disappeared with time. It

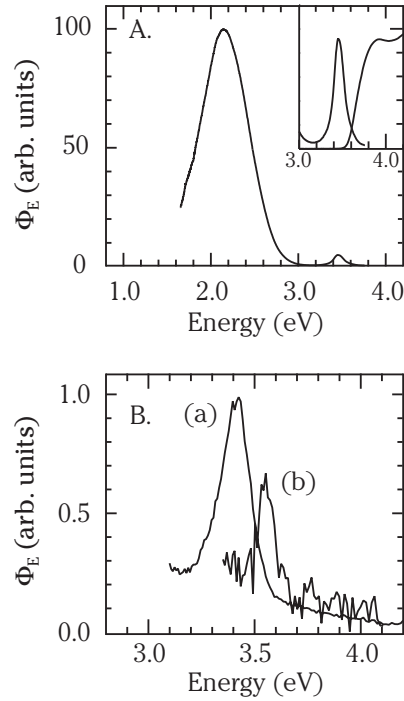


**Figure 2.12** : A : Emission spectrum of an aqueous suspension of nanocrystalline ZnO particles. The inset shows the exciton emission band together with the absorption spectrum of the suspension. B : Emission spectra showing the exciton emission bands of an aqueous suspension of ZnO particles before illumination (a) and after illumination (b) for 16 hours through glass with a cut-off energy of about 4 eV. Spectrum (b) was multiplied by a factor 10.  $\Phi_E$  denotes the photon flux per constant energy interval. The emission spectra were recorded upon excitation with 4.1 eV.

was not possible to record an absorption spectrum of the ZnO suspension after illumination because the signal had become too low due to the loss of material during the photoetching process.

Similar to CdS, more information about the mean particle size and the particle size distribution can be obtained by using an empirical relationship between the onset of absorption and the particle size for ZnO particles [14]. In our case, emission measurements have to be used instead of absorption measurements. To be able to use the relationship it is assumed that shift between the maximum of the exciton emission band and the onset of absorption is the same before photoetching as afterwards. In this way, it is determined that a mean particle radius of  $35 \text{ \AA} \pm 15 \text{ \AA}$  before photoetching is decreased to  $15 \text{ \AA} \pm 5 \text{ \AA}$  after photoetching. It is clear that not only the mean particle size has decreased upon photoetching but also the width of the particle size distribution has decreased.

As can be seen in figure 2.12B, the width of the exciton emission band has become slightly smaller upon photoetching. At a radius of 15 Å, the ZnO particles have not yet entered the range in which the bandgap energy depends very strongly on the particle size. According to Haase et al. [14], a strong dependence of the absorption onset on particle size starts at particle radii of about 10 Å corresponding to an absorption onset of about 3.6 eV.



---

## 2.5 CONCLUSION.

The experiments described in this chapter demonstrate the feasibility of size selective photoetching as a means to adjust the size of nanocrystalline semiconductor particles with a high degree of control. The particle size after photoetching is determined by the energy of the light that is used for photoetching. The technique works very well for nanocrystalline CdS particles and enables one to prepare a series of samples with different well-defined particle radii, covering a wide range from 35 Å to 7.5 Å. The decrease in mean particle size is accompanied by a narrowing of the particle size distribution from some 40% to 10-15%.

The applicability of the technique to nanocrystalline semiconductor particles of ZnS and ZnO has been demonstrated but the wide bandgap of these compounds limits the range for size selective photoetching experiments.

Nanocrystalline PbS particles are very difficult to photoetch, most probably due to the insolubility of PbSO<sub>4</sub> in water which could result in the formation of a passivating sulphate layer on the surface of the PbS particles.

## REFERENCES.

- [1] L.E. Brus, *J. Chem. Phys.* 80(9) (1984) 4403.
- [2] A. Henglein, *Top. Curr. Chem.* 143 (1988) 113.
- [3] A. Henglein, *Chem. Rev.* 89 (1989) 1861.
- [4] H. Weller, U. Koch, M. Gutiérrez, A. Henglein, *Ber. Bunsenges. Phys. Chem.* 88 (1984) 649.
- [5] A. Henglein, *Ber. Bunsenges. Phys. Chem.* 86 (1982) 301.
- [6] Y. Wang, N. Herron, *J. Phys. Chem.* 95 (1991) 525.
- [7] H. Weller, *Angew. Chem. Int. Ed. Engl.* 32 (1993) 41.
- [8] A. Henglein, A. Fojtik, H. Weller, *Ber. Bunsenges. Phys. Chem.* 91 (1987) 441.
- [9] D. Meissner et al., *Ber. Bunsenges. Phys. Chem.* 89 (1985) 121.
- [10] T. Vossmeier, L. Katsikas, M. Giersig, I.G. Popovic, K. Diesner, A. Chemseddine, A. Eychmüller, H. Weller, *J. Phys. Chem.* 98 (1994) 7665.
- [11] S. Gallardo, M. Gutiérrez, A. Henglein, E. Janata, *Ber. Bunsenges. Phys. Chem.* 93 (1989) 1080.
- [12] D.W. Bahnemann, *Israel J. Chem.* 33 (1993) 115.
- [13] D.W. Bahnemann, C. Kormann, M.R. Hoffmann, *J. Phys. Chem.* 91 (1987) 3789.
- [14] M. Haase, H. Weller, A. Henglein, *J. Phys. Chem.* 92 (1988) 482.
- [15] L. Spanhel, M.A. Anderson, *J. Am. Chem. Soc.* 113 (1991) 2826.
- [16] D.W. Bahnemann, A. Henglein, J. Lilie, L. Spanhel, *J. Phys. Chem.* 88 (1984) 709.
- [17] C. Kormann, D.W. Bahnemann, M.R. Hoffmann, *J. Phys. Chem.* 92 (1988) 5196.
- [18] W. Chen, Z.G. Wang, Z.J. Lin, J.J. Qian, L.Y. Lin, *Solid State Commun.* 100 (1996) 101.
- [19] W. Chen, Z.G. Wang, Z.J. Lin, J.J. Qian, L.Y. Lin, *Appl. Phys. Lett.* 68(14) (1996) 1990.
- [20] Y. Wang, N. Herron, *J. Phys. Chem.* 91 (1987) 257.
- [21] G. Counio, S. Esnouf, T. Gacoin, J.-P. Boilot, *J. Phys. Chem.* 100 (1996) 20021.
- [22] M.L. Steigerwald, A.P. Alivisatos, J.M. Gibson, T.D. Harris, R. Kortan, A.J. Muller, A.M. Thayer, T.M. Duncan, D.C. Douglas, L.E. Brus, *J. Am. Chem. Soc.* 110 (1988) 3046.
- [23] A.R. Kortan, R. Hull, R.L. Opila, M.G. Bawendi, M.L. Steigerwald, P.J. Carroll, L.E. Brus, *J. Am. Chem. Soc.* 112 (1990) 1327.
- [24] C.H. Fischer, H. Weller, L. Katsikas, A. Henglein, *Langmuir* 5 (1989) 429.
- [25] A. Eychmüller, L. Katsikas, H. Weller, *Langmuir* 6 (1990) 1605.
- [26] C.B. Murray, D.J. Norris, M.G. Bawendi, *J. Am. Chem. Soc.* 115 (1993) 8706.
- [27] M.G. Bawendi, P.J. Carroll, W.L. Wilson, L.E. Brus, *J. Chem. Phys.* 96(2) (1992) 946.
- [28] D.J. Norris, M.G. Bawendi, *Phys. Rev. B* 53(24) (1996) 16338.
- [29] A. Chemseddine, H. Weller, *Ber. Bunsenges. Phys. Chem.* 97 (1993) 636.
- [30] H. Matsumoto, T. Sakata, H. Mori, H. Yoneyama, *Chem. Lett.* (1995) 595.
- [31] H. Matsumoto, T. Sakata, H. Mori, H. Yoneyama, *J. Phys. Chem.* 100 (1996) 13781.
- [32] A. van Dijken, D. Vanmaekelbergh, A. Meijerink, *Chem. Phys. Lett.* 269 (1997) 494.
- [33] D. Meissner, C. Benndorf, R. Memming, *Appl. Surf. Sci.* 27 (1987) 423.
- [34] D. Meissner, R. Memming, B. Kastening, *J. Phys. Chem.* 92 (1988) 3476.
- [35] P.H.L. Notten, J.E.A.M. van den Meerakker, J.J. Kelly, *Etching of III-V Semiconductors. An Electrochemical Approach*, Elsevier Advanced Technology, Oxford (1991).
- [36] A. Fojtik, H. Weller, U. Koch, A. Henglein, *Ber. Bunsenges. Phys. Chem.* 88 (1984) 969.

- 
- [37] A. Eychmüller, A. Hässelbarth, L. Katsikas, H. Weller, *J.Lumin.* 48&49 (1991) 745.
- [38] J. Tittel, W. Göhde, F. Koberling, Th. Basché, A. Kornowski, H. Weller, A. Eychmüller, *J. Phys. Chem. B* 101 (1997) 3013.
- [39] O. Madelung (ed.), *Landolt-Börnstein. Numerical data and functional relationships in science and technology. Volume III-17: Semiconductors*, Springer Verlag, Berlin (1988), 17b pp. 35-115, 166-194; 17f pp. 155-161.



**ABSTRACT.**

The emission properties of suspensions of nanocrystalline ZnO particles with different particle sizes are studied. Two emission bands are observed, one being an exciton emission and the other the visible emission of ZnO. The energy of both emissions depend on the particle dimensions due to size quantisation. A linear relationship between the energetic maxima of the two emission bands is found. Because of the difference in effective masses of electrons and holes in ZnO, the slope of the linear relationship clearly indicates that the visible emission is due to the transition of an electron from the conduction band to a deep trap. The nature of the deep trap is also considered.

### 3.1 INTRODUCTION.

ZnO has been known as a luminescent material for a century, and some fifty years ago it was discovered that firing ZnO powder in a reducing atmosphere gives a particularly efficient blue-green luminescent material. This is usually represented as ZnO:Zn because of the loss of oxygen during the reducing treatment [1]. This material has a high efficiency as a low-voltage phosphor and the material has been used in vacuum fluorescent displays (VFD's) and field emission displays (FED's). Especially the latter application has become important recently, since FED's are one of the promising candidates for flat panel displays [2]. Inspired by the application of ZnO, numerous studies have appeared on the nature of the visible luminescence from ZnO. In spite of all this research, the mechanism behind the visible luminescence has been very difficult to establish, as is clear from a statement in the 1999 edition of the Phosphor Handbook [2] :

*“The origin of the luminescence center and the luminescence mechanism of ZnO:Zn phosphors are barely understood”.*

Much of the research on the luminescence of ZnO is performed on single crystalline powders ( $\mu\text{m}$  size) or single crystals. Two emission bands are usually found. A relatively weak and narrow UV emission band is observed around 380 nm (3.25 eV), just below the onset of absorption. A much stronger and broader emission band is situated in the green part of the visible spectrum, with a maximum between 500 and 530 nm (2.35-2.50 eV). The UV emission band is due to the radiative annihilation of excitons. The binding energy of excitons in ZnO is 59 meV and the exciton emission can still be observed at temperatures far above room temperature [3]. The lifetime of this exciton emission is very short, on the order of several tens to hundreds of picoseconds [4].

As mentioned before, the nature of the visible emission has been the subject of much research. At first, this emission was thought to be associated with divalent copper impurities [5] but later intrinsic defects such as interstitial zinc ions [6] or oxygen vacancies [7] were assumed to be the recombination centres. Alternative explanations involved zinc vacancies [8], chemisorbed oxygen [9], and sulphur impurities [10]. During the last years, oxygen vacancies have been assumed to be the most likely candidates for the recombination centres involved in the visible luminescence of ZnO [11-13]. In contrast to the exciton emission, the lifetime of the visible emission is much longer, viz. in the  $\mu\text{s}$  range [11].

---

Studies on the nature of defect centres involved in the visible emission often use treatment of macrocrystalline ZnO in a reducing or oxidizing atmosphere [12-14]. In this way, the number of oxygen vacancies or other defects can be varied and this is then related to changes in the luminescence intensity. A problem is that the intensity of the luminescence is influenced by the width of the depletion layer, which is also strongly dependent on defect concentrations. This makes it difficult to draw conclusions on the origin of the visible luminescence from the observed changes in the luminescence intensity and defect concentrations [12-16]. In this study, nanocrystalline ZnO particles are used which has two main advantages. First, there is no band bending in the particle as the particles are much smaller than the width of the depletion layer. Changes in luminescence intensity due to depletion layer effects are therefore absent. Second, the mean particle size can be varied and its influence on the emission properties can be studied since the electronic structure of ZnO is size-dependent when the particles are in the quantum size regime ( $R < 19 \text{ \AA}$  [17]). The characteristics of the visible emission of macrocrystalline ZnO (single crystals or powders) are very similar to those of nanocrystalline ZnO particles. In both cases, the energetic position as well as the luminescence lifetime are comparable. This similarity suggests that the origin of the visible emission is the same for all forms of ZnO. Furthermore, the recombination centres are probably not at the surface of the material because in single crystals of ZnO - with a very low surface-to-volume ratio - the intensity of the visible emission is still high. The idea that the recombination centres that are involved in the visible emission of ZnO must be in the bulk of the material is corroborated by results from temperature-dependent steady-state luminescence measurements that will be presented in chapter 4.

In this chapter, results will be presented of steady-state luminescence measurements performed at room temperature during the growth of ZnO particles. Studies on the variation of the energetic positions of the maxima of both the visible and the UV emission band of ZnO as a function of particle size provide novel information on the nature of the transition responsible for the visible emission, which is valid for ZnO in general.

## **3.2 THEORY.**

Photoexcitation of a semiconductor particle results in the formation of Wannier excitons. Radiative recombination of these excitons yield photons with an energy close to that of the bandgap. Such a process is normally referred to as exciton emission. Wannier excitons are spatially delocalised and when the semiconductor particle is very

small (i.e. in the quantum size regime) they will be delocalised over the entire particle volume. The photogenerated charge carriers can also get trapped somewhere in the particle. This can take place in shallow levels or in deep traps. Shallowly trapped charge carriers are still spatially delocalised. Due to this delocalisation the energetic position of such shallow traps is related to the band structure of the material [19]. When the band edges shift as a function of particle size, as is the case for quantum-confined semiconductor particles, the energetic position of the shallow traps in these particles will show a similar size-dependency.

When a charge carrier is trapped deeper, a localised energetic state is obtained. Such deep traps can be found either in the bulk or at the surface of a semiconductor particle. Their energetic position is more or less independent on particle size and is determined by the local surroundings of the trapped charge carrier. Trapping of a charge carrier can occur via a radiative process. This type of emission is referred to as trap emission. Next to these two kinds of emission (exciton and trap emission), non-radiative processes are very important in semiconductor particles. Often surface states are involved in non-radiative relaxation processes. The surface of a semiconductor is a strong perturbation of the lattice where a high concentration of both shallow and deep levels provide a pathway for non-radiative recombination of photogenerated charge carriers [20]. Figure 3.1 schematically shows the energy levels for macrocrystalline as well as nanocrystalline semiconductors, similar to figure 1.1 but now including various trap levels. Note that in figure 3.1, the lines representing the shallow traps (ST) are longer than the one representing the deep trap (DT). This is to indicate a higher degree of delocalisation.

### **3.3 EXPERIMENTAL METHODS.**

#### **3.3.1 Sample preparation.**

Suspensions of nanocrystalline ZnO particles can be prepared in a non-aqueous solvent such as 2-propanol [8]. For this preparation 25 ml of a 0.02 M NaOH solution was slowly added while stirring to 225 ml of a 0.001 M  $\text{Zn}(\text{CH}_3\text{COO})_2 \cdot 2\text{H}_2\text{O}$  solution, after both solutions were first cooled to 0 °C. A rapid formation of extremely small ZnO particles is followed by a relatively slow growth of the particles. The rate of particle growth depends strongly on the temperature. When the suspension is aged at room temperature, it takes several days for the particles to attain their final size. TEM-measurements on the fully grown particles have shown a crystalline structure and a



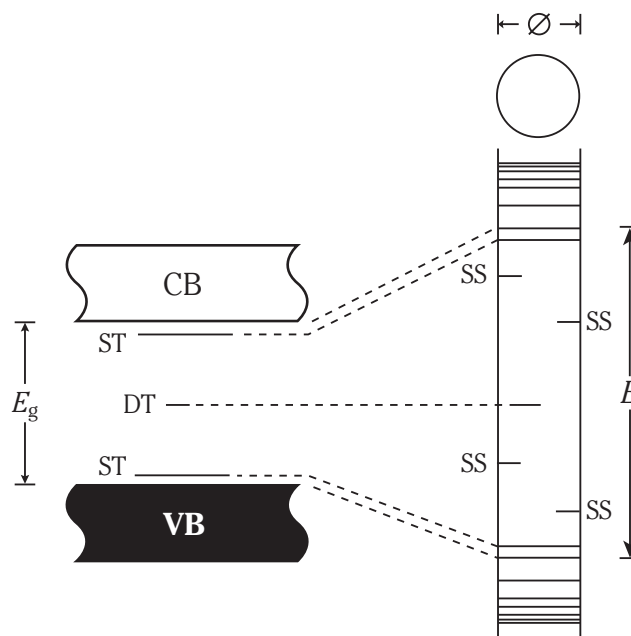


**Figure 3.1** : Schematic picture of the energy levels of a macrocrystalline (left) and a nanocrystalline semiconductor (right).  $E_g$  is the bandgap of the macrocrystalline semiconductor while  $E$  denotes the corresponding energy difference for a nanocrystalline semiconductor. Two different bulk trap levels are shown, ST being a shallow trap and DT a deep trap. The shift of the energetic positions of these trap levels upon a decrease of particle size are indicated by dashed lines. For the nanocrystalline semiconductor, also surface states (SS) are shown.

mean radius of about 30 Å [21]. This corresponds to particles that contain approximately 5000 molecular ZnO units. By comparing our results to those obtained by Haase et al. [22] we have estimated the mean radius of the smallest ZnO particles that were studied to be about 7 Å, corresponding to 60 molecular ZnO units. Directly after mixing the two starting solutions, the resulting reaction mixture is stored at room temperature. At regular intervals, a sample is taken from this reaction mixture which is used for optical measurements. In this way, it is possible to study nanocrystalline ZnO particles with different sizes.

### 3.3.2 Optical measurements.

Emission measurements were performed on a SPEX Fluorolog spectrophotometer model F2002 equipped with two double-grating 0.22 m SPEX 1680 monochromators and a 450 W Xe lamp as the excitation source. The emission spectra were corrected for the spectral response of the emission monochromator and the PM

tube. Absorption measurements were performed on a Perkin Elmer Lambda 16 UV/VIS spectrophotometer. The absorbance ( $A$ ) was measured as the logarithm of the transmission ( $T=I/I_0$ ) with 2-propanol as a reference.

## **3.4 RESULTS AND DISCUSSION.**

### **3.4.1 Emission measurements.**

Figure 3.2 shows a typical room temperature emission spectrum of a suspension of ZnO particles upon photoexcitation, together with the accompanying absorption spectrum. The emission spectrum contains two bands. The maximum of the relatively weak and narrow emission band in the UV (3.6 eV) overlaps with the onset of absorption. This band can be assigned to the radiative recombination of shallowly-trapped charge carriers (exciton emission).

A more intense broad emission band is observed in the visible part of the spectrum (2.2 eV). This emission must involve a deeply trapped charge carrier as the maximum of the band lies at an energy about 1.5 eV lower than the onset of absorption.

Figure 3.3 contains three emission spectra taken at different times during the growth of ZnO particles in 2-propanol at room temperature. Spectrum (a) is taken after 15 min, spectrum (b) after 120 min, and spectrum (c) after 420 min of particle growth. Each spectrum contains a weak solvent Raman peak at 4 eV, shifted with respect to the excitation energy by about 0.4 eV ( $3500\text{ cm}^{-1}$ , corresponding to an OH-vibration). All the emission spectra in figure 3.3 show both a visible and a UV emission band, even for the smallest particles (spectrum (a)). Previously, for ZnO particles with a radius smaller than about  $25\text{ \AA}$  only a visible emission was observed [8].

As can be seen in figure 3.3, the UV emission band as well as the visible emission band shift to lower energies upon particle growth. For the visible emission process this indicates that, next to a deep trap level, also one of the band edges (or a shallow level close to one of these edges) must be involved. For a collection of emission spectra, the maximum of the visible emission band is plotted versus that of the UV emission band in figure 3.4. There is an approximate linear relationship between the energetic positions of these two maxima, with a slope of about 0.6.

Similar experiments as described above for suspensions in 2-propanol have been carried out for suspensions of ZnO particles in ethanol. The preparation of ZnO suspensions in ethanol has been described in the literature [23,24]. Again a linear

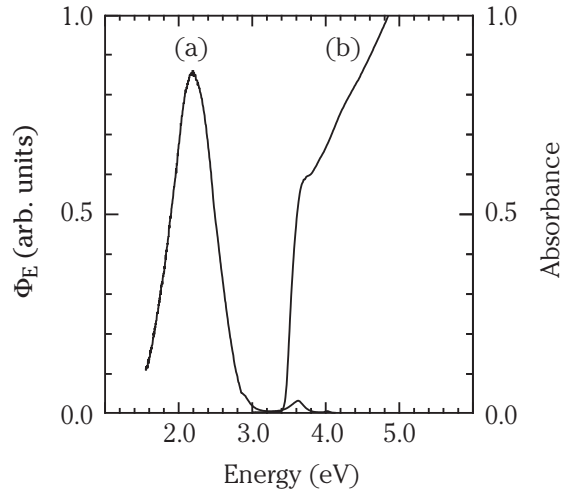


**Figure 3.2** : Emission spectrum of a suspension of ZnO particles in 2-propanol, taken at room temperature upon excitation with light of 4.4 eV (a).  $\Phi_E$  denotes the photon flux per constant energy interval. Spectrum (b) shows the absorption spectrum of the same suspension.

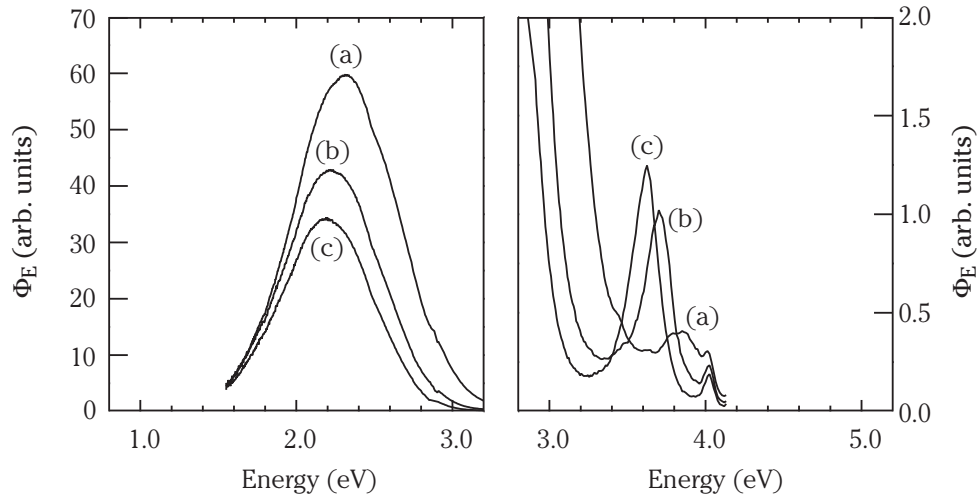


**Figure 3.3** : Emission spectra of suspensions of nanocrystalline ZnO particles in 2-propanol taken after different periods of particle growth at room temperature : (a) 15 min, (b) 120 min, and (c) 420 min. On the left, the broad visible emission band is shown and on the right the sharp UV band.  $\Phi_E$  denotes the photon flux per constant energy interval. The ZnO particles were excited with light of 4.4 eV.

dependence with a slope of 0.6 was found between the onset of the absorption band and the maximum of the visible emission band [25].

### 3.4.2 Identification of the visible emission transition.

One can think of two possible mechanisms for the visible emission : (1) recombination of a shallowly-trapped (delocalised) electron with a deeply-trapped hole, or (2) recombination of a shallowly-trapped hole with a deeply-trapped electron. These two possibilities are shown in figure 3.5. To distinguish between the two processes, we consider the size-dependence of the positions of both emission bands. As discussed in chapter 1, the size-dependence of the bandgap energy ( $E$ ) can be represented by the following equation [19] :

$$E = E_g + \frac{\hbar^2}{8m_0R^2} \cdot \left( \frac{1}{m_e^*} + \frac{1}{m_h^*} \right) - \frac{1.8e^2}{4\pi\epsilon_0\epsilon_\infty R} \quad (3.1)$$

In equation (3.1),  $E_g$  is the bandgap of the macrocrystalline material,  $m_e^*$  and  $m_h^*$  the effective masses of the electron and hole respectively (both in units  $m_0$ ),  $\epsilon_\infty$  the high-frequency dielectric constant, and  $R$  the radius of the particle. In equation (3.1), two size-corrections on the bandgap of a macrocrystalline semiconductor are shown. The first correction is a confinement term ( $\propto R^{-2}$ ) and the second a Coulomb interaction term ( $\propto R^{-1}$ ). Although equation (3.1) is not adequate for calculating absolute values for  $E$ , the dependency of  $E$  on  $R$  as given by equation (3.1) can be used to describe the experimental results [24]. Furthermore, as we have studied ZnO particles that were crystalline and consisted of about 50-5000 molecular ZnO units, the validity of the effective mass approximation can be assumed.

In figure 3.5, the edge of the conduction band ( $e$ ) and of the valence band ( $h$ ) is shown versus particle size. Using equation (3.1), the following expressions can be given for the absolute values of the shifts of the band edges as a function of particle radius  $R$  :

$$(e) = E_g + \frac{\hbar^2}{8m_e^*R^2} - \frac{0.9e^2}{4\pi\epsilon_0\epsilon_\infty R} \quad (3.2a)$$

$$(h) = \frac{\hbar^2}{8m_h^*R^2} - \frac{0.9e^2}{4\pi\epsilon_0\epsilon_\infty R} \quad (3.2b)$$

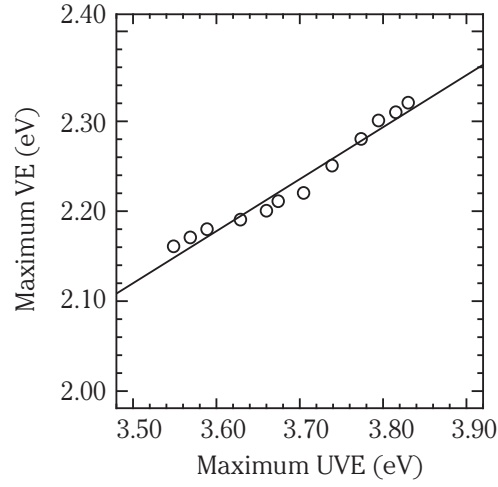


**Figure 3.4** : Energy of the maximum of the visible emission band (VE) versus the energy of the maximum of the UV emission band (UVE). The straight line is a linear fit to the experimental data points.

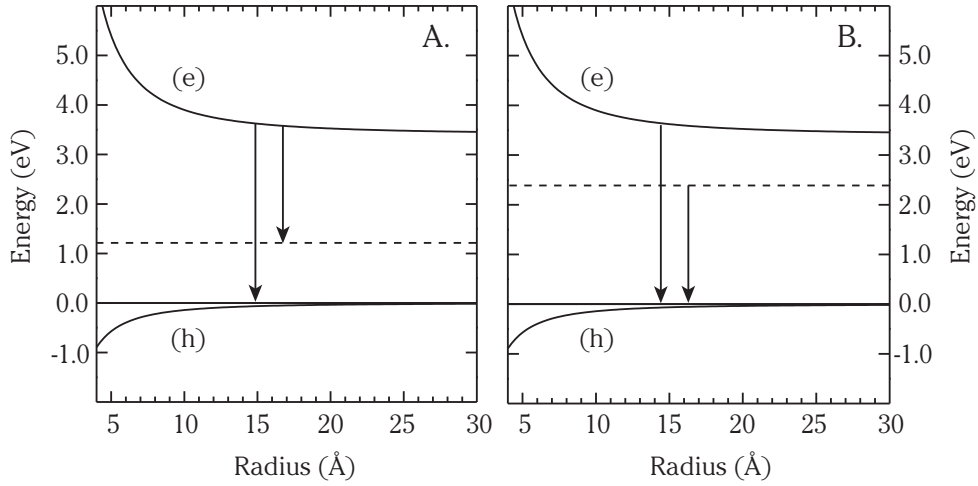


**Figure 3.5** : Schematic overview of the two possibilities for trap emission in nanocrystalline ZnO particles. A : recombination of a delocalised electron with a deeply-trapped hole. B : recombination of a delocalised hole with a deeply-trapped electron. In both pictures, (e) represents the shift of the conduction band edge versus particle radius, (h) the shift of the valence band edge versus particle radius and the dashed line the energetic position of a trapped charge carrier.

The shift of the conduction band edge as a function of particle size, as given by equation (3.2a), is determined by the effective mass of the electron ( $m_e^*$ ), which is  $0.28m_0$  for ZnO [17]. For the shift of the valence band edge (equation (3.2b)), the effective mass of the hole ( $m_h^*$ ) has to be used, which has a value of  $0.50m_0$  for ZnO

[17]. This difference in effective masses of the charge carriers leads to a different size-dependent shift for both band edges. The energetic position of the deeply trapped charge carrier (dashed line in figure 3.5) is assumed to be independent of particle size, as was explained previously in the theory. If the visible emission is due to recombination of a delocalised electron with a deeply-trapped hole (figure 3.5A), the shift of the energetic position of the trap emission as a function of particle size is determined by the shift of the conduction band edge. For the other option, recombination of a delocalised hole with a deeply-trapped electron (figure 3.5B), the shift of the valence band edge determines the shift of the visible emission.

Because the energetic positions of both band edges can be calculated as a function of particle size it is possible to show the relationship between the energies of the exciton emission and the trap emission for the two possibilities shown in figure 3.5. For both cases an approximate linear relationship is obtained as can be seen in figure 3.6 (dashed lines). When the Coulomb interaction - the  $R^{-1}$  term from equation (3.1) - is not taken into account, exact linear relationships between the energies of the two emissions are found (solid lines in figure 3.6). The slope of the linear relationship for each of the two cases shown in figure 3.5 does not depend much on whether a Coulomb interaction is included or not. The exact linear relationship between the emission energies without taking into account the Coulomb interaction gives a slope of  $\mu/m^*$  ( $\mu$  is the reduced mass of the exciton which has a value of  $0.18m_0$  for ZnO). For the situation in figure 3.5A, using  $m_e^*$ , a value of 0.64 is obtained for the slope. In the case of figure 3.5B,  $m_h^*$  has to be used which gives a value of 0.36 for the slope. In figure 3.4, the linear relationship between the energies of the two emission maxima from our experiments is shown. The slope is about 0.6, in good agreement with the value as found for the situation represented in figure 3.5A. This indicates that in the case of nanocrystalline ZnO particles the visible emission involves a transition of an electron from the conduction band (or a shallow level close to this band) to a trap level approximately 2 eV below the conduction band edge. As was mentioned in the introduction, oxygen vacancies are often identified as the recombination centres for the visible emission of macrocrystalline ZnO [5,6]. As was mentioned in the introduction to this chapter, the characteristics of the visible emission are very similar for macrocrystalline and nanocrystalline ZnO and it is very likely that the origin of this emission is the same in both cases. Chapter 4 contains more experimental results that confirm this assertion. In this chapter, size-dependent and temperature-dependent measurements of both the emission bands (UV and visible) are presented. Based on the results, a model is derived in which the visible emission is assigned to the recombination of an electron with a  $V_o^{\bullet\bullet}$  centre (deeply trapped hole).

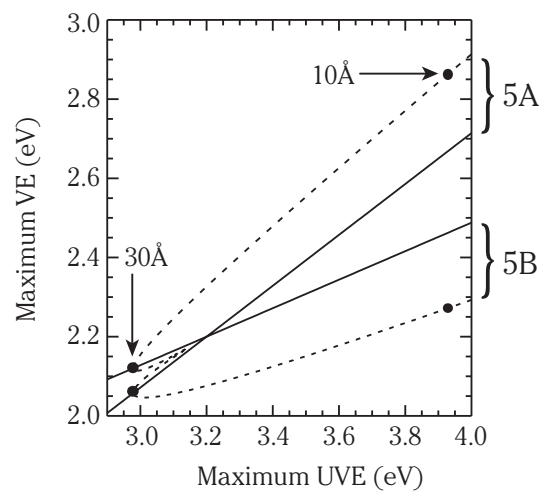


**Figure 3.6** : Theoretical relationship between the energetic maxima of the trap emission band and the UV emission band. The dashed lines result from a calculation including the Coulomb interaction while the solid lines represent the relationship without taking the Coulomb interaction into account. The arrows point to the values obtained for particle radii of 10 Å and 30 Å respectively. On the right axis of the graph it is indicated which model from figure 3.5 is used for the calculation.

### **3.5 CONCLUSION.**

Emission measurements were performed at room temperature on suspensions of nanocrystalline ZnO particles of different sizes in 2-propanol. All the suspensions show two emission bands. One is a relatively weak and sharp UV band with a maximum close to the absorption onset which is assigned to the radiative recombination of excitons. The second band is a more intense and broad emission band in the visible part of the spectrum, shifted by approximately 1.5 eV with respect to the absorption onset. This emission process involves a deeply trapped charge carrier.

The energetic positions of the maxima of both emission bands depend on the size of the ZnO particles : they shift to lower energies as the particle size increases. This is a quantum size effect and can be understood in terms of spatial confinement of charge carriers. From the size-dependency, the visible emission band is assigned to a transition of a photogenerated electron from the conduction band edge (or from a shallow level close to the conduction band edge) to a trap level, positioned approximately 2 eV below the conduction band edge. This transition occurs in the bulk of the material and applies to ZnO in general.



---

## REFERENCES.

- [1] R.E. Shrader, H.W. Leverenz, *J. Opt. Soc. Am.* 37 (1947) 939.
- [2] S. Shionoya, W.M. Yen (editors), *Phosphor Handbook*, CRC Press LCC, Boca Raton 1999, p. 255.
- [3] K. Shibahara, N. Kuroda, S. Nishino, H. Matsunami, *Jpn. J. Appl. Phys.* 26 (1987) L1815.
- [4] V.V. Travnikov, A. Freiberg, S.F. Savikhin, *J. Lumin.* 47 (1990) 107.
- [5] R. Dingle, *Phys. Rev. Lett.* 23(11) (1969) 579.
- [6] E. Mollwo, *Z. Phys.*, 138 (1954) 478.
- [7] F.A. Kröger, H.J. Vink, *J. Chem. Phys.* 22(2) (1954) 250.
- [8] J.M. Smith, W.E. Vense, *Phys. Rev. A* 31(3) (1970) 147.
- [9] F. van Craeynest, W. Maenhout-van der Vorst, W. Dekeyser, *Phys. Status Solidi* 8 (1965) 841.
- [10] W. Lehman, *J. Electrochem. Soc.* 115 (1968) 538.
- [11] M. Anpo, Y. Kubokawa, *J. Phys. Chem.* 88 (1984) 5556.
- [12] K. Vanheusden, W.L. Warren, C.H. Seager, D.R. Tallant, J.A. Voigt, B.E. Gnade, *J. Appl. Phys.* 79(1) (1996) 7983.
- [13] K. Vanheusden, C.H. Seager, W.L. Warren, D.R. Tallant, J.A. Voigt, *Appl. Phys. Lett.* 68(3) (1996) 403.
- [14] T. Sekiguchi, N. Ohashi, Y. Terada, *Jpn. J. Appl. Phys. II* 36(3A) (1997) L289.
- [15] A. Pfanel, *J. Electrochem. Soc.* 109 (1962) 502.
- [16] G.H. Schoenmakers, D. Vanmaekelbergh, J.J. Kelly, *J. Phys. Chem.* 100 (1996) 3215.
- [17] O. Madelung (ed.), *Landolt-Börnstein. Numerical data and functional relationships in science and technology. Volume III-17: Semiconductors*, Springer Verlag, Berlin (1988), 17b pp. 35-115.
- [18] D.W. Bahnemann, C. Kormann, M.R. Hoffmann, *J. Phys. Chem.* 91 (1987) 3789.
- [19] L.E. Brus, *J. Chem. Phys.* 80(9) (1984) 4403.
- [20] J.I. Pankove, *Optical Processes in Semiconductors*, Dover Publications, New York (1971).
- [21] A. van Dijken, A.H. Jansen, M.H.P. Smitsmans, D. Vanmaekelbergh, A. Meijerink, *Chem. Mater.* 10(11) (1998) 3513.
- [22] M. Haase, H. Weller, A. Henglein, *J. Phys. Chem.* 92 (1988) 482.
- [23] L. Spanhel, M.A. Anderson, *J. Am. Chem. Soc.* 113 (1991) 2826.
- [24] E.A. Meulenkaamp, *J. Phys. Chem. B* 102 (1998) 5566.
- [25] E.A. Meulenkaamp, unpublished results.



---

**II. The Kinetics of the Radiative and  
Non-Radiative Processes upon Photoexcitation**

---

**ABSTRACT.**

In this second chapter on the optical properties of nanocrystalline ZnO particles, the results of steady-state and time-resolved luminescence measurements are presented. The experiments were performed on suspensions of nanocrystalline ZnO particles of different sizes and at different temperatures. In all cases two emission bands are observed. One is an exciton emission band and the second an intense and broad visible emission band, shifted by approximately 1.5 eV with respect to the absorption onset. As the size of the particles increases, the intensity of the visible emission decreases while that of the exciton emission increases. As the temperature decreases, the relative intensity of the exciton emission increases. In accordance with the results presented in chapter 3, it is assumed that the visible emission is due to a transition of an electron from a level close to the conduction band edge to a deeply-trapped hole in the bulk ( $V_O^\bullet$ ) of the ZnO particle. The temperature- and size-dependence of the ratio of the visible to exciton luminescence and the kinetics are explained by a model in which the photogenerated hole is transferred from the valence band to a  $V_O^\bullet$  level in the bulk of the particle in a two-step process. The first step of this process is an efficient surface-trapping, probably at a  $O^{2-}$  site.

## 4.1 INTRODUCTION.

ZnO as a luminescent material was already introduced in the previous chapter. There it was mentioned that ZnO shows an efficient blue-green emission which has resulted in the implementation of the material in various applications, such as vacuum fluorescent displays (VFD's) and field emission displays (FED's) [1]. Despite much research it turned out to be very difficult to elucidate the mechanism of this visible emission process. An important reason for this is that most of the research has been carried out on macrocrystalline ZnO (powders or single crystals). This involves taking into account such effects as band bending when considering the emission intensities as a function of defect concentration. In chapter 3, an overview was given of the attempts to identify the transition responsible for the visible emission. These attempts have led to the assumption that oxygen vacancies are the most likely candidates for the recombination centres involved in the visible luminescence of ZnO [2-4].

It was shown in the previous chapter that by using nanocrystalline ZnO particles the visible emission can be assigned to a transition of a photogenerated electron from a shallow level close to the conduction band edge to a deeply trapped hole. Furthermore, it was suggested that this transition occurs in the bulk of the material and applies to ZnO in general. In this chapter, we will elaborate on this assignment by presenting results of steady-state and time-resolved luminescence measurements, as a function of particle size and temperature. Such detailed measurements have not been reported before. The temperature-dependence of the emission intensities and emission lifetimes was studied by freezing the suspensions to liquid helium temperature. The results presented in this chapter will show that, although the actual transition that gives the visible emission is the same all forms of ZnO, the kinetics involved in the total process can be very different for nanocrystalline and macrocrystalline ZnO. A model is proposed for the competition between ultraviolet exciton recombination, trap recombination giving rise to visible luminescence and non-radiative recombination in fair agreement with the results from the steady-state and time-resolved measurements. Also, the nature of the trap involved in the visible emission process will be considered.

---

## **4.2 EXPERIMENTAL METHODS.**

### **4.2.1 Sample preparation.**

Suspensions of nanocrystalline ZnO particles can be prepared in non-aqueous solvents such as ethanol or 2-propanol. For the preparation in 2-propanol [5], 25 ml of a 0.02 M NaOH solution was slowly added while stirring to 225 ml of a 0.001 M  $\text{Zn}(\text{CH}_3\text{COO})_2 \cdot 2\text{H}_2\text{O}$  solution, after both solutions were first cooled to 0 °C. The preparation in ethanol is very similar [6,7]. In this case, 50 ml of a 0.14 M  $\text{LiOH} \cdot \text{H}_2\text{O}$  solution (prepared using an ultrasonic bath) was added to 50 ml of a 0.1 M  $\text{Zn}(\text{CH}_3\text{COO})_2 \cdot 2\text{H}_2\text{O}$  solution. Again, both solutions were first cooled to 0 °C before the hydroxide solution was added slowly to the zinc solution while stirring. The preparation in ethanol yields a suspension with a particle concentration about two orders of magnitude higher than the 2-propanol preparation. The kinetics of the particle growth is not the same for both preparations but in both cases, a rapid formation of extremely small ZnO particles is followed by a relatively slow growth of the particles [7,8]. The rate of particle growth depends strongly on the temperature. When the suspension is aged at room temperature, it takes several days for the particles to attain their final size. In ethanol, the rate of growth of ZnO particles is somewhat slower than in 2-propanol. TEM-measurements have shown that the mean particle diameter of the fully grown particles is about 60 Å (see chapter 2 of this thesis). This corresponds to particles that contain approximately 5000 molecular ZnO units.

Directly after mixing the two starting solutions, the resulting reaction mixture is stored at room temperature. At regular intervals, a sample is taken from this reaction mixture which is used for optical measurements. In this way, one can study nanocrystalline ZnO particles with different sizes.

### **4.2.2 Optical measurements.**

The photoluminescence measurements were performed on a SPEX Fluorolog spectrofluorometer model F2002 equipped with two double-grating 0.22 m SPEX 1680 monochromators and a 450 W xenon lamp as the excitation source. The emission spectra were corrected for the spectral response of the emission monochromator and the PM tube. Absorption measurements were performed on a Perkin-Elmer Lambda 16 UV/Vis spectrophotometer.

Decay time measurements were performed on a Lambda Physik LPX100 XeCl Excimer laser set-up (excitation with 308 nm - corresponding to 4.03 eV - with a pulse

width of about 10 ns) equipped with a Jobin Yvon HR1000M monochromator and a Tektronix 2440 digital oscilloscope for the lifetime measurements.

Measurements at low temperatures were performed in the following way. A small quartz cuvet was filled with a few  $\mu\text{l}$  of a ZnO suspension. This cuvet was mounted on a sample holder and inserted into a flow cryostat. By flowing with liquid helium, the suspension could be cooled to 4 K, well below its freezing point. The solvent, whether it is ethanol or 2-propanol, freezes into a transparent solid.

For the decay time measurements and the low-temperature measurements, only suspensions of nanocrystalline ZnO particles in ethanol were used because of their high luminescence intensity.

## **4.3 RESULTS.**

### **4.3.1 Absorption.**

Absorption spectra were taken at regular intervals during the growth of ZnO particles in 2-propanol at room temperature. Four of these spectra can be seen in figure 4.1A. Two effects are clearly visible from these spectra. First, the absorption onset shifts to lower energies upon particle growth. Second, at the early stages of particle growth the absorption spectra exhibit a distinct maximum directly after the onset of absorption. This feature becomes less pronounced as the ageing process progresses. Both effects can be understood in terms of a decrease in quantum confinement upon particle growth. As the particle size increases, the bandgap gradually shifts towards the value for macrocrystalline ZnO ( $\sim 3.2$  eV), hence the shift in absorption onset. Also, the density of states at the edges of the energy bands changes which leads to a less pronounced structure in the absorption spectra. From the extrapolation of the steep part of the absorption curve one can estimate the mean particle radius by using results obtained by Haase et al. [9]. In this way, one can visualize the ageing process of ZnO particles by plotting the mean particle radius versus time (see figure 4.1B). Figure 4.1B shows that within a few minutes after adding the hydroxide solution to the zinc solution very small ZnO clusters are formed, with a mean radius of approximately 7 Å, corresponding to about 60 molecular ZnO units. These ZnO particles show very strong quantum confinement effects. This is expected, as they are much smaller than the Bohr radius of the exciton, which is about 20 Å for macrocrystalline ZnO.

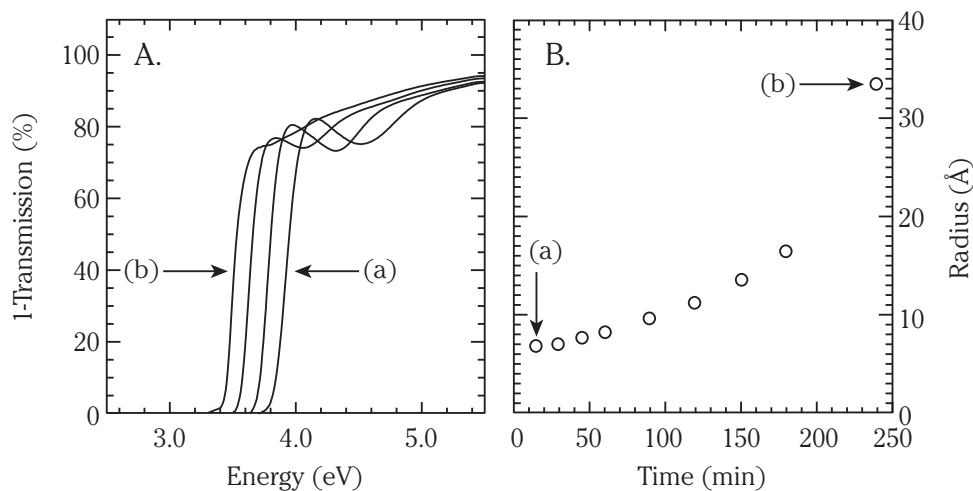


**Figure 4.1** : A : Absorption spectra of a suspension of nanocrystalline ZnO particles in 2-propanol measured at regular intervals during particle growth at room temperature. Spectrum (a) is taken after 15 min and spectrum (b) after 240 min. The two spectra in between (a) and (b) are taken after 60 min and 120 min respectively. B : Mean particle radii as determined by extrapolating the steep part of the absorption spectrum to the energy axis and using an empirical relationship between this energy value and the mean particle radius as obtained by Haase et al. [24].

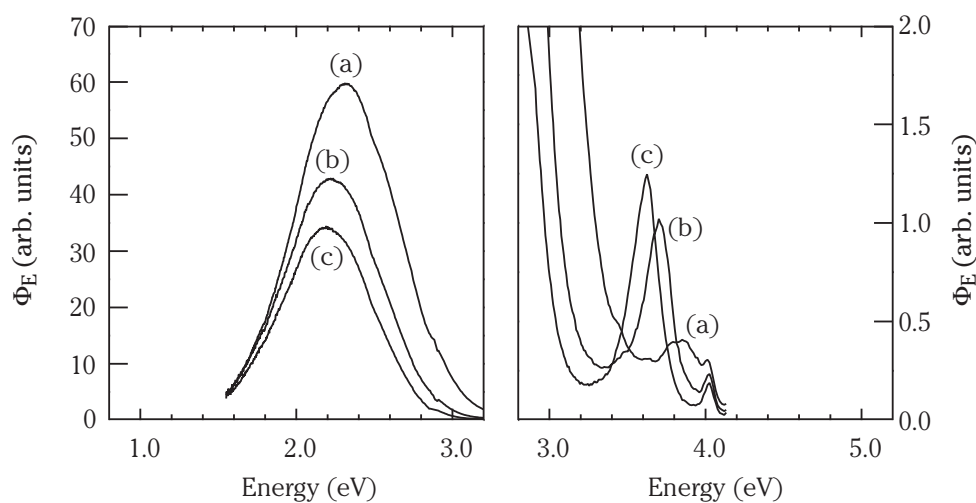


**Figure 4.2** : Emission spectra of suspensions of nanocrystalline ZnO particles in 2-propanol taken after different periods of particle growth at room temperature : (a) 15 min, (b) 120 min, and (c) 420 min. On the left, the broad visible emission band is shown and on the right the sharp UV band.  $\Phi_E$  denotes the photon flux per constant energy interval. The ZnO particles were excited with light of 4.4 eV.

### 4.3.2 Steady-state luminescence.

Figure 4.2 contains three emission spectra, taken at regular intervals during the growth of ZnO particles in 2-propanol at room temperature. Each spectrum contains a weak solvent Raman peak at 4 eV, shifted with respect to the excitation energy by about 0.4 eV ( $3500\text{ cm}^{-1}$ , corresponding to an OH-vibration). The relatively narrow emission band in the UV ( $\sim 3.5\text{--}3.8\text{ eV}$ ) is due to the direct recombination of photogenerated charge carriers (exciton emission). A more intense broad emission band is observed in the visible part of the spectrum ( $\sim 2.1\text{--}2.3\text{ eV}$ ). As can be seen from figure 4.2, the UV emission band as well as the visible emission band shift to lower energies upon particle growth.

A second feature is evident from figure 4.2. As the ZnO particles grow bigger, the intensity of the UV emission increases while that of the visible emission decreases. Figure 4.3 shows the intensities of both emission bands as a function of particle size. From figure 4.1 it is clear that the absorbance of the samples at the excitation energy (4.4 eV) does not change much. The intensity of the visible emission decreases to about half of its original value, while that of the UV emission increases with 60%. As the intensity of the UV emission band is only a fraction of that of the visible emission band, the total integrated emission intensity decreases upon particle growth. It is well known that the visible emission band is quenched upon UV illumination in the absence of adsorbed oxygen on the surface of ZnO particles [5]. We have studied the emission of nanocrystalline ZnO particles in the presence and absence of adsorbed oxygen, the results of which can be found in chapter 5 of this thesis. The size- and temperature-dependent effects as described in this chapter do not result from the absence of adsorbed oxygen as all measurements were performed in the presence of oxygen. Also, variations on a timescale of seconds or minutes - which are associated with the absence of adsorbed oxygen - are not observed.

### 4.3.3 Time-resolved luminescence.

Decay time measurements were performed on a suspension of nanocrystalline ZnO particles in ethanol. The time evolution of the emission intensity was monitored at the maximum of the visible emission band ( $\sim 2.3\text{ eV}$ ). The measurements were performed both at an early stage of particle growth ( $R \sim 10\text{ \AA}$ ) as well as on fully grown ZnO particles ( $R \sim 30\text{ \AA}$ ). The results are plotted in figure 4.4. In both cases the decay of the visible emission intensity shows a multi-exponential behaviour. The experimental data points were fitted to a bi-exponential decay function. The fastest of the two decay



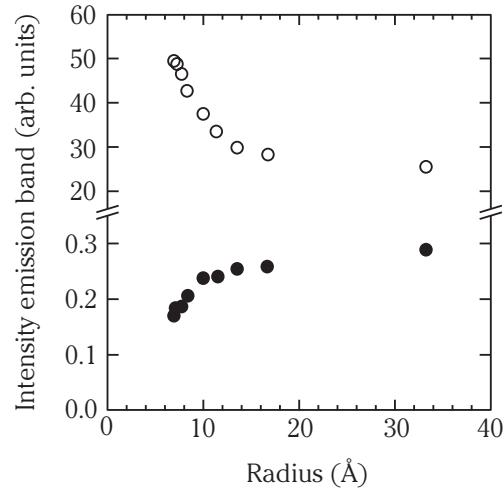


**Figure 4.3** : Dependence of the emission intensities on the particle radius for the two types of emission from nanocrystalline ZnO particles at room temperature. The solid circles represent the UV emission band and the open circles the visible emission band.

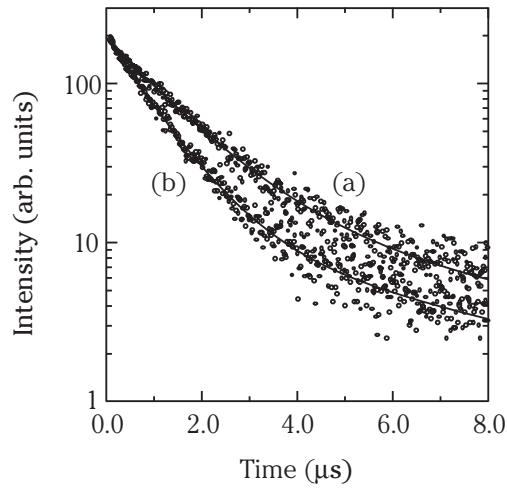


**Figure 4.4** : Luminescence lifetime measurements of the visible emission from two suspensions of nanocrystalline ZnO particles in ethanol, measured at room temperature. Curve (a) : suspension of particles that are fully grown ( $R=30$  Å) and curve (b) : suspension at an early stage of particle growth ( $R=10$  Å). The excitation is at 4 eV (308 nm).

components obtained in this way made up more than 90% of the decay signal. The value of the decay time of this component is 1.34  $\mu\text{s}$  for the large particles (a), and 0.92  $\mu\text{s}$  for the small particles (b). This indicates that the lifetime of the visible emission increases upon particle growth. The decay time of the slower component was approximately 5  $\mu\text{s}$ . For the UV emission, the lifetime was shorter than the pulse width of the laser ( $\sim 10$  ns) and could therefore not be measured.

#### **4.3.4 Temperature-dependent luminescence.**

The emission characteristics of a suspension of nanocrystalline ZnO particles in ethanol were measured in a temperature range from 4 K to room temperature. The results of this measurement are presented in figure 4.5. As the temperature increases, the intensity of both emission bands decreases. The observation that at temperatures between 70 K and 120 K the intensity of the visible emission band increases is probably an artefact. Also, both emission bands shift to lower energies as the temperature increases. The temperature-dependence of the maximum of the ultraviolet emission band closely resembles the temperature-dependence of the bandgap of macrocrystalline ZnO [10]. The maximum of the visible emission shows a different behaviour. Up to 75 K, the energetic position of the maximum of the visible emission is independent of temperature. At temperatures between 75-180 K the maximum shifts towards lower energies by approximately  $1 \text{ meV}\cdot\text{K}^{-1}$ . At temperatures higher than 180 K, the energetic position is more or less independent of temperature again. In the same temperature range, the lifetime of the visible emission was monitored. In figure 4.6, the decay curves at 4 K, 75 K and room temperature are shown. At 4 K, the decay of the visible emission is single exponential with a decay time of 275 ns. At 75 K, a second component with a decay time of about 1.5  $\mu\text{s}$  appears in the decay curve of the visible emission. The appearance of this  $\mu\text{s}$ -component coincides with the shift of the maximum of the visible emission to lower energies. As the temperature is increased above 75 K, the contribution of the  $\mu\text{s}$ -component to the total decay signal increases while the intensity of the short lived luminescence decreases. At room temperature the decay of the visible emission is almost single exponential with a decay time of 1.34  $\mu\text{s}$ , as was mentioned before. This means that at low temperatures the lifetime of the visible emission is much shorter than at room temperature.

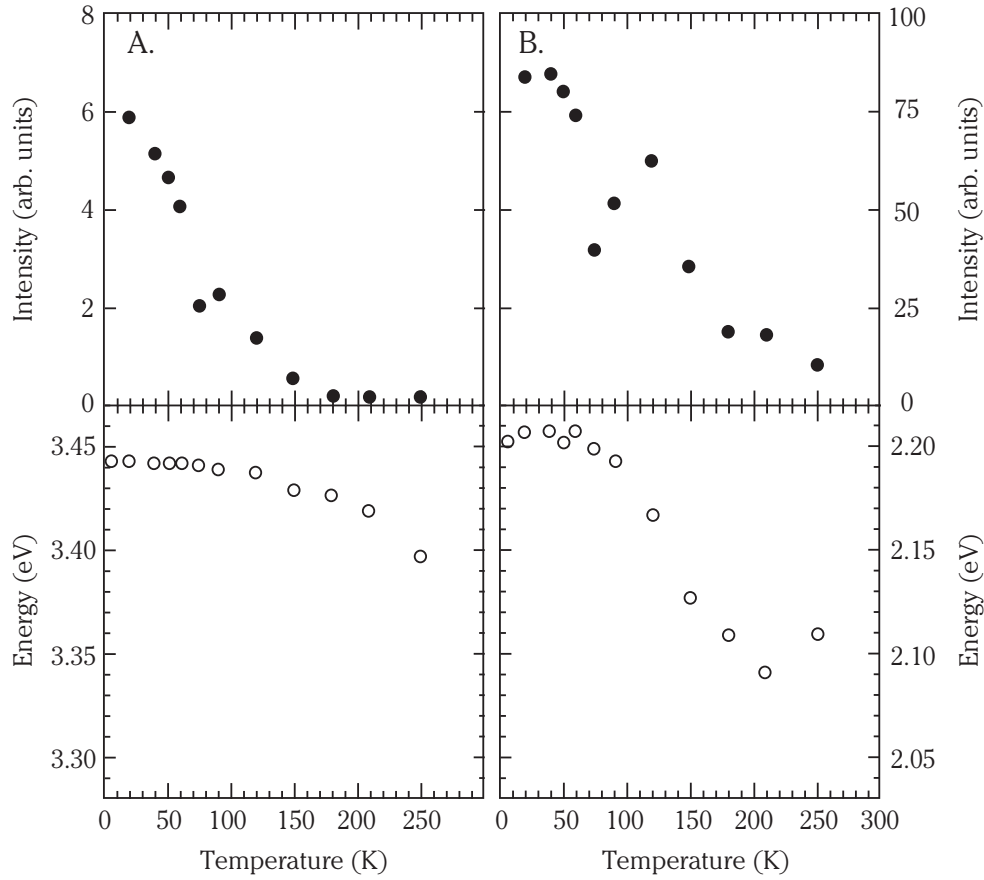


**Figure 4.5** : Temperature dependence of the emission characteristics of a suspension of nanocrystalline ZnO particles in ethanol ( $R=30$  Å). A : Ultraviolet emission. B : Visible emission. The solid circles (upper graphs) represent the integrated intensities and the open circles (lower graphs) the energetic positions of the maxima of the emission bands.

## 4.4 DISCUSSION.

### 4.4.1 Steady-state luminescence.

The size-dependent emission spectra of ZnO particles show both a visible and a UV emission band, even for the smallest particles (see figure 4.2). Previously, for ZnO particles with a radius smaller than  $25$  Å only a visible emission was observed [5]. The energy of the maximum of the UV emission band is close to the absorption onset. This band can be assigned to the radiative recombination of Wannier excitons (exciton emission) which is a very fast process occurring on a sub-nanosecond timescale.

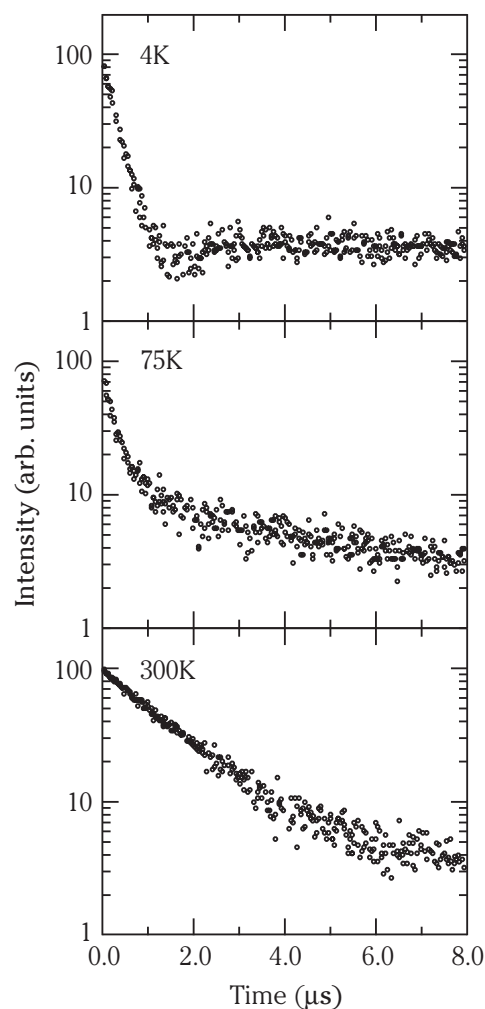


**Figure 4.6** : Luminescence decay curves of the visible emission from a suspension of nanocrystalline ZnO particles ( $R=30 \text{ \AA}$ ) in ethanol at different temperatures. Excitation is at 4 eV (308 nm).

The visible emission must involve a deeply trapped charge carrier as this band is shifted by about 1.5 eV with respect to the absorption onset. Next to a deep trap level, also one of the band edges must be involved in the visible emission process because the position of this emission band depends on the particle size, as can be seen in figure 4.2. By analyzing the size-dependence of the emission bands, we have demonstrated in chapter 3 that the visible emission is due to a transition of a photogenerated electron from a shallow level close to the conduction band edge to a deeply trapped hole (a  $V_{\text{O}}^{\bullet\bullet}$  centre).

---

In figure 4.2 it can be seen that the intensity of the visible emission band is much higher than that of the exciton emission band. However, the lifetime of the visible emission is much longer than that of the exciton emission. As both process are in competition with each other, the visible emission process must involve a step in which the photogenerated hole is trapped efficiently somewhere in the particle. The rate of this hole trapping must be much faster than the radiative recombination rate of the exciton emission. In the literature, there are indications that efficient hole-trapping occurs at interfacial states in macrocrystalline ZnO [11]. Because of the large surface-to-volume ratio of our ZnO particles, efficient and fast trapping of photogenerated holes at surface sites can be expected. A good candidate for the trapping of holes are  $O^{2-}$  ions at the surface [12]. These surface ions can trap holes, thereby acting as a kind of  $O^{2-}/O^-$  redox couple. Evidence for the involvement of surface states in the visible emission process is provided by measurements on the temperature- and size-dependence of the emission intensity, as will be discussed later.

#### **4.4.2 Time-resolved luminescence.**

The lifetime of the visible emission at room temperature is 1.34  $\mu s$  for the aged particles ( $R \sim 30 \text{ \AA}$ ) and 0.92  $\mu s$  for the smaller particles ( $R \sim 10 \text{ \AA}$ ). Lifetimes of the order of  $\mu s$  are typically observed for broad band trap emission in semiconductors [13,14]. If the rate-determining step in the visible emission process is the transition of a shallowly-trapped electron to a deeply-trapped hole, the small - but significant - size-dependence of the emission lifetime can be explained by an increase in wavefunction overlap between the charge carriers. For macrocrystalline semiconductors it is well known that the recombination rate of trapped charge carriers is proportional to the square of the wavefunction overlap [13,15]. In the smaller particles the charge carriers are closer together, resulting in a larger wavefunction overlap, which gives a higher oscillator strength. In the case of nanocrystalline semiconductor particles this size-dependence of the lifetime can be observed as long as the particles do not become much smaller than the spatial extension of the wavefunction of the shallowly trapped charge carrier. In the limit of very small particle sizes, the wavefunction of the shallowly trapped charge carrier is delocalised over the particle volume and the overlap with the wavefunction of a deeply trapped charge carrier will not increase when the particle becomes even smaller. It is interesting to compare the present results on nanocrystalline ZnO particles to lifetime measurements performed on the trap emission of nanocrystalline CdS particles of different sizes [13]. For CdS particles with a mean diameter of 22  $\text{\AA}$  and 38  $\text{\AA}$  the same lifetime has been observed for the trap emission. Since particles of these sizes

are well within the quantum confinement regime of CdS, this case represents the situation of very small particles for which no size-dependence of the wavefunction overlap is expected due to a strong confinement of the shallowly trapped charge carriers.

The lifetime of the exciton emission in the UV is shorter than the time resolution of the laser set-up ( $\sim 10$  ns). This is to be expected as a sub-nanosecond lifetime is typically observed for exciton emission in semiconductors. The short lifetime is due to the high oscillator strength of the transition and to fast non-radiative trapping of charge carriers. The observation that at room temperature the exciton emission is only a weak band in the UV shows that the trapping rate must be much higher than the (fast) radiative decay rate.

#### **4.4.3 Temperature-dependent luminescence.**

The results from the temperature-dependent emission measurements given in figure 4.5 show that the intensity of both the exciton and the trap emission increases when the temperature decreases. The increase of the exciton emission is more pronounced. It is a general observation that the luminescence efficiency is higher at low temperatures. Non-radiative pathways become more probable at higher temperatures, while radiative recombination rates are usually not significantly affected by temperature. This explains the common observation of temperature quenching.

The temperature dependence of the luminescence lifetime (as illustrated in figure 4.6) is peculiar : at low temperatures ( $T < 50$  K) the lifetime of the luminescence is shorter than at higher temperatures. Usually the opposite is observed : a longer lifetime at low temperatures becomes shorter at higher temperatures due to extra (non-radiative) decay paths which require thermal activation. An explanation for the observed behaviour involves a temperature-dependent population of a distribution of shallow electron traps near the conduction band edge. At low temperatures, the most shallow traps from this distribution are significantly occupied by electrons. The wavefunction overlap of the delocalised shallowly trapped electron and the deeply trapped hole is relatively large, resulting in a short lifetime (275 ns). Above about 50 K the shallow electron traps start to be thermally depopulated. This results in a decrease of the emission intensity since the electrons can now reach the surface and recombine non-radiatively (see also below). Alternatively, the electrons may be trapped again in somewhat deeper traps and recombine with the deeply trapped holes. This results in emission at a slightly different energy than the emission observed at lower temperatures, explaining the shift to lower energies of the emission maximum between 50 and 200 K.

---

Since the electron wavefunction is less delocalised in the slightly deeper electron trap, the overlap with the wavefunction of the deeply trapped hole is reduced resulting in an increase of the lifetime. The thermal detrapping of the shallowly trapped electrons occurs between 50 K and 200 K and in this temperature range the trap emission shifts to lower energies. The decay curve of the emission is two-exponential in this temperature range : both the short lifetime component (recombination of the shallowly trapped electrons) and the long life time component are observed. The contribution of the short decay component (275 ns) decreases between 50 and 200 K, while the contribution of the long decay component ( $\sim 1 \mu\text{s}$ ) increases. Above 200 K only the 'slow'  $\mu\text{s}$  decay is observed, indicating that detrapping is complete. A similar explanation has been used before to explain temperature-dependent luminescence measurements on colloidal suspensions of CdS particles [16].

In a study on the luminescence of nanocrystalline CdS particles temperature quenching of the CdS trap emission was also observed, where it was explained by a multi-phonon relaxation process [13]. In the case of the trap emission from nanocrystalline ZnO particles, multi-phonon relaxation cannot explain the temperature quenching of this emission band. The best evidence comes from the temperature-dependent lifetime measurements as discussed above. Furthermore, the energy gap of 2 eV is too high compared to the energy of optical phonons in ZnO (0.05-0.07 eV [17]).

#### **4.4.4 Nature of the deep hole trap.**

Now that the luminescence properties of nanocrystalline ZnO particles have been discussed as a function of particle size and temperature, a more quantitative model is proposed. The nature of the deep trap involved in the visible emission is still an important issue, as discussed in the introduction. In chapter 3 we have shown that the visible emission is due to recombination of a shallowly trapped electron with a deeply trapped hole. To be more specific about the nature of the deep trap the defect chemistry of ZnO is considered. ZnO can have several types of defects such as interstitial atoms or vacancies, both anionic and cationic [18]. EPR studies have shown that oxygen vacancies containing one electron ( $V_{\text{O}}^{\bullet}$ ) are the predominant paramagnetic defects [2-4]. In macrocrystalline ZnO these defects are represented by a level approximately 2 eV below the conduction band edge [18] and they are often assumed to be the recombination centres for the visible emission in ZnO. In some publications the visible emission is represented as the recombination of an electron from the conduction band with the  $V_{\text{O}}^{\bullet}$  centre (which has an effective monovalent positive charge with respect to the regular  $\text{O}^{2-}$  site) [14]. After this recombination the effectively neutral

$V_O^\times$  centre is formed. The  $V_O^\times$  centre has an energy very close to the conduction band edge and at room temperature almost all  $V_O^\times$  centres are thermally dissociated into  $V_O^\bullet$  centres and conduction band electrons. The shift from 2 eV below the conduction band edge for  $V_O^\bullet$  to just below the conduction band edge for  $V_O^\times$  is due to the correlation energy of the two electrons in the oxygen vacancy [18]. A transition of an electron from the conduction band to a  $V_O^\bullet$  level can therefore not yield photons with an energy of 2 eV, as such a transition effectively takes place between the conduction band edge and the  $V_O^\times$  level. This means that a mechanism in which  $V_O^\bullet$  is the recombination centre for the visible emission of ZnO is not correct. Recombination of a conduction band electron with a  $V_O^{\bullet\bullet}$  centre (an oxygen vacancy containing no electrons, having an effective divalent positive charge with respect to the normal  $O^{2-}$  site) can yield photons with an energy of about 2 eV. Such  $V_O^{\bullet\bullet}$  centres can be formed when a hole is trapped at a  $V_O^\bullet$  centre. In the model presented below the visible emission is assigned to the recombination of a shallowly trapped electron with a deeply trapped hole in a  $V_O^{\bullet\bullet}$  centre.

#### 4.4.5 Model.

The dependence of the luminescence intensities on temperature and particle size indicates that the particle surface plays a role in the process leading to the visible emission. In view of the large surface area of the particles this is to be expected. In the preceding text it has been argued that the visible emission results from a transition that takes place in the bulk of the ZnO particle and that the recombination centre is a  $V_O^{\bullet\bullet}$  defect which traps an electron from a level close to the conduction band edge. In figure 4.7, a schematic overview is presented of the relaxation processes of a photoexcited ZnO particle. In this figure, the band edges are shown as well as a deep trap level ( $V_O^\bullet/V_O^{\bullet\bullet}$ ) and the energy distribution of a  $O^{2-}/O^-$  surface system. For reasons of simplicity, the shallow trapping of a photogenerated electron is not shown. A transition is indicated with an arrow and represented by the letter  $T$ , having a subscript that specifies the transition. This subscript consists of the initial and final state of the electron. These states are C (conduction band), V (valence band), S (surface) and T (deep trap). Non-radiative recombination is denoted with the subscript NR. In principle, this can occur at the surface (S) or at quenching centres in the particle. In view of the large surface area of the ZnO particles, only non-radiative recombination at the surface is considered.



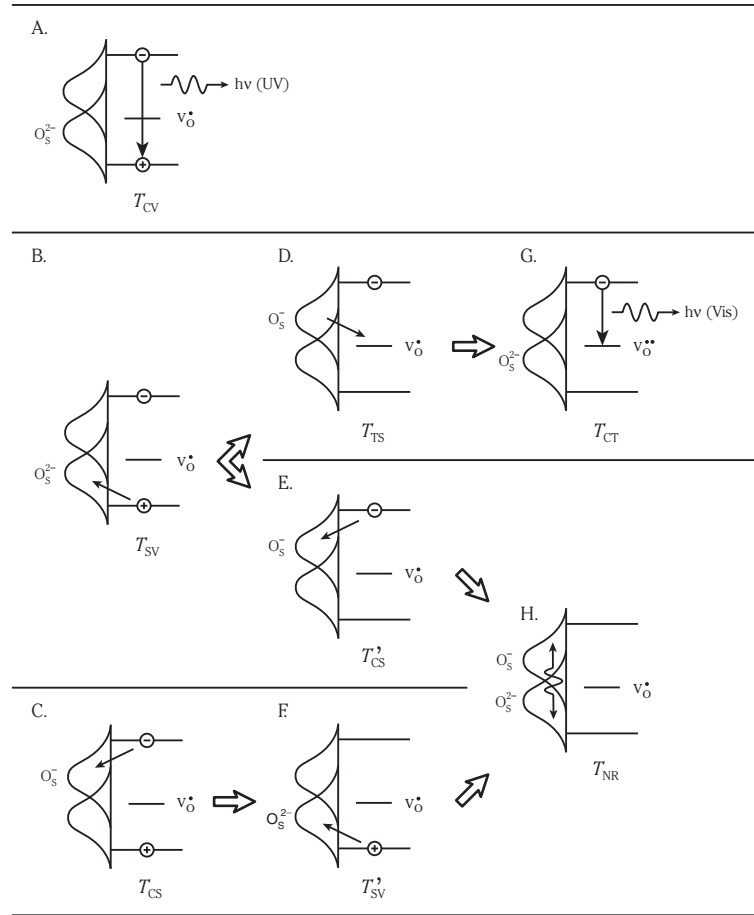


**Figure 4.7 :** A schematic overview of the relaxation processes that take place upon photoexcitation of a ZnO particle. The bandedges are shown as well as a deep trap level in the bulk of the particle. At the surface of the particle, an energy distribution of a  $O^{2-}/O^-$  system is shown. The arrows indicate a transition that is represented by the letter  $T$ . The subscript to this letter specifies the transition in a way that it contains the initial and final state of the electron. These states can be the conduction band (C), the valence band (V), the trap (T) or the surface (S). It is assumed that non-radiative recombination (NR) only occurs at the particle surface. A-C : Three competitive processes on the level of the exciton : exciton emission and trapping of either of the charge carriers at the surface. D-E : possible processes following surface trapping of a hole. G : Visible emission, following the tunneling of the surface-trapped hole back into the particle. H : Non- radiative recombination, which can be the result of either of two different processes : trapping of a hole at the surface followed by trapping of an electron at the surface (B and E) or trapping of an electron at the surface followed by trapping of a hole at the surface (C and F).

The three competitive processes on the excitonic level - shown in figure 4.7A-C - are : radiative recombination with transition rate  $T_{cv}$ , trapping of the hole at the surface with rate  $T_{sv}$  (while the electron remains in the conduction band), and trapping of the electron at the surface  $T_{cs}$  (while the hole remains in the valence band). The probabilities ( $P$ ) for these three processes are :

$$P_{cv} = \frac{T_{cv}}{T_{cv} + T_{sv} + T_{cs}} \quad (4.1a)$$

$$P_{sv} = \frac{T_{sv}}{T_{cv} + T_{sv} + T_{cs}} \quad (4.1b)$$

$$P_{cs} = \frac{T_{cs}}{T_{cv} + T_{sv} + T_{cs}} \quad (4.1c)$$

The rates for both surface trapping processes ( $T_{sv}$  and  $T_{cs}$ ) decrease as the particle size increases since the surface-to-bulk ratio decreases. The transition rate of the exciton recombination ( $T_{cv}$ ) will not be influenced strongly by the particle size and thus the intensity of the exciton emission will increase with increasing particle size, as is shown in figure 4.2.

On the right of figure 4.7A-C, the possible consecutive relaxation steps are shown. The transition  $T_{cv}$  returns the ZnO particle to its ground state so it has no consecutive step. Trapping of the hole at the surface (figure 4.7B) can have either of two possible consecutive steps. One possibility is that the surface-trapped hole tunnels back into the particle to recombine with an electron in a deep trap ( $T_{ts}$ , shown in figure 4.7D). The other possibility is that a photogenerated electron - which is still in the conduction band - gets trapped at the surface and recombines with the surface-trapped hole ( $T'_{cs}$ , figure 4.7E, the accent is used to indicate that this process is not identical to  $T_{cs}$  shown in figure 4.7C). While the former step (figure 4.7D) leads to the transition responsible for the visible emission ( $T_{ct}$ , figure 4.7G), the latter (figure 4.7E) results in non-radiative recombination ( $T_{nr}$ , figure 4.7H). When the first step in the relaxation process is the surface-trapping of an electron (figure 4.7C), this will always result in non-radiative recombination ( $T_{nr}$ , figure 4.7H) via surface-trapping of a hole ( $T'_{sv}$ , figure 4.7F).

The three relaxation processes that return a photoexcited ZnO particle to its ground state are radiative exciton recombination (UV emission,  $T_{cv}$ ), radiative trap

---

recombination (visible emission,  $T_{CT}$ ) and non-radiative recombination at the surface ( $T_{NR}$ ). The probabilities for these three processes are given by :

$$P_{CV} = \frac{T_{CV}}{T_{CV} + T_{SV} + T_{CS}} \quad (4.2a)$$

$$P_{NR} = P_{CS} + P_{SV} \cdot \frac{T'_{CS}}{T_{TS} + T'_{CS}} \quad (4.2c)$$

$$P_{CT} = P_{SV} \cdot \frac{T_{TS}}{T_{TS} + T'_{CS}} \quad (4.2b)$$

It can easily be seen that the sum of equations (2a), (2b) and (2c) is equal to unity.

The model as presented in this chapter implies that both the tunneling rate of a surface-trapped hole to a  $V_O^\bullet$  centre ( $T_{TS}$ ) as well as the trapping rate of a conduction band electron at the surface ( $T_{CS}$  and  $T'_{CS}$ ) decrease with increasing particle size. The tunneling rate decreases more strongly since tunneling takes place between two localised states while the surface trapping of the conduction band electron (leading to non-radiative relaxation) involves a delocalised state. Also, the defect concentration (including  $V_O^\bullet$  centres) may decrease when the size of the particles increases, which has been put forward before based on studies of the size-dependence of the dissolution rate of nanocrystalline ZnO particles [19]. Both effects result in a decrease of the probability for the trap emission compared to the probability for non-radiative decay at the surface. Finally, for the bigger particles also non-radiative decay in the bulk of the particle may become important and contribute to the total loss by non-radiative processes. As a result the intensity of the trap emission decreases with increasing particle size in agreement with the experimental results (see figures 4.2 and 4.3).

Both the trap emission and the exciton emission show thermal quenching. The quenching of the exciton emission is more pronounced. In the case of nanocrystalline ZnO particles non-radiative relaxation predominantly takes place at the surface. Non-radiative relaxation at surface sites is generally observed and because of the large surface-to-volume ratio of nanoparticles the surface will play an important role in the quenching of the luminescence. The quenching at the surface involves trapping of both photogenerated charge carriers at the surface. With increasing temperatures the probability for surface trapping of charge carriers increases. Similar to redox couples, surface systems such as  $O^{2-}/O^-$  have a certain energy distribution due to solvation

effects. The width of this distribution depends on the temperature : the higher the temperature, the broader the energy distribution. The larger overlap in energy between the conduction band or valence band and the surface states at higher temperatures will lead to higher trapping rates  $T_{SV}/T_{SV}^*$  and  $T_{CS}/T_{CS}^*$ . The exciton emission is affected by both trapping processes and therefore the temperature quenching of this emission is more pronounced. For the quenching of the trap emission, trapping of a photogenerated electron at the surface is important. Besides the increase in overlap between the conduction band states and the surface states, thermal detrapping of a shallowly trapped electron will occur at higher temperatures and the probability that an electron is trapped at surface sites at higher temperatures increases, resulting in quenching of the trap luminescence.

The model containing the possible relaxation processes of a photoexcited nanocrystalline ZnO particles as shown in figure 4.7 can explain the observations qualitatively. The identification of the visible luminescence as the recombination of a conduction band electron with a deeply trapped hole at a  $V_O^{\bullet\bullet}$  centre is in agreement with previous work on macrocrystalline ZnO which has provided evidence for a role of oxygen vacancies in the visible luminescence of ZnO, although in these publications  $V_O^{\bullet}$  centres were incorrectly assumed to be the recombination centres. In macrocrystalline ZnO also direct trapping of holes by  $V_O^{\bullet}$  centres will occur. In nanocrystalline ZnO particles an important role of the surface can be expected. Evidence for the role of fast surface-trapping of holes in the trap emission process comes from the size-dependence of the overall emission intensities and the relative intensities of the exciton and visible emission as presented in this chapter. The model is supported by previous work on the luminescence of nanocrystalline ZnO particles where it was observed that ions like  $Fe^{2+}$  [5] and  $I^-$  [14] - which can accept holes that are trapped at the surface of the particle - are efficient quenchers of the visible luminescence.

---

## 4.5 CONCLUSION.

Temperature-dependent steady-state and time-resolved luminescence measurements were performed on suspensions of nanocrystalline ZnO particles of different sizes. All the suspensions show two emission bands, a relatively weak and sharp UV band which can be assigned to exciton emission and a more intense and broad emission band in the visible part of the spectrum, shifted by approximately 1.5 eV with respect to the absorption onset.

A model for the kinetics of the radiative and non-radiative processes in nanocrystalline ZnO particles is proposed based on the identification of the transition responsible for the visible emission as being a recombination of a shallowly-trapped electron with a deeply-trapped hole. From the particle size dependence and the temperature dependence of the emission properties it is concluded that the photogenerated hole is trapped at a surface system (probably  $O^{2-}/O^-$ ). The surface-trapped hole can tunnel back into the particle where it recombines with an electron in an oxygen vacancy ( $V_O^\bullet$ ) resulting in the creation of a  $V_O^{\bullet\bullet}$  centre, the recombination centre for the visible emission. The dependence on particle size of the probability for this tunneling process is much stronger than that of the non-radiative processes. This results in an increase of the visible emission intensity as the size of the ZnO particles decreases.

## REFERENCES.

- [1] S. Shionoya, W.M. Yen (editors), *Phosphor Handbook*, CRC Press LCC, Boca Raton 1999, p. 255.
- [2] M. Anpo, Y. Kubokawa, *J. Phys. Chem.* 88 (1984) 5556.
- [3] K. Vanheusden, C.H. Seager, W.L. Warren, D.R. Tallant, J.A. Voigt, *Appl. Phys. Lett.* 68(3) (1996) 403.
- [4] K. Vanheusden, W.L. Warren, C.H. Seager, D.R. Tallant, J.A. Voigt, B.E. Gnade, *J. Appl. Phys.* 79(1) (1996) 7983.
- [5] D.W. Bahnemann, C. Kormann, M.R. Hoffmann, *J. Phys. Chem.* 91 (1987) 3789.
- [6] L. Spanhel, M.A. Anderson, *J. Am. Chem. Soc.* 113 (1991) 2826.
- [7] E.A. Meulenkaamp, *J. Phys. Chem. B* 102(29) (1998) 5566.
- [8] E.M. Wong, J.E. Bonevich, P.C. Searson, *J. Phys. Chem. B* 102 (1998) 7770.
- [9] M. Haase, H. Weller, A. Henglein, *J. Phys. Chem.* 92 (1988) 482.
- [10] G.H. Edstrup Jensen, *Phys. Stat. Sol. (b)* 64 (1974) K51.
- [11] S.R. Morrison, *Electrochemistry at Semiconductor and Oxidized Metal Electrodes*, Plenum Press, First Edition, New York 1980, p. 227-233.
- [12] G.H. Schoenmakers, D. Vanmaekelbergh, J.J. Kelly, *J. Phys. Chem.* 100 (1996) 3215.
- [13] N. Chestnoy, T.D. Harris, R. Hull, L.E. Brus, *J. Phys. Chem.* 90 (1986) 3393.
- [14] P.V. Kamat, B. Patrick, *J. Phys. Chem.* 96 (1992) 6829.
- [15] B. Henderson, G.F. Imbusch, *Optical Spectroscopy of Inorganic Solids*, Clarendon Press, First Edition, Oxford 1989.
- [16] A. Eychmüller, A. Hässelbarth, L. Katsikas, H. Weller, *Ber. Bunsenges. Phys. Chem.* 95 (1991) 79.
- [17] O. Madelung (ed.), *Landolt-Börnstein, Numerical data and functional relationships in science and technology. Volume III-17: Semiconductors*; Springer Verlag: Berlin, 1988; 17b pp. 35-115.
- [18] F.A. Kröger, *The Chemistry of Imperfect Crystals*, North-Holland Publishing Company, First Edition, Amsterdam 1964, p. 691.
- [19] E.A. Meulenkaamp, *J. Phys. Chem. B* 102 (1998) 7764.

---





---

**III. The Influence of Adsorbed Oxygen  
on the Emission Properties**

---

**ABSTRACT.**

The third and final chapter on the optical properties of nanocrystalline ZnO particles presents the results of studies on the influence of electron scavengers (such as oxygen) on the emission properties. Emission measurements are performed on deaerated suspensions of ZnO particles in alcohols (2-propanol and ethanol) and other organic solvents (DMF and propylene carbonate). Upon UV irradiation the visible emission quenches while the intensity of the exciton emission increases. Admission of oxygen restores the initial emission properties. Using the mechanism of the visible emission process as developed in chapters 3 and 4, the results as presented in this chapter are explained by charging of the ZnO particles with electrons. The presence of excess electrons on ZnO particles results in the removal of  $V_O^\bullet$  centres which are involved in the visible emission.

## 5.1 INTRODUCTION.

Due to the high surface-to-volume ratio of nanocrystalline semiconductor particles the nature of the surface is very important when considering the properties of such particles. The surface is a strong perturbation of the lattice where a high concentration of both shallow and deep levels provide pathways for non-radiative recombination of photogenerated charge carriers [1]. This explains why the quantum efficiency of the emission of nanocrystalline semiconductor particles is generally far below unity and is strongly dependent on surface passivation. However, surface states can also be of importance for radiative transitions, as we have demonstrated for ZnO in chapter 4.

Next to these intrinsic surface properties it is known that surface adsorbates - such as reaction byproducts, solvent molecules or dissolved gases - can influence various properties of a colloidal suspension of semiconductor particles. For instance, using zinc perchlorate instead of zinc acetate yields a less stable ZnO suspension [2]. It was suggested that weakly bound acetic acid plays the role of a stabilizer [3]. Surface adsorbates can also influence the optical properties of a suspension of semiconductor particles, viz. by scavenging charge carriers that are created upon photoexcitation [4]. The photogenerated holes can be removed by oxidation of solvent molecules while adsorbed oxygen molecules can scavenge photogenerated electrons. The influence of surface adsorbates, more particularly solvent molecules and oxygen, on the optical properties of suspensions of ZnO particles will be the main topic of this chapter.

It has been observed that a deaerated suspension of ZnO particles in methanol or 2-propanol exhibits remarkable emission properties. A freshly prepared sample shows two types of emissions under UV irradiation. One is a relatively weak and narrow emission band in the UV due to exciton recombination while the other is a strong and broad emission band in the visible part of the spectrum. As explained in chapter 3, the visible emission can be assigned to the recombination of an electron from a level close to the conduction band edge with a deeply trapped hole. UV irradiation (using photons with an energy higher than the bandgap) of a deaerated suspension of ZnO particles quenches the trap emission while the intensity of the exciton emission slightly increases. Simultaneously, a shift of the absorption onset to higher energies was observed [5]. The initial emission and absorption properties are restored some time after the UV irradiation is stopped or after the admission of air.

First, these observations were explained by assuming a photodissolution of the ZnO particles [5]. In this model,  $\text{Zn}^+$  is formed at the particle surface which quenches the trap emission by reacting with photogenerated holes to form  $\text{Zn}^{2+}$ . Furthermore, the

---

shift of the absorption onset was thought to be a quantum size effect as a result of the decrease in size of the ZnO particles. In the mean time, comparable photodissolution mechanisms have been described mainly for sulphidic semiconductor particles (see chapter 2). However, in the case of the observed behaviour for ZnO particles, the explanation of the shift of the absorption onset and the quenching of the visible emission by a photodissolution mechanism was rejected after it was recognised that the presence of even a single excess electron on a semiconductor particle causes a shift of the absorption onset to higher energies [6]. This was explained by a model based on the Stark effect in semiconductors. The excess electron is treated as a localised point charge producing a strong electric field in the semiconductor particle. In this way, the energy for the lowest exciton state is increased. The blue-shift of the absorption onset can also be explained by the Burstein-Moss effect in which excess electrons fill the lowest states of the conduction band [7-9]. In this way, subsequent absorption requires photons of higher energies in order to access the lowest empty states.

An alternative model for the quenching of the trap emission of ZnO particles was proposed which was based on an oxygen-mediated shuttle mechanism [2]. In this mechanism, photogenerated electrons are scavenged by adsorbed oxygen molecules that subsequently transfer these electrons to deep traps. Recombination of the deeply trapped electrons with trapped holes gives the visible emission. Additional experiments were performed on colloidal suspensions of ZnO in which  $O_2$  was formed by pulse radiolysis [10]. If the shuttle mechanism is correct, an emission should be observed when  $O_2$  transfers an electron to a ZnO particle. However, no emission was observed.

In this chapter, the results of studies on the influence of oxygen (as electron scavenger) on the emission properties of nanocrystalline ZnO particles are presented. Emission measurements are performed before and after saturating a suspension with nitrogen and the influence of UV irradiation is studied. Secondly, the influence of adsorbed hole scavengers on the emission properties is investigated by using different organic solvents.

## **5.2 EXPERIMENTAL METHODS.**

### **5.2.1 Sample preparation.**

Suspensions of nanocrystalline ZnO particles can be prepared in organic solvents such as ethanol or 2-propanol. For the preparation in 2-propanol [2], 25 ml of a 0.02 M NaOH solution were slowly added while stirring to 225 ml of a 0.001 M

$\text{Zn}(\text{CH}_3\text{COO})_2 \cdot 2\text{H}_2\text{O}$  solution, after both solutions were first cooled to 0 °C. The preparation in ethanol is very similar [11,12]. In this case, 50 ml of a 0.14 M  $\text{LiOH} \cdot \text{H}_2\text{O}$  solution (prepared using an ultrasonic bath) were added to 50 ml of a 0.1 M  $\text{Zn}(\text{CH}_3\text{COO})_2 \cdot 2\text{H}_2\text{O}$  solution. Again, both solutions were first cooled to 0 °C before the hydroxide solution was added slowly to the zinc solution while stirring. For the preparation in 2-propanol, TEM-measurements have shown that the mean particle radius of the fully grown particles is about 30 Å (see chapter 2). This corresponds to particles that contain approximately 5000 molecular ZnO units. The preparation in ethanol yields particles of a similar size but the concentration of ZnO particles is about two orders of magnitude higher than for the preparation in 2-propanol. Upon addition of hexane to the suspension in ethanol (volume ratio hexane to ZnO sol of 2:1) the ZnO particles precipitate [12]. The ZnO particles can be separated from the mixture by centrifuging followed by decantation of the supernatant. The precipitated ZnO particles can be resuspended in another solvent. To make sure that none of the initial solvent was still present in the new suspension, the ZnO particles were carefully dried in a nitrogen atmosphere. In this way, suspensions of ZnO particles were prepared in propylene carbonate (anhydrous 99.7%) and N,N-dimethylformamide (DMF, 99.8%).

### 5.2.2 Optical measurements.

The photoluminescence measurements were performed on a SPEX Fluorolog spectrofluorometer model F2002 equipped with two double-grating 0.22 m SPEX 1680 monochromators and a 450 W xenon lamp as the excitation source. The emission spectra were corrected for the spectral response of the emission monochromator and the PM tube. UV irradiation of the suspensions was carried out inside the spectrofluorometer using the excitation beam. The suspension was measured in a quartz cuvet of dimensions 1:1:4 cm (width:depth:height). The excitation beam had a rectangular shape with a height of about 1 cm and a width of approximately 1 mm. The penetration depth of the UV radiation was such that absorption took place over the entire width of the cuvet.

## 5.3 RESULTS.

When a suspension of nanocrystalline ZnO particles in 2-propanol is saturated with nitrogen, the emission properties do not change much as can be seen in figure 5.1 when comparing spectrum (a) to spectrum (b). In both cases two emission bands are

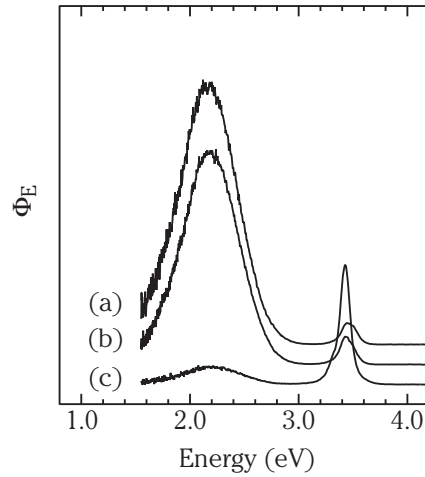


**Figure 5.1** : Room temperature emission spectra of a suspension of nanocrystalline ZnO particles in 2-propanol upon excitation with 4.3 eV.  $\Phi_E$  denotes the photon flux per constant energy interval. The emission spectra are plotted with an offset relative to each other. Spectrum (a) is taken before, and spectrum (b) after saturating the suspension with nitrogen. Spectrum (c) is taken after the nitrogen-saturated suspension has been illuminated with UV radiation (4.3 eV) for 75 min.

observed. The relatively weak and narrow emission band at 3.4 eV is due to the radiative annihilation of excitons (exciton emission). The intense broad emission band at 2.2 eV is assigned to a transition of a photogenerated electron from a shallow level close to the conduction band to a deeply trapped hole (see chapter 3). The emission properties change when the nitrogen-saturated suspension is illuminated with UV radiation. From figure 5.1 it can be seen that upon UV irradiation for 75 min the trap emission band has been quenched while the intensity of the exciton emission band has increased. Furthermore, the exciton emission band has shifted to lower energies and the trap emission to higher energies, both by about 30 meV. The FWHM of the exciton emission band has decreased to about 60% of the initial value while the width of the trap emission band did not change significantly. Turning off the radiation or adding oxygen restores the initial luminescence properties.

To investigate the quenching of the trap emission in more detail we have measured the intensity of this emission at 2.2 eV as a function of time while illuminating with UV radiation. The results of this measurement are shown in figure 5.2. After about 30 minutes the intensity of the trap emission has reached a constant value of about 10% of the initial value. When the UV irradiation is interrupted for a period of time by using a shutter, the emission intensity recovers. The degree of recovery depends on the time that the suspension is kept in the dark. From figure 5.2 it can be seen that keeping the suspension in the dark for about 5 minutes results in a full recovery of the intensity of

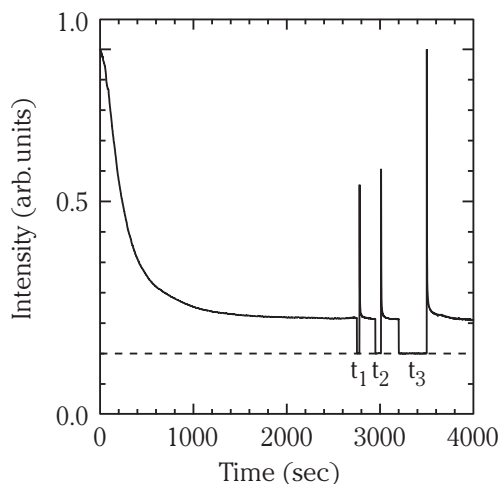


**Figure 5.2** : Intensity of the trap emission at 2.2 eV as a function of time while illuminating with UV radiation (4.3 eV). The measurement is performed at room temperature using a suspension of nanocrystalline ZnO particles in 2-propanol which has first been saturated with nitrogen. During the periods  $t_1$  (30 sec),  $t_2$  (60 sec), and  $t_3$  (300 sec) the suspension is kept in the dark.

the trap emission. Following such a recovery, the intensity decreases much faster upon UV irradiation than for the freshly prepared sample. Within 10 seconds the intensity of the trap emission decreases to 25% and a constant intensity ( $\sim 10\%$ ) is reached in less than a minute. For the exciton emission the opposite behaviour is observed. Figure 5.3 shows in more detail the fast quenching of the trap emission and the fast increase of the intensity of the exciton emission upon UV irradiation.

The influence of the intensity of the UV beam on the quenching rate of the trap emission was studied by using filters with a known transmission at the UV wavelength. Before the measurements were performed, the suspension was first saturated with nitrogen, illuminated with UV radiation until the trap emission intensity has reached its minimum intensity after which it was kept in the dark for a few minutes to allow the trap emission to recover. Figure 5.4 shows the results of these measurements.

Similar experiments as described above were performed on suspensions of nanocrystalline ZnO particles in ethanol, propylene carbonate and DMF. The suspension in ethanol behaved completely identical to the suspension in 2-propanol. For the other two suspensions, the intensity of the visible emission during UV irradiation is shown in figure 5.5A. In general, the visible emission intensity decreases to a constant value after a certain time. For propylene carbonate and DMF successively, this constant value is 75% and 40% of the initial intensity. Before this constant value is reached, the change of the visible emission intensity with time shows a different behaviour for each

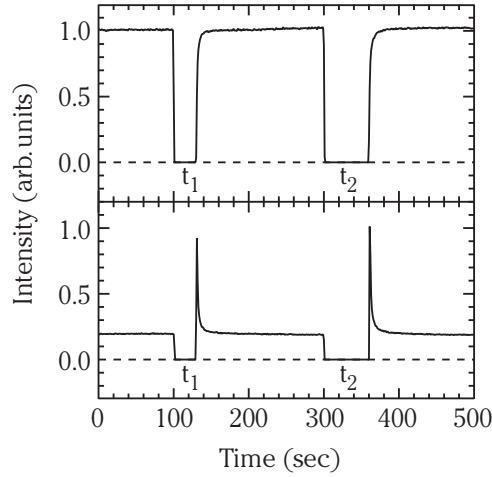


**Figure 5.3** : Intensity of the exciton emission band at 3.4 eV (upper graph) and of the trap emission band at 2.2 eV (lower graph) as a function of time while illuminating with UV radiation (4.3 eV). The experiment is performed on a suspension that has first been saturated with nitrogen and illuminated with UV radiation for 45 minutes. During the periods  $t_1$  (30 sec) and  $t_2$  (60 sec) the suspension is kept in the dark.

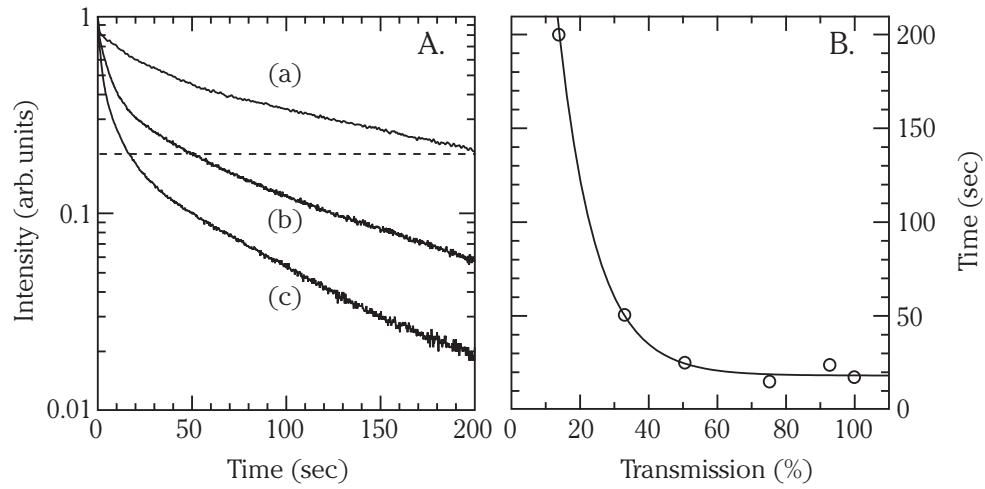


**Figure 5.4** : A : Intensity of the trap emission at 2.2 eV as a function of time while illuminating with UV radiation (4.3 eV). Filters with varying transmission at 4.3 eV were placed in the UV beam : (a) no filter, (b) 33%, and (c) 14% transmission. For each of the three graphs, the intensity at  $t=0$  was set to unity and the constant intensity at high  $t$  to zero. B : Time at which the trap emission intensity has decreased to 20% of its initial value (see dashed line in A) versus the transmission of the filter at 4.3 eV. The solid line is a guide to the eye.

of the solvents. It has to be remarked that the suspensions in propylene carbonate and DMF showed some light scattering. A complete redispersion of precipitated colloidal particles can be difficult due to clustering of the particles. For ethanol as a solvent, experiments were performed on a suspension directly after preparation (no light scattering) and on a suspension after redispersion of the particles (light scattering). During the first period of UV irradiation (directly after saturating the suspension with nitrogen), the intensity of the visible emission decreased at similar rates for both ethanolic suspensions. This rate was also similar to that of the suspension in 2-propanol. However, the constant value that was reached eventually, was higher for the suspension that showed light scattering. After keeping the suspensions in the dark for a couple of minutes, both the transparent and the non-transparent suspension behaved identically, and again similar to the suspension in 2-propanol. For the other solvents (propylene carbonate and DMF), the results of these measurements are presented in figure 5.5B. In the case of propylene carbonate as a solvent, the intensity of the visible emission quenches only very slowly. For DMF, a similar quenching behaviour is observed as for ethanol and 2-propanol. With respect to the amount of time it takes for the visible emission intensity to recover completely, differences were observed for the various solvents. It was already mentioned that for a suspension in 2-propanol (and ethanol), the visible emission intensity recovers within about 5 minutes. For DMF as a solvent, keeping the suspension in the dark for 30 minutes only leads to a recovery of 50% and for propylene carbonate the recovery time is even longer.

## 5.4 DISCUSSION.

Oxygen molecules can be chemisorbed quite strongly to the surface of ZnO particles. This means that upon saturating a suspension with an inert gas, only the free oxygen molecules are removed which explains why the emission properties have not changed after saturating with nitrogen. UV irradiation (with photon energies higher than the bandgap) of a suspension of ZnO particles can lead to a photoinduced desorption of chemisorbed oxygen molecules as the result of a reaction with protons to form hydrogen peroxide [2]. When there are no other oxygen molecules present in solution to replace the desorbed ones, it is possible to make the surface of the ZnO particles free of adsorbed oxygen by UV irradiation. The photodesorption process is accompanied by a decrease of the intensity of the visible emission, as shown in figure 5.2 between  $t=0$  and  $t=2000$  seconds. A detailed explanation for this quenching will be given later. The fact that the rate of quenching is slow is due to the experimental conditions. The UV



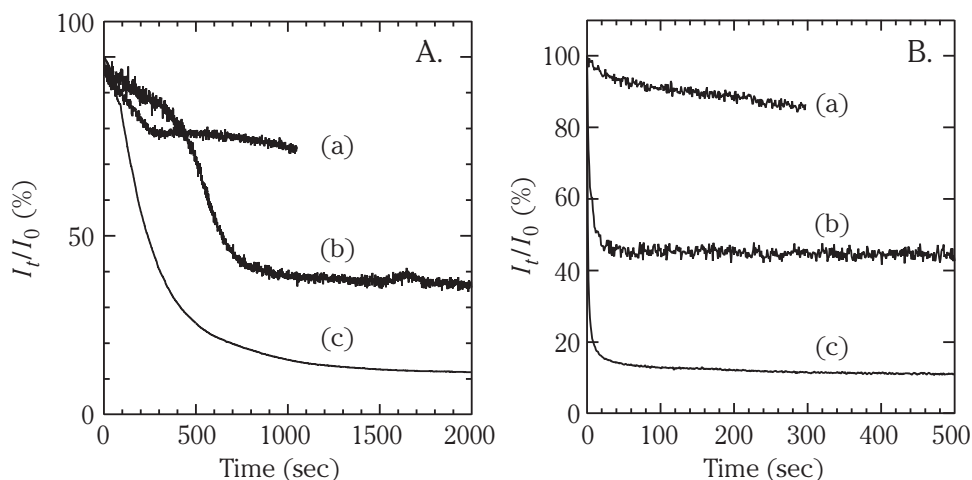


**Figure 5.5** : Intensity of the visible emission of suspensions of nanocrystalline ZnO particles in propylene carbonate (a) and DMF (b) during UV irradiation (4.3 eV). For comparison, the result of the measurement in 2-propanol is shown as graph (c). The fact that graphs (a) and (b) have a lower signal-to-noise ratio than graph (c) is due to a difference in concentration with respect to the 2-propanol suspension. On the vertical axis the intensity at time  $t$  ( $I_t$ ) is given as a percentage of the the intensity at  $t=0$  ( $I_0$ ). A : Emission intensity versus irradiation time of freshly prepared samples after saturation with nitrogen. B : Emission intensity versus time of the same samples as in A, but after the suspensions have been kept in the dark for several minutes.

radiation beam only illuminates a small part of the suspension inside the quartz cuvet and the semiconductor particles can diffuse in and out of this area. At any given time, less than 5% of the total number of ZnO particles will be illuminated by the UV beam.

As was mentioned in the introduction to this chapter, different explanations have been suggested for the quenching of the visible emission of ZnO under UV irradiation. Subsequent experiments have indicated that a photoinduced dissolution of the material is not responsible for the observed behaviour [6]. Also, a shuttle mechanism based on adsorbed oxygen [2] was not in agreement with results obtained by further experiments [10]. The results presented in this chapter provide further evidence that the shuttle mechanism is not responsible for the visible emission. The mechanism requires the presence of adsorbed oxygen to observe trap emission for nanocrystalline ZnO particles. This would mean that the recovery of the trap emission intensity while the ZnO suspension is in the dark, is due to a resorption of oxygen molecules that are still present in solution. Suppose that such a resorption can take place, UV irradiation should quench the recovered trap emission at a similar rate as before. It can be seen in figure 5.2 that this is not the case. After the initial slow desorption of chemisorbed oxygen (accompanied by a slow quenching of the visible emission), the decrease of the visible emission intensity is fast following the recovery of

the signal. To explain these results we propose a mechanism based on charging of the ZnO particles to account for the quenching of the trap emission upon UV irradiation.

When a ZnO particle is photoexcited in the absence of adsorbed electron scavengers (such as oxygen) it can be negatively charged because the photogenerated holes are efficiently scavenged by solvent molecules such as alcohols (resulting in the oxidation of the hydroxide group). The alcohol radicals produced by this reaction may inject additional electrons into the semiconductor particle [13]. For a thin film consisting of ZnO particles it has been observed that charging with electrons leads to a decrease of the trap emission intensity while at the same time the intensity of the exciton emission increases [14]. This was explained by a filling of electron traps resulting in an increase of the number of free electrons. It was assumed that the recombination of free electrons with free holes (exciton emission) was the most probable radiative process. Charging effects have not only been observed for nanoparticulate ZnO electrodes, but also for suspensions of nanocrystalline ZnO particles [5,6], as was already mentioned in the introduction. The observed quenching of the trap emission can be explained by the presence of excess electrons on the ZnO particles. The recovery of the trap emission intensity while the suspension is kept in the dark, is due to decharging of the ZnO particles. Even in the absence of electron scavengers like oxygen, a slow decharging of the particles will take place. From the timescale of the recovery (full recovery after 5 minutes) information can be obtained on the lifetime of the charged particles. The present explanation for the quenching of the visible emission explains the observations shown in figure 5.2. In a freshly prepared colloidal suspension, the oxygen which is adsorbed on the surface of the ZnO particles acts as an electron scavenger. The quenching of the visible emission is slow, because all the oxygen has to be removed before the particle can be charged. After the recovery of the signal in the dark, the quenching is much faster. Photoexcitation of electron-hole pairs and the subsequent scavenging of the holes by 2-propanol (or ethanol) immediately results in the formation of charged particles, as no efficient electron scavengers are present.

As was mentioned before, the quenching of the visible emission upon UV irradiation is accompanied by a shift of this emission band of 30 meV to higher energies. The intensity of the exciton emission band increases and shifts by some 30 meV to lower energies. This suggests that predominantly the emission characteristics of the bigger particles in the suspension are affected by UV irradiation. For nanocrystalline ZnO particles that show quantum size effects, it is known that the emission bands are broadened due to particle size distribution. The low energy side of the emission band originates mainly from the bigger particles and the high energy side from the smaller

---

particles in the distribution. Charging of particles results in an increase of the UV emission and a quenching of the visible emission, as discussed above. The shift of the UV and visible emission to lower and higher energies respectively, can be explained if the larger particles are charged more easily upon UV irradiation. When the visible emission from the bigger particles is quenched this is manifested by a shift of the maximum of the visible emission band to higher energies due to a larger contribution from the smaller particles, as is observed. The opposite applies for the exciton emission band. The exciton emission originating from the bigger particles increases upon UV irradiation resulting in a shift of this emission band to lower energies. Apparently, the bigger ZnO particles can be charged with electrons more easily than the smaller ones. It has been shown before that the redox potential of nanoparticulate electrodes consisting of quantum-confined ZnO particles depends on the particle size [13]. The potential at which electron injection into ZnO occurs increases with decreasing particle size. This behaviour is expected when electrons are transferred into the quantised electronic levels of ZnO.

To describe in more detail the way in which the presence of excess electrons in a ZnO particle results in a decrease of the trap emission intensity, it is necessary to know what kind of transition is responsible for this emission. We have been able to assign the trap emission of ZnO to a transition of a photogenerated electron from a shallow level close to the conduction band to a deeply trapped hole in the bulk of the particle (see chapter 3). Furthermore, we have identified the trapped hole as being a  $V_O^{\bullet\bullet}$  centre. The  $V_O^{\bullet\bullet}$  trapped hole centre is created by trapping of a hole by a  $V_O^\bullet$  centre, probably via surface states (see chapter 4).  $V_O^\bullet$  centres (oxygen vacancies containing one electron) are the most abundant paramagnetic defects in ZnO [15] and they are located about 2 eV below the conduction band edge [16]. Each of these centres can trap an additional electron to form  $V_O^{\bullet\bullet}$  centres (oxygen vacancies with two electrons). Charging of the ZnO particles with electrons will raise the electron quasi Fermi level which means that the oxygen vacancies will exist as  $V_O^{\bullet\bullet}$  for most of the time during which the particle is charged. Effectively, this means a removal of the  $V_O^\bullet$  centres by a charging of the particles which explains the quenching of the visible emission. At the same time, the higher concentration of conduction band electrons will increase the recombination rate of excitons, thus explaining the increase of the exciton emission intensity.

The possibility to charge a semiconductor particle with electrons is influenced by the nature of surface adsorbates. Of course, an electron scavenger (such as oxygen) should not be present which is why the suspensions were saturated with nitrogen. Next, the photogenerated holes should be removed from the particle by a suitable hole

scavenger. From the results as presented in figure 5.5B it is clear that 2-propanol, ethanol and DMF are equally capable of scavenging photogenerated holes from a ZnO particle. For these solvents, the visible emission intensity quenches at a similar rate under UV irradiation. From figure 5.5B it can also be seen that propylene carbonate is much less able to scavenge holes as the emission intensity hardly decreases at all upon UV irradiation. This is in agreement with results from experiments on ZnO electrodes in propylene carbonate under comparable conditions [17]. In these experiments no significant oxidation of propylene carbonate was observed.

The observation that in DMF the visible emission of the ZnO particles only quenches to about 40% - instead of 10% in 2-propanol - could be due to cluster formation of ZnO particles. This would mean that clusters of particles are difficult to charge. Possibly the particles inside such a cluster are hardly charged because they are “shielded” by the outer particles from the cluster.

---

## 5.5 CONCLUSION.

Experimental evidence is presented for a model explaining the quenching of the visible emission from oxygen-free suspensions of nanocrystalline ZnO particles in alcohols such as 2-propanol and ethanol under UV irradiation. The quenching is due to charging of the ZnO particles. In the absence of an electron scavenger such as oxygen, the removal of photogenerated holes from the particles by solvent molecules results in the formation of negatively charged ZnO particles. In these particles, the  $V_O^\bullet$  centres which are involved in the visible emission process, are converted into  $V_O^\times$  centres resulting in a quenching of the visible emission.

## REFERENCES .

- [1] J.I. Pankove, *Optical Processes in Semiconductors*, Dover Publications, New York (1971).
- [2] D.W. Bahnemann, C. Kormann, M.R. Hoffmann, *J. Phys. Chem.* 91 (1987) 3789.
- [3] S. Sakohara, M. Ishida, M.A. Anderson, *J. Phys. Chem. B* 102 (1998) 10169.
- [4] J. Rabani, D. Behar, *J. Phys. Chem.* 93 (1989) 2559.
- [5] U. Koch, A. Fojtik, H. Weller, A. Henglein, *Chem. Phys. Lett.* 122 (1985) 507.
- [6] A. Henglein, A. Kumar, E. Janata, H. Weller, *Chem. Phys. Lett.* 132 (1986) 133.
- [7] E. Burstein, *Phys. Rev.* 93 (1954) 632.
- [8] T.S. Moss, *Proc. Phys. Soc. (London) B* 76 (1954) 775.
- [9] P.V. Kamat, N.M. Dimitrijevic, A.J. Nozik, *J. Phys. Chem.* 93 (1989) 2873.
- [10] M. Haase, H. Weller, A. Henglein, *J. Phys. Chem.* 92 (1988) 482.
- [11] L. Spanhel, M.A. Anderson, *J. Am. Chem. Soc.* 113 (1991) 2826.
- [12] E.A. Meulenkaamp, *J. Phys. Chem. B* 102(29) (1998) 5566.
- [13] P. Hoyer, H. Weller, *Chem. Phys. Lett.* 221 (1993) 479.
- [14] P. Hoyer, R. Eichberger, H. Weller, *Ber. Bunsenges. Phys. Chem.* 97 (1993) 630.
- [15] K. Vanheusden, W.L. Warren, C.H. Seager, D.R. Tallant, J.A. Voigt, B.E. Gnade, *J. Appl. Phys.* 79(1) (1996) 7983.
- [16] F.A. Kröger, *The Chemistry of Imperfect Crystals*, North-Holland Publishing Company, Amsterdam (1964), p. 691.
- [17] P.E. de Jongh, E.A. Meulenkaamp, D. Vanmaekelbergh, J.J. Kelly, to be submitted.

---





## QUANTUM EFFICIENCIES

---

**The Influence of Preparation,  
Surface Passivation and Particle Size**

---

**ABSTRACT.**

A detailed analysis of the luminescence quantum efficiencies of nanocrystalline CdS and ZnO particles is presented in this chapter. For CdS particles, it is shown that a preparation using  $\text{Na}_2\text{S}$  yields particles with a higher quantum efficiency than when  $\text{H}_2\text{S}$  is used. The quantum efficiency can be increased by surrounding the particles with a cadmium hydroxide layer or by cooling the suspension to below its freezing point. Both methods lead to a removal of the non-radiative recombination centres at the surface of the particle. For ZnO, the influence of particle size on the quantum efficiency of the visible emission is studied. It is shown that the quantum efficiency of the visible emission decreases from 20% for particles with a mean radius of 7 Å to 12% for particles with a mean radius of 10 Å. An explanation for the size-dependence of the quantum efficiency is presented

## 6.1 INTRODUCTION

A large variety of colloidal semiconductor particles has been investigated by luminescence measurements. One of the first II-VI semiconductors that was investigated is CdS [1,2]. Generally, a colloidal suspension of CdS particles shows two emission bands upon photoexcitation. The first is a relatively weak and narrow emission band at an energy close to that of the bandgap, which is about 2.4 eV for macrocrystalline CdS. This band is known as the exciton emission band. The second band is a trap emission band which is broader and more intense than the exciton emission. This emission band has a maximum at approximately 1.8 eV. However, the dominating process for relaxation is usually radiationless decay, as is evident from the low quantum yield, which is generally below 1%. The absolute intensity of the emission of colloidal CdS suspensions is strongly dependent on several conditions, the most important one being the nature of the surface. The reason for this is the fact that surface states are usually involved in non-radiative processes and small particles have a large surface-to-volume ratio. It has been reported that covering the surface of CdS particles with a cadmium hydroxide layer results in an increase of the luminescence intensity [3,4]. Not only the nature of the particle surface itself, but also that of the solvent is of importance. Upon exchanging the aqueous solvent by an alcohol such as methanol, the luminescence intensity also increases [3]. Especially the exciton emission is sensitive to surface passivation. In fact, this emission is dominant in suspensions of well-passivated particles [3,5]. In this chapter, the influence of surface passivation on the luminescence quantum efficiency for CdS particles prepared by two synthesis methods is reported.

It is also interesting to consider the influence of particle size on the luminescence efficiency. In some papers it has been reported that the luminescence quantum efficiency of nanocrystalline semiconductor particles increases with decreasing particle size. At first sight this may seem surprising since the probability for non-radiative decay via surface sites can be expected to increase as the particle size decreases due to a larger surface-to-volume ratio. Still, for CdS it was shown that photocorrosion results in a decrease of the particle size and an increase of the luminescence efficiency which was explained by a preferential removal of surface defect sites acting as non-radiative recombination centres [5]. For ZnS particles doped with  $\text{Mn}^{2+}$  an increase in the  $\text{Mn}^{2+}$  emission was observed with a decrease of the particle size. This was explained by more efficient trapping of electron-hole pairs by  $\text{Mn}^{2+}$  in smaller ZnS particles as a result of an increased wavefunction overlap [6]. Finally, for ZnO it has been reported that smaller particles luminesce more efficiently although no detailed analysis has been reported. Whether a size-dependence of the luminescence quantum efficiency can be observed depends on the mechanisms of the radiative and

---

non-radiative processes that can occur in a certain semiconductor. For nanocrystalline ZnO particles, these mechanisms have been described in detail (see chapters 3 and 4). This forms the basis for a study of the size-dependence of the luminescence quantum efficiency for nanocrystalline ZnO particles as presented in this chapter.

## 6.2 EXPERIMENTAL METHODS.

The experiments as described in this chapter were performed on colloidal suspensions of nanocrystalline II-VI semiconductor particles. The materials that were used are CdS and ZnO. The colloidal CdS particles were prepared in two ways, differing only in the nature of the sulphur source. For each of these preparations, part of the suspension was subjected to a procedure in which the surface of the colloidal particles was passivated by creating a hydroxide layer around them. In this way, four different colloidal suspensions of CdS were prepared and investigated.

### 6.2.1 Sample preparation.

**CdS.** First, 2.4 ml of a 0.01 M  $\text{Cd}(\text{ClO}_4)_2 \cdot 6\text{H}_2\text{O}$  solution in water were diluted to 45 ml in a round-bottom flask equipped with a septum. To this solution, 1 ml of a 0.01 M sodium polyphosphate solution in water was added. Next, 500  $\mu\text{l}$   $\text{H}_2\text{S}$  (Aldrich lecture bottle, 99.5+ %) were injected using an airtight syringe. Vigorously shaking the sample for several minutes at room temperature resulted in a transparent suspension with a yellow colour. According to the literature, this preparation of an aqueous colloidal CdS suspension should yield particles with a mean radius of about 35 Å [7]. For a second preparation, 6 ml of a 0.01 M  $\text{Cd}(\text{ClO}_4)_2 \cdot 6\text{H}_2\text{O}$  solution in water were diluted to 95 ml before 5 ml of a 0.01 M sodium polyphosphate solution in water were added. Next, 5 ml of a 0.01 M  $\text{Na}_2\text{S} \cdot 9\text{H}_2\text{O}$  solution were diluted to 10 ml and added to the  $\text{Cd}^{2+}$  solution while stirring. Again this resulted in a transparent suspension with a yellow colour. Part of both suspensions was used for a surface passivation step. This step involved the adjustment of the pH to 11.5 by adding a few droplets of a 1 M NaOH solution in water. Subsequently, the suspension was kept at 95 °C for two hours using a waterbath.

**ZnO.** For the preparation of a colloidal suspension of ZnO in 2-propanol, 12.5 ml of a 0.02 M solution of NaOH and 140 ml of a 0.001 M solution of  $\text{Zn}(\text{CH}_3\text{COO})_2 \cdot \text{H}_2\text{O}$  were first cooled to 0 °C before slowly adding the hydroxide solution to the zinc acetate solution while stirring. After a few minutes, ZnO particles with a radius of about 10 Å have been formed (see chapter 4). When the solution is allowed to age at room temperature, the ZnO particles slowly grow until after several hours they have attained

their final size, having a radius of about 30 Å. At different times during the particle growth a sample is taken to be used for absorption and emission measurements. After the emission measurement, again an absorption spectrum was taken to check whether the particle size has changed during the emission measurement that generally took about 5 minutes. As the ZnO absorption spectrum did not change during this time period, it is concluded that the particles did not grow significantly.

### **6.2.2 Luminescence quantum efficiencies.**

To determine the quantum efficiency of the luminescence of a colloidal suspension of semiconductor particles, the emission spectrum is compared to that of a reference solution with a known quantum efficiency. For an accurate determination of the quantum efficiency, the absorbance at the excitation wavelength should be low and similar for both the sample and the reference solution. When the absorption strength is high, all excitation light is absorbed in the first thin layer of the sample which is not focussed on the slit of the emission monochromator. Furthermore, the spectral position of the emission band of the sample was chosen to be as close as possible to that of the reference solution. The overlap between the emission band and the absorption band of the reference solution should be as low as possible to prevent re-absorption of the emitted light by the reference itself. The concentration of the reference solution has to be in the regime where the emission intensity scales linearly with the number of absorbed photons.

For the experiments described in this chapter, solutions of different dyes were used as a reference. The luminescence quantum efficiency of the dye solutions is close to 90%. The dyes that were used were sulforhodamine 101 for CdS and coumarine 153 for ZnO. Solutions of these dyes were prepared in the same solvent as used for the preparation of the colloidal semiconductor suspensions, with a range of concentrations that shows a linear relationship between the number of absorbed photons and the emission intensity. If necessary, the colloidal suspensions were diluted in order to have an absorbance that is in the same range as that of the concentration series of the reference.

---

### **6.2.3 Optical characterisation.**

Absorption measurements were performed on a Perkin-Elmer Lambda 16 UV/Vis spectrophotometer. The photoluminescence measurements were performed on a SPEX Fluorolog spectrofluorometer model F2002 equipped with two double-grating 0.22 m SPEX 1680 monochromators and a 450 W xenon lamp as the excitation source. The emission spectra were corrected for the spectral response of the emission monochromator and the PM tube.

## **6.3 RESULTS AND DISCUSSION.**

### **6.3.1 CdS prepared with $H_2S$ .**

As can be seen in figure 6.1A, the absorption spectrum of the colloidal suspension of CdS particles prepared with  $H_2S$  did not change significantly after the suspension had been subjected to the passivation procedure. The formation of a hydroxide layer around the CdS particles did not change the size of these particles. Also, the suspension showed no light scattering due to clustering of particles. Figure 6.1A also contains the emission spectrum of a suspension of non-passivated CdS particles which shows a broad band with a maximum at approximately 1.5 eV. The low energy side of this emission band cannot be recorded with the luminescence setup that was used for these experiments as the PM tube has a very low sensitivity for photons with an energy lower than 1.5 eV. To determine the total intensity of the emission, the broad band was fitted to a gaussian function, the area of which can be used as a measure for the total emission intensity. Upon passivating the surface of the CdS particles, the intensity of the emission band increases strongly.

### **6.3.2 CdS prepared with $Na_2S$ .**

Contrary to the results for the preparation of CdS particle with  $H_2S$ , the absorption spectrum of a colloidal suspension of CdS particles prepared with  $Na_2S$  did change upon passivation of the particle surface. This can be seen in figure 6.1B. The onset of absorption - as determined by extrapolating the steep part of the absorption curve to the energy axis - stays at the same position indicating that the size of the largest particles in the suspension has not changed upon surface passivation. However, the structure of the spectrum has changed. After the onset of absorption, the absorbance

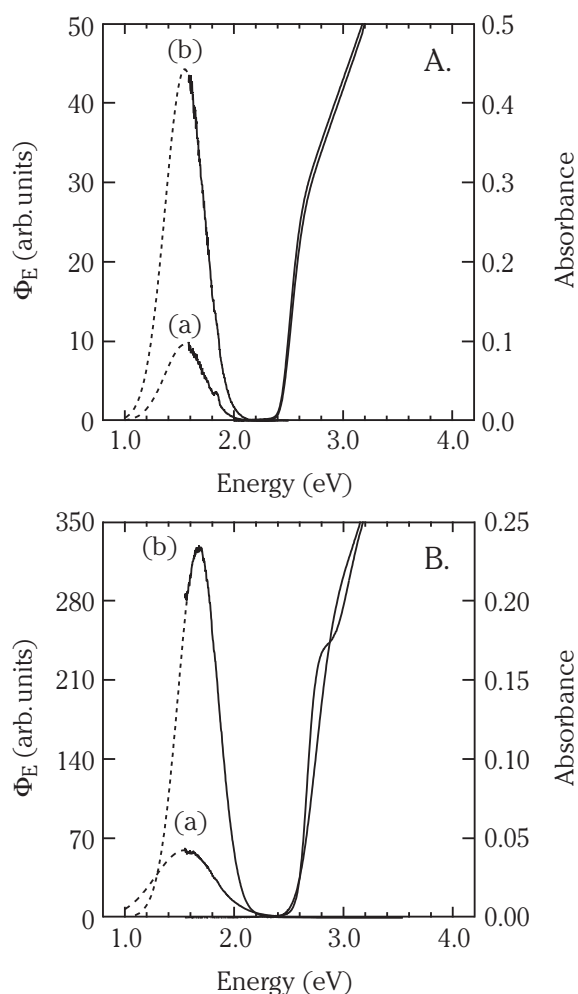


**Figure 6.1** : Room temperature emission (excitation with 4 eV) and absorption spectra of colloidal suspensions of CdS particles in water. A :  $\text{H}_2\text{S}$  preparation, before (a) and after (b) surface passivation. B :  $\text{Na}_2\text{S}$  preparation, before (a) and after (b) surface passivation.  $\Phi_E$  denotes the photon flux per constant energy interval.

risks more steeply for the passivated particles than for the non-passivated particles. Also, a maximum can be observed at about 2.8 eV in the absorption spectrum of the passivated CdS particles. These observations can be explained by a narrowing of the particle size distribution which could have resulted from temperature-induced Ostwald ripening of the particles. Comparison of the absorption spectra of the  $\text{Na}_2\text{S}$  preparation to those of the  $\text{H}_2\text{S}$  preparation shows that in the latter case the onset of absorption is at lower energies. Apparently the  $\text{H}_2\text{S}$  preparation results in the formation of larger particles than the  $\text{Na}_2\text{S}$  preparation. Although the exact reason for this is unclear it could be due to the fact that in the  $\text{Na}_2\text{S}$  preparation a larger concentration of “free” sulphur anions ( $\text{S}^{2-}$ ) will be present while in the  $\text{H}_2\text{S}$  preparation a large part of the sulphur

---

anions will be in present as  $\text{HS}^-$  or  $\text{H}_2\text{S}$  in solution. A higher concentration of  $\text{S}^{2-}$  results in faster growth kinetics and the formation of smaller colloidal particles. Similar to the  $\text{H}_2\text{S}$  preparation, the intensity of the emission band increases upon passivation of the particle surface.

### 6.3.3 Luminescence quantum efficiencies of CdS.

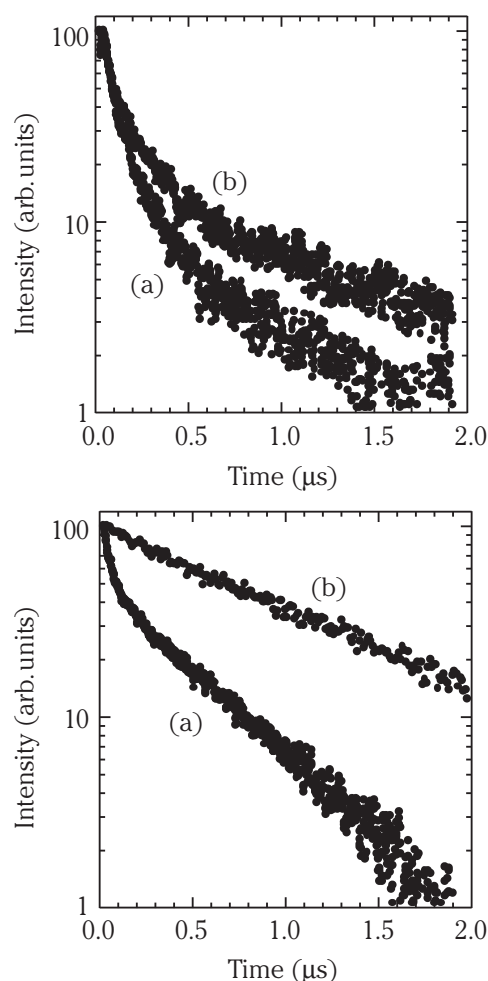
In table 1, the results of the determination of the luminescence quantum efficiencies of colloidal suspensions of CdS particles are presented. It is clear that the preparation with  $\text{H}_2\text{S}$  generally leads to the formation of particles that have lower luminescence quantum efficiencies than the particles obtained from the  $\text{Na}_2\text{S}$  preparation. Based on the absorption spectra it was concluded that the preparation of CdS with  $\text{Na}_2\text{S}$  yielded smaller particles than when  $\text{H}_2\text{S}$  is used. The particle size could be related to the higher luminescence quantum efficiency. More probably, the different synthesis methods result in particles with a different concentration of non-radiative surface sites.

Table 1. Luminescence quantum efficiencies of colloidal suspensions of CdS particles in water, prepared by injecting  $\text{H}_2\text{S}$  or by adding a solution of  $\text{Na}_2\text{S}\cdot 9\text{H}_2\text{O}$ . Part of the suspensions was subjected to a procedure in which the surface of the particles was passivated by forming a hydroxide layer.

preparation method	QE (%) before surface passivation	QE (%) after surface passivation
$\text{H}_2\text{S}$	0.2	0.8
$\text{Na}_2\text{S}$	1.5	8.0

From table 1 it is also clear that passivation of the particle surface leads to an increase of the luminescence quantum efficiency. The surface of a semiconductor particle is a strong perturbation of the lattice where a high concentration of both shallow and deep levels provide a pathway for non-radiative recombination of photogenerated charge carriers [8]. Passivating the surface by forming a hydroxide layer leads to the removal of surface states and therefore a lower probability for non-radiative decay.

This lower probability is also evident from lifetime measurements that were performed on suspensions of CdS particles. Figure 6.2 shows the results of these measurements on particles with and without surface-passivation. At room temperature,



**Figure 6.2** : Luminescence lifetime measurements of the trap emission (1.7 eV) from colloidal suspensions of CdS particles in water. The CdS particles were prepared with  $\text{Na}_2\text{S}$ . A : Measurement at 8K for non-passivated (a) and passivated (b) CdS particles. B : Measurement at room temperature for non-passivated (a) and passivated (b) CdS

surface-passivation has a pronounced influence on the lifetime of the trap emission (see figure 6.2B). The decay curve of the trap emission from the particles with no surface-passivation can be fitted to a bi-exponential function. The strongest of the two decay components - which accounts for almost 90% of the signal - has a decay time of about 500 ns while the other component is much faster, with a decay time of 40 ns. Upon passivation of the surface, the decay curve of the trap emission becomes mono-exponential with a decay time of about 900 ns. Upon blocking the non-radiative pathways at the particle surface, the lifetime of the trap emission increases by almost a factor 2. At low temperatures (8K, see figure 6.2A), the influence of surface-passivation on the lifetime of the trap emission is much less pronounced. For both samples the



---

decay curves are multi-exponential with a similar shape. This indicates that cooling a suspension of CdS particles below its freezing point has a similar effect as surrounding these particles with a hydroxide layer, viz. blocking the non-radiative routes at the particle surface.

#### **6.3.4 ZnO.**

Absorption spectra that were taken at regular intervals during the growth of ZnO particles in 2-propanol at room temperature can be seen in figure 6.3. The onset of absorption shifts to lower energies as the size of the particles increases, which is due to a decrease in quantum confinement. Using a relationship between the particle radius and the onset of absorption [9], it is determined that the radius of the ZnO particles increases from 7 Å a few minutes after the reaction was started to 10 Å after 500 min of particle growth. The emission spectrum of a colloidal suspension of ZnO particles shows two emission bands : a weak and narrow band at energies close to the absorption onset (exciton emission band) and a strong and broad emission band about 1.5 eV below the onset of absorption (trap emission band). As the intensity of the exciton emission band is negligible compared to that of the trap emission band, only the latter is used to determine the luminescence quantum efficiencies. For macrocrystalline ZnO, the efficiency of the visible emission upon irradiation with UV light is about 20% [10].

#### **6.3.5 Luminescence quantum efficiencies of ZnO.**

The luminescence quantum efficiencies are plotted versus the mean particle radius in figure 6.4. It can be seen that the quantum efficiency decreases non-linearly from about 20% for particles with a radius of 7 Å to 12% for particles with a radius of 10 Å. To explain why the luminescence quantum efficiency decreases as the particle size increases it is necessary to know the mechanism which is responsible for the trap emission. New information concerning this mechanism has been described in detail in chapters 3 and 4 of this thesis and a schematic overview is presented in figure 4.7. The key features of the trap emission process are a very fast trapping of the photogenerated hole at a surface site followed by tunnelling of this surface-trapped hole back into the bulk of the ZnO particle to a  $V_O^\bullet$  oxygen vacancy. In this way, a  $V_O^{\bullet\bullet}$  centre is created which can recombine with a photogenerated electron from a level close to the conduction band to give the trap emission. Apart from the other radiative process (exciton emission), the most important process competing with the trap emission is non-radiative decay. In nanocrystalline particles non-radiative decay predominantly

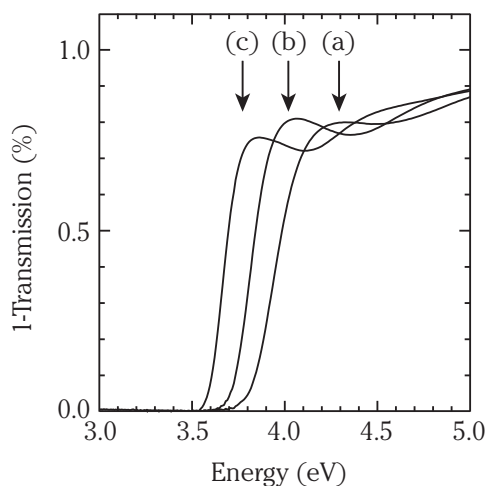


**Figure 6.3** : Absorption spectra of a suspension of nanocrystalline ZnO particles in 2-propanol, taken after 20 min (a), 90 min (b), and 500 min (c) of particle growth at room temperature. On the vertical axis, the amount of absorption is given as 1 minus the transmission.

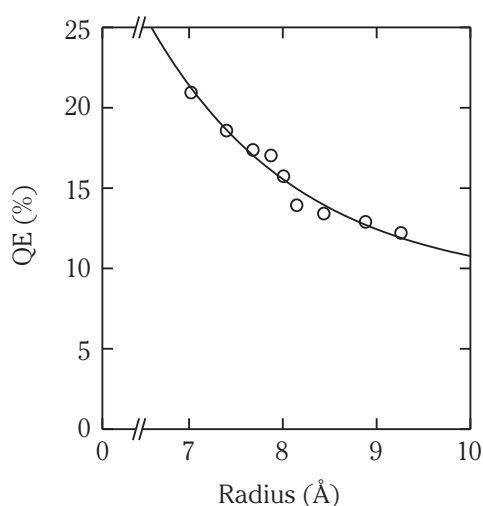


**Figure 6.4** : Room temperature luminescence quantum efficiencies (QE) versus particle radius for nanocrystalline ZnO particles.

takes place at the surface. The larger the surface-to-volume ratio is, the higher the probability for non-radiative decay will be. Nevertheless, the smaller ZnO particles have a higher luminescence quantum efficiency than the larger ones. To understand this, the two important competing processes (trap emission and non-radiative decay) have to be analyzed. The first step in both processes is trapping of a delocalised photogenerated charge carrier at the surface. This step shows a similar size-dependence for both processes which means that the second step is important for the observed size-

---

dependence of the luminescence quantum efficiency. In the case of non-radiative decay, the second step is again surface-trapping of a delocalised charge carrier. For the trap emission, the second step is tunneling of a surface-trapped hole back into the bulk of a ZnO particle to a  $V_O^\bullet$  centre. In this process, two localised states are involved. The probability for such a process decreases more strongly when the distance between the charge carriers increases than the probability for a process involving a delocalised charge carrier. In the latter case, the wavefunction overlap is less sensitive to the particle size. It is important to note that the quenching of the visible luminescence of ZnO particles takes place before the actual recombination centre is created.

The fact that the luminescence quantum efficiency decreases when the size of the ZnO particles increases indicates that the distance between the surface-trapped hole and the deeply trapped electron in the bulk oxygen vacancy increases. This is in agreement with results that indicate that the defect concentration (including  $V_O^\bullet$  centres) decreases when the size of the particles increases, as derived from studies on the size-dependence of the dissolution rate of nanocrystalline ZnO particles [11]. The explanation for the decrease of the quantum efficiency with increasing particle size is also in agreement with results of time-dependent luminescence measurements on ZnO particles of different sizes as presented in chapter 4. Figure 4.4 contains a decay curve of the visible emission from ZnO particles with a mean radius of 10 Å as well as a decay curve of the emission from particles with a mean radius of 30 Å. The emission from the larger particles has a longer lifetime than that of the smaller particles.

## 6.4 CONCLUSION.

For several colloidal suspensions of nanocrystalline II-VI semiconductor particles the luminescence quantum efficiencies were determined by comparing the emission intensity to that of a dye solution with a known quantum efficiency. For CdS, the influence of the nature of the sulphur source ( $\text{H}_2\text{S}$  or  $\text{Na}_2\text{S}$ ) and the influence of passivation of the particle surface on the luminescence quantum efficiencies was investigated. It was found that the quantum efficiency is highest when using  $\text{Na}_2\text{S}$  to prepare a colloidal suspension of CdS particles. By creating a hydroxide layer around the particle the non-radiative recombination centres at the surface are passivated which results in an increase of the quantum efficiency.

For ZnO the influence of particle size on the luminescence quantum efficiency was investigated. The quantum efficiency decreases as the size of the particles increases. The majority of the radiative recombination in ZnO is trap emission. An important step in this emission process is the tunnelling of a surface-trapped hole to a deeply trapped electron in the bulk of the ZnO particle. The probability for this tunnelling process decreases strongly when the particle size increases, and as a result the luminescence quantum efficiency decreases.

---

## REFERENCES.

- [1] A. Henglein, *Ber. Bunsenges. Phys. Chem.* 86 (1982) 301.
- [2] A. Henglein, *J. Phys. Chem.* 86 (1982) 2291.
- [3] L. Spanhel, H. Weller, A. Fojtik, A. Henglein, *Ber. Bunsenges. Phys. Chem.* 91 (1987) 88.
- [4] A. Eychmüller, L. Katsikas, H. Weller, *Langmuir* 6 (1990) 1605.
- [5] L. Spanhel, M. Haase, H. Weller, A. Henglein, *J. Am. Chem. Soc.* 109 (1987) 5649.
- [6] R.N. Bhargava, D. Gallagher, X. Hong, A. Nurmikko, *Phys. Rev. Lett.* 72(3) (1994) 416.
- [7] A. Eychmüller, A. Hässelbarth, L. Katsikas, H. Weller, *J. Lumin.* 48&49 (1991) 745.
- [8] J.I. Pankove, *Optical Processes in Semiconductors*, Dover Publications: New York, 1971.
- [9] M. Haase, H. Weller, A. Henglein, *J. Phys. Chem.* 92 (1988) 482.
- [10] A. Schleede, *Leuchten und Struktur fester Stoffe* (R. Tomaschek, ed.), R. Oldenbourg : Munich, 1943.
- [11] E.A. Meulenkaamp, *J. Phys. Chem. B* 102 (1998) 7764.





## SAMENVATTING

---

Halfgeleiders zijn materialen die al ruim honderd jaar uitvoerig bestudeerd worden en inmiddels op grote schaal zijn verwerkt in allerlei soorten toepassingen. Een belangrijk voorbeeld hiervan zijn opto-elektronische apparaten zoals fotodiodes, licht-emitterende diodes en zonnecellen. De laatstgenoemde toepassing is een elektrochemische cel waarmee met behulp van zonlicht een elektrische stroom kan worden opgewekt. Op basis van hetzelfde principe kunnen ook chemische reacties worden geïnitieerd. Om dergelijke processen zo efficiënt mogelijk te laten verlopen worden halfgeleidermaterialen met een zo groot mogelijk oppervlak gebruikt. Een manier om dit te bereiken is door te werken met kleine halfgeleiderdeeltjes. Vanaf het begin van de jaren tachtig wordt dit intensief gedaan. Naast de interesse in kleine halfgeleiderdeeltjes vanwege toepassingen in elektrochemische cellen, zijn deze systemen eveneens interessant vanuit een fundamenteel opzicht. Immers, wanneer de afmetingen van een halfgeleider vergelijkbaar worden met de grootte van een exciton in dit materiaal, dan treden kwantum opsluitingseffecten op. Het gevolg van deze effecten is dat de energetische structuur van een halfgeleiderdeeltje afhankelijk wordt van zijn grootte. Dit manifesteert zich onder andere door een toename van de bandafstand bij een afnemende deeltjesgrootte en een geleidelijke overgang van energiebanden naar discrete energieniveaus. Dergelijke effecten worden al jaren bestudeerd in zeer dunne halfgeleider heterostructuren waar ze in één of twee dimensies optreden. In kleine deeltjes - bijvoorbeeld colloïden in suspensie - kunnen kwantum opsluitingseffecten in alle dimensies optreden. Vooral deeltjes van II-VI materialen zoals CdS, ZnS en ZnO zijn uitermate geschikt als systeem voor het

bestuderen van kwantum opsluitingseffecten in drie dimensies. Zij zijn eenvoudig te maken en hun energetische structuur begint al een grootte-afhankelijkheid te vertonen bij afmetingen van enkele nanometers.

De in dit proefschrift beschreven experimenten zijn uitgevoerd aan colloïdale suspensies van II-VI halfgeleiderdeeltjes die kwantum opsluitingseffecten vertonen. Er wordt beschreven hoe deze effecten kunnen worden gebruikt om halfgeleiderdeeltjes op een gecontroleerde manier kleiner te maken. Dit gebeurt door ze te foto-etsen waarbij de uiteindelijke deeltjesgrootte afhangt van de kleur van licht dat gebruikt wordt. Verder worden kwantum opsluitingseffecten gebruikt om het mechanisme op te helderen dat verantwoordelijk is voor de bekende zichtbare luminescentie van ZnO. Hiertoe worden temperatuurafhankelijke luminescentiemetingen uitgevoerd aan deeltjes met verschillende afmetingen, zowel tijdsgeïntegreerd als tijdsopgelost. De metingen bij lage temperatuur werden uitgevoerd door een kwarts cuvet gevuld met enkele microliters van een suspensie af te koelen in een cryostaat met behulp van vloeibaar helium.

Het zojuist genoemd foto-etsproces wordt beschreven in hoofdstuk 2. Het betreft hier een post-preparatieve methode waarmee het mogelijk is om van een bepaald halfgeleidermateriaal een reeks van deeltjes met verschillende afmetingen te maken, elk met een relatief smalle deeltjesgrootteverdeling. Deze methode wordt *grootte-selectief foto-etsen* genoemd en berust op het feit dat sommige halfgeleiders fotocorrosie vertonen (oplossen onder belichting). Wanneer halfgeleiderdeeltjes die kwantum opsluitingseffecten vertonen oplossen onder belichting dan veranderen hun eigenschappen. Dit heeft als gevolg dat er een moment komt waarop zij niet meer in staat zijn om het ingestraalde licht te absorberen. Op dat moment zal het foto-etsen ophouden en zullen de deeltjes een bepaalde grootte hebben bereikt die afhangt van de golflengte van het ingestraalde licht. Door deze golflengte te variëren kan een reeks van verschillende deeltjesgroottes worden gemaakt. Experimenten aan het modelsysteem CdS hebben aangetoond dat met behulp van grootte-selectief foto-etsen deeltjes met een straal van 35 Å op een gecontroleerde manier kleiner gemaakt kunnen worden tot een straal van 7.5 Å, terwijl tegelijkertijd de deeltjesgrootteverdeling afneemt van 40% tot 10-15%. Ook voor andere II-VI materialen blijkt de methode te werken, zij het met wisselend succes.

De hoofdstukken 3 tot en met 5 zijn gewijd aan de studie van één soort II-VI verbinding, te weten ZnO. Wat betreft het bestuderen van kwantum opsluitingseffecten is er aan ZnO veel minder aandacht besteed dan aan de sulfiden. Toch is het vrij eenvoudig om nanokristallijne ZnO deeltjes te maken die deze effecten vertonen.



---

Verder is ZnO interessant omdat het een efficiënte zichtbare (groene) emissie vertoont waardoor het materiaal als luminescerende verbinding wordt toegepast. In tegenstelling tot nanokristallijne deeltjes is ZnO als macrokristallijn materiaal wel veel bestudeerd maar desondanks is het mechanisme achter de zichtbare emissie nog niet opgehelderd. Aangezien deze emissie zowel in nanokristallijne deeltjes als in macrokristallijn ZnO optreedt - en waarschijnlijk berust op hetzelfde mechanisme - kan het eerstgenoemde systeem gebruikt worden voor het ophelderen van de aard van de zichtbare emissie van ZnO.

Een dergelijke studie is het onderwerp van hoofdstuk 3 en omvat emissiemetingen aan een reeks van ZnO deeltjes met verschillende groottes. Naast de zichtbare emissie vertonen deze deeltjes ook een zogenaamde exciton emissieband. Deze emissie is het gevolg van de recombinatie van excitonen (elektron-gat paren) en de energie van het maximum van deze band komt overeen met de bandafstand van het materiaal. Het blijkt dat er een lineair verband bestaat tussen de energetische positie van de zichtbare emissieband en dat van de exciton emissieband. Uit de helling van het lineaire verband tussen de energetische posities van de twee emissiebanden kan worden afgeleid dat de overgang die verantwoordelijk is voor de zichtbare emissie een recombinatie is van een elektron uit de geleidingsband met een gat dat zich bevindt in een niveau ongeveer 2 eV onder de geleidingsband. Op basis van de kennis over de defectstructuur van ZnO wordt aangenomen dat het bedoelde niveau gevormd wordt door een zuurstofvacature waarin zich geen enkel elektron bevindt.

Daar waar in hoofdstuk 3 conclusies over ZnO in het algemeen worden getrokken, wordt in hoofdstuk 4 dieper ingegaan op de eigenschappen die specifiek zijn voor nanokristallijne ZnO deeltjes. De experimenten die in dit hoofdstuk beschreven worden, leiden uiteindelijk tot het opstellen van een model waarin alle relaxatieprocessen worden beschreven die plaatsvinden nadat een elektron-gat paar is gecreëerd in een ZnO deeltje totdat dit deeltje weer terug is in zijn grondtoestand. Eén van deze relaxatieprocessen is de zichtbare emissie en het wordt duidelijk gemaakt dat dit proces uit meerdere stappen bestaat. De eerste stap is een uiterst snel en efficiënt proces waarin het gat wordt gevangen aan het oppervlak van het ZnO deeltje, waarschijnlijk door een  $O^{2-}$  ion. Vervolgens bestaat er een kans dat dit gat terug het deeltje in tunnelt waar het terecht kan komen in een zuurstofvacature waarin zich één elektron bevindt. Het is bekend dat dergelijke zuurstofdefecten veel voorkomen in ZnO. Dit proces zorgt voor de vorming van de uiteindelijke recombinatiecentra voor de zichtbare emissie, zoals die al worden verondersteld in hoofdstuk 3.

Tenslotte wordt in hoofdstuk 5 beschreven hoe - met behulp van het model dat wordt opgesteld in hoofdstuk 4 - verklaard kan worden waarom in bepaalde suspensies de zichtbare emissie van ZnO deeltjes dooft wanneer er voor gezorgd wordt dat er geen zuurstof meer in het systeem aanwezig is. Deze verklaring berust op het feit dat ZnO deeltjes kunnen worden opgeladen met elektronen in de afwezigheid van geadsorbeerde zuurstofmoleculen. Deze extra elektronen kunnen vervolgens de zuurstofvacatures opvullen wat leidt tot het verdwijnen van de recombinatiecentra voor de zichtbare emissie.

De experimenten die beschreven zijn in hoofdstuk 6 hebben betrekking op de kwantumefficiëntie van de emissie van nanokristallijne deeltjes van zowel ZnO als CdS. Voor CdS wordt onderzocht wat de invloed is van de synthesesmethode en de oppervlakte-eigenschappen op de kwantumefficiëntie met als resultaat dat een synthese uitgaande van Na<sub>2</sub>S meer efficiënt luminescerende deeltjes oplevert dan met H<sub>2</sub>S. In beide gevallen kan de kwantumefficiëntie nog worden verbeterd door een laagje cadmiumhydroxide te groeien rondom de deeltjes. Hierdoor worden de plekken aan het oppervlak gepassiveerd waar normaal gesproken niet-stralend verval kan plaatsvinden. Voor ZnO deeltjes wordt de invloed van de deeltjesgrootte op de kwantumefficiëntie bepaald. Het blijkt dat de kwantumefficiëntie afneemt wanneer de deeltjes groter worden. Dit is in overeenstemming met het model voor de kinetiek van de relaxatieprocessen in een geëxciteerd ZnO deeltje zoals dat in hoofdstuk 4 wordt gepresenteerd.

---

---



## LIST OF PUBLICATIONS

---

### JOURNAL ARTICLES.

- [1] A. van Dijken, A. Meijerink, D. Vanmaekelbergh, *Chem. Phys. Lett.* 269 (1997) 494 [Chapter 2].
- [2] A. van Dijken, A.H. Janssen, M.H.P. Smitsmans, D. Vanmaekelbergh, A. Meijerink, *Chem. Mater.* 10(11) (1998) 3513 [Chapter 2].
- [3] A. van Dijken, E.A. Meulenkamp, D. Vanmaekelbergh, A. Meijerink, *J. Lumin.* (accepted for publication) [Chapter 3].
- [4] A. van Dijken, E.A. Meulenkamp, D. Vanmaekelbergh, A. Meijerink, *J. Phys. Chem. B* (submitted for publication) [Chapter 4].
- [5] A. van Dijken, E.A. Meulenkamp, D. Vanmaekelbergh, A. Meijerink, manuscript in preparation [Chapter 5].
- [6] A. van Dijken, J. Makkinje, A. Meijerink, manuscript in preparation [Chapter 6].

### CONFERENCE PROCEEDINGS.

- [1] A. van Dijken, D. Vanmaekelbergh, A. Meijerink, *Proceedings of the Symposium on Photoelectrochemistry* (1997 Joint Meeting of the Electrochemical Society and the International Society of Electrochemistry in Paris, France), p. 79-83.
- [2] A. van Dijken, E.A. Meulenkamp, D. Vanmaekelbergh, A. Meijerink, *Proceedings of the Fifth International Symposium on Quantum Confinement : Nanostructures* (1998 Meeting of the Electrochemical Society in Boston, USA), p. 392-401.
- [3] A. van Dijken, E.A. Meulenkamp, D. Vanmaekelbergh, A. Meijerink, *Proceedings of the 1999 International Conference on Luminescence and Optical Spectroscopy of Condensed Matter (Osaka)*, to be published.





# OVER DE INHOUD

## VAN DIT PROEFSCHRIFT

---

Een overzicht voor niet-ingewijden

---

### HALFGELEIDERS.

Halfgeleiders vormen een speciale klasse van materialen die vanwege hun eigenschappen zeer veel worden gebruikt. In de loop der jaren is aan deze materialen veel onderzoek gedaan met als gevolg dat de hoeveelheid kennis inmiddels groot is. Net zoals ieder ander materiaal bevat een halfgeleider *elektronen*, deeltjes met een negatieve lading. Voor elk soort materiaal gedragen de elektronen zich op een bepaalde manier waardoor de specifieke eigenschappen van dit materiaal worden veroorzaakt. Wanneer bijvoorbeeld elektronen vrij kunnen bewegen - zoals het geval is in metalen - dan kan het materiaal een elektrische stroom geleiden. De elektronen in halfgeleiders kunnen niet zomaar vrij bewegen omdat ze sterk gebonden zijn aan de atomen waaruit de halfgeleider is opgebouwd. Het is echter mogelijk om een gebonden elektron los te maken van een atoom, waarna het wél door het materiaal kan bewegen. Hier is een zekere hoeveelheid energie voor nodig die kan worden geleverd door warmte of door licht, dat door de halfgeleider wordt geabsorbeerd. Pas daarna kan een halfgeleider stroom geleiden. De plek waar het elektron zat kan nu worden ingenomen door een ander elektron, die op zijn beurt weer een lege plaats op een atoom achterlaat. Het steeds maar weer opvullen van lege plekken betekent dat er elektronen door de halfgeleider bewegen. Het blijkt zo te zijn dat je dit ook kunt beschrijven als het bewegen van *gaten* door de halfgeleider. Een gat gedraagt zich alsof het een elektron is, maar dan met een positieve lading. Het vrij maken van een elektron in een halfgeleider heeft dus niet alleen tot gevolg dat dit elektron door het materiaal kan gaan bewegen maar tevens dat een gat hetzelfde kan gaan doen.

Bekende voorbeelden van toepassingen van halfgeleiders zijn transistoren (onder andere terug te vinden in computerchips), licht-emitterende diodes (LED's, de lichtgevende onderdelen van bijvoorbeeld wekkerradio's) en zonnecellen. Zoals uitgelegd leidt de absorptie van licht door een halfgeleider tot het ontstaan van elektronen en gaten die vervolgens voor een elektrische stroom kunnen zorgen. Op dit principe berust de werking van een zonnecel. De elektronen en gaten kunnen ook gebruikt worden om bepaalde chemische verbindingen om te zetten in verbindingen die meer gewenst zijn. Dit is de reden waarom halfgeleiders worden toegepast bij de productie van brandstoffen en bij het afbreken van schadelijke verbindingen in afvalwater.

## **M E R K W A A R D I G   V E R S C H I J N S E L .**

De mogelijkheid om halfgeleiders te gebruiken om bepaalde chemische reacties uit te voeren, heeft aan het begin van de jaren tachtig tot een interessante ontwikkeling geleid. Om licht zo efficiënt mogelijk om te zetten in vrije elektronen en gaten is een groot oppervlak belangrijk. Een manier om het oppervlak van een halfgeleider te vergroten is door van het materiaal een poeder te maken. Hoe kleiner de poederdeeltjes zijn, hoe groter het totale oppervlak is. Tijdens het maken van kleine deeltjes van het halfgeleidermateriaal CdS (cadmiumsulfide), namen onderzoekers op een bepaald moment een merkwaardig verschijnsel waar : wanneer de deeltjes extreem klein worden, verandert de kleur van het CdS poeder van geel naar wit.

## **K W A N T U M   O P S L U I T I N G S E F F E C T E N .**

In een heel klein halfgeleiderdeeltje kunnen elektronen en gaten nooit echt vrij bewegen. Ze zitten altijd opgesloten in het deeltje en omdat ze een tegengestelde lading hebben zullen ze elkaar aantrekken. De toestand die op deze manier ontstaat kan worden gezien als een gat waar een elektron omheen cirkelt. Een dergelijke toestand wordt een *exciton* genoemd. Absorptie van licht door een klein halfgeleiderdeeltje leidt dus altijd tot de vorming van een exciton.

De kleur van een materiaal hangt af van welk gedeelte van het zichtbare licht door deze stof geabsorbeerd kan worden. Zonlicht bevat alle kleuren en wanneer dit op een materiaal valt dat alleen rood licht kan absorberen, dan zal dit materiaal er blauw uitzien. Deze kleur wordt namelijk door het materiaal gereflecteerd zodat het vervolgens

---

door het menselijk oog kan worden waargenomen. In eerste instantie lijkt de kleur van een materiaal onafhankelijk te zijn van zijn afmetingen. Echter, de eerder genoemde experimenten aan CdS deeltjes hebben aangetoond dat voor halfgeleiders de kleur wel degelijk afhangt van de afmetingen. Wanneer een halfgeleiderdeeltje steeds maar kleiner wordt gemaakt dan komt er een moment waarop zijn kleur begint te veranderen.

Vanaf deze grootte is steeds meer energie nodig om excitonen te maken wat tot uitdrukking komt in een verschuiving van de absorptie van licht naar een andere kleur. De kleurverandering van steeds kleiner wordende halfgeleiderdeeltjes is één van de meest in het oog springende gevolgen van het optreden van zogenaamde *kwantum opsluitingseffecten*. In theorie waren deze effecten al jaren lang bekend en ze waren ook al waargenomen in hele dunne lagen van halfgeleiders. In halfgeleiderdeeltjes met afmetingen van een miljoenste millimeter (nanometer) manifesteren deze effecten zich echter bijzonder sterk. Inmiddels heeft zich rondom deze *nanokristallijne* halfgeleiderdeeltjes een geheel nieuw onderzoeksgebied ontwikkeld waarin vooral veel aandacht wordt geschonken aan het bestuderen van kwantum opsluitingseffecten. Alhoewel men veel weet over de eigenschappen van halfgeleiders met “normale” afmetingen, valt er nog veel onderzoek te verrichten aan deeltjes met afmetingen van slechts enkele nanometers. Dergelijke nanokristallijne halfgeleiderdeeltjes zijn het onderwerp van dit proefschrift.

## S U S P E N S I E S .

Voor een gedegen onderzoek naar kwantum opsluitingseffecten in halfgeleiderdeeltjes is het ten eerste uitermate belangrijk dat de deeltjes die bestudeerd worden allemaal ongeveer dezelfde afmetingen hebben. In de loop der jaren heeft men veel ervaring opgedaan met het maken van dergelijke deeltjes, vooral in de vorm van suspensies. Een suspensie is een vloeistof waarin de vaste stof zich als een fijnverdeeld materiaal bevindt. Alle experimenten die beschreven zijn in dit proefschrift zijn gedaan aan suspensies van halfgeleiderdeeltjes. De materialen die gebruikt zijn, zijn sulfiden - zoals CdS, ZnS (zinksulfide) en PbS (loodsulfide) - maar vooral ZnO (zinkoxide). Een overeenkomst tussen deze materialen is dat ze behoren tot de klasse van *II-VI* materialen.

De experimenten hebben een aantal belangrijke resultaten opgeleverd. Zo is aangetoond dat het mogelijk is om halfgeleiderdeeltjes die zich in een suspensie bevinden kleiner te maken door er licht op te stralen. Dit gebeurt op een gecontroleerde manier en de uiteindelijke deeltjesgrootte wordt bepaald door de kleur van het licht.



Deze methode wordt *grootte-selectief foto-etsen* genoemd en wordt uitgebreid beschreven in hoofdstuk 2.

Een tweede interessant resultaat heeft te maken met ZnO. Dit materiaal wordt niet alleen als halfgeleider gebruikt, maar ook als *fosfor*. Een fosfor is een vaste stof die *luminescentie* vertoont. Luminescentie is het verschijnsel dat bepaalde verbindingen zichtbaar licht uitzenden wanneer zij worden bestraald met ultraviolette (UV) straling. Deze straling kan niet worden waargenomen door het menselijk oog maar is bijna overal aanwezig. Zonlicht bevat bijvoorbeeld een zekere hoeveelheid UV straling wat de oorzaak is voor het bruin worden van de huid wanneer deze wordt blootgesteld aan de zon. Ook in verlichting wordt UV straling en luminescentie gebruikt. Zo wordt in een TL-buis UV straling opgewekt en vervolgens door poeders, die zich aan de binnenkant van de buis bevinden, omgezet in wit licht. Wanneer ZnO wordt bestraald met UV straling dan wordt door het materiaal groen licht afgegeven. Vanwege deze eigenschap wordt ZnO toegepast in lichtgevende schermpjes die bijvoorbeeld zijn verwerkt in audio- en video-apparatuur. Waar deze groene luminescentie van ZnO precies door veroorzaakt werd was echter onduidelijk. Door bepaalde experimenten te doen aan kleine ZnO deeltjes van verschillende groottes en bij verschillende temperaturen is het mogelijk gebleken om meer informatie over de groene luminescentie te verkrijgen. Deze experimenten worden beschreven in de hoofdstukken 3 en 4.

---





## TOT BESLUIT

---

### Een woord van dank

---

In 1887 heeft Sherlock Holmes gezegd dat hij de “*kleine dingen*” altijd het meest belangrijk vindt. Dat hij zeker niet de enige is die op de kleintjes let, bleek in 1995 toen Andries Meijerink besloot om iemand aan te nemen die zich vier jaren lang bezig zou gaan houden met kleine halfgeleiderdeeltjes. Inmiddels kan ik zeggen dat ik erg blij ben dat ik deze rol heb mogen vervullen. Andries, de manier waarop jij je promovendi begeleidt heb ik ontzettend prettig gevonden. Het is indrukwekkend om te zien hoe leuk jij je vak vindt. Zoals een oud-voetballer die coach wordt vaak nog even een balletje mee trapt, zo kan jij het niet laten om actief met wetenschappelijk onderzoek bezig te blijven zijn. Dat mijn onderzoek naast luminescentie ook de andere specialiteit van onze vakgroep (elektrochemie van halfgeleiders) omvatte, vond ik erg interessant. John Kelly en Daniël Vanmaekelbergh hebben mij meerdere malen op weg geholpen als ik een halfgeleiderprobleem had. Daniël, jouw commentaar is van onschatbare waarde geweest voor de inhoud van mijn proefschrift en voor de waardering van Luc Nilis als voetballer. De samenwerking met een andere elektrochemicus, Eric Meulenkamp, heeft geresulteerd in de drie ZnO hoofdstukken en menig telefoongesprek en/of e-mailcontact tussen Eric en mijzelf. Eric, naast verstand van zaken heb je een oog voor detail, een combinatie die het bespreken van mijn werk soms tot een middagvullende bezigheid maakte maar vooral tot gevolg had dat ik er een stuk wijzer op werd. Vooral tijdens het begin van mijn promotieperiode werd ik vanuit colloïdchemische kant geholpen door Carlos van Kats van de *Colloid Synthesis Facility* in Utrecht. Hij bracht me enkele kneepjes bij en heeft zijn uiterste best gedaan om die wel hele kleine colloïden onder de microscoop zichtbaar te maken. Wat dit laatste betreft verdient zeker ook Marcel Verheijen van het *Philips Centre for Manufacturing*

*Technology* (Eindhoven) een pluim. Hij maakte de TEM-opnamen die uiteindelijk in dit proefschrift zijn gebruikt. De gemotoriseerde technicus Hans Ligthart verstaat zijn vak en is op de vakgroep en in de sportzaal een gewaardeerde kracht. Verder is er een viertal studenten geweest waarop ik blijkbaar mijn enthousiasme heb weten over te brengen aangezien zij besloten om mij gedurende een bepaalde periode te helpen met mijn onderzoek. De inspanningen van de hoofdvakkers Alrik van den Brom, Monique Smitsmans en Jeroen Makkinje en die van de klein-bijvakker Ries Janssen, hebben een aanzienlijke bijdrage geleverd aan dit proefschrift. Tenslotte wil ik nog iemand bedanken wiens aanwezigheid in onze groep uitermate belangrijk is geweest : Arnim Henglein, pionier op het gebied van onderzoek aan kleine halfgeleiderdeeltjes. Dear Prof. Henglein, it was a great pleasure for me to work with you during the first months of my Ph.D. research. Your knowledge on nanocrystalline semiconductor particles and your enthusiasm for your work is most impressive.

Tegelijk met mij begonnen op 1 september 1995 nog twee andere mensen aan hun promotie-onderzoek en met z'n drieën kwamen we terecht in kamer 268. In vier jaar tijd is die kamer uitgegroeid tot een goed geoliede werkomgeving, voorzien van alle gemakken. Luxe bureaustoelen, een uitgebreide verzameling kantoorartikelen en een computer-infrastructuur waar menige multinational zijn vingers bij af zou likken. Petra, ik weet dat ik het vaak niet kon laten om een pijnlijke opmerking te maken over de gebreken van de Mac, die jij dan weer pareerde door mij op het geratel van mijn PC te wijzen. En René, ik ben mij er van bewust dat ik je regelmatig lastig viel met deuntjes waar zelfs een getrainde scout zoals jij nog simpel van kon worden. Desondanks hoop ik dat jullie je de afgelopen vier jaar net zo goed hebben vermaakt als ik zelf. Wie had gedacht dat we alledrie uiteindelijk bij het Nat. Lab. terecht zouden komen? (ik in ieder geval niet!). Ik hoop dat we elkaar nog regelmatig zullen zien.

Ook andere prominente figuren - ik noem een Arjan Vink - dienen zeker vermeld te worden. Arjan, eerst practicumpartner en daarna collega, ik dacht dat ik nooit van je af zou komen! Toch moet ik toegeven dat ik waarschijnlijk met weemoed terug zal denken aan de tijd waarin ik dagelijks door jou werd gestalkt via ICQ en iedere maandagochtend imbossiaanse verhalen moest aanhoren over de plaatselijke FC. Maar ook Ageeth, Koert, Liesbeth+Erik, Ferry, Freek, Marcel, Aarnoud, Xinghua, Marjolein en Jeroen hebben zeker bijgedragen een plezierige tijd. Een speciale vermelding gaat uit naar Gijs, talent van de eerste verdieping en vaak zo kapot. Maar wat kon 'ie losgaan! Legendarisch zijn de avonden waarop we samen naar het partycentrum aan de Bemuurde Weerd trokken om aldaar de een of andere onbenullige pot uit de Champions League te bekijken. Natuurlijk kwamen we eigenlijk voor de uitbater van het

---

etablissement, De Valk, en voor zijn onuitputtelijke voorraadkast (de Kast is OK!). De Valk, zijn grootsheid kent geen grenzen.....

Buiten mijn werk kon ik altijd rekenen op bepaalde mensen voor de nodige doses entertainment : Diederik, met wie ik terug ga tot de *old school*, en Surfgod Reinoud. CJ de Vergruizer (21:00 België?), die altijd te porren was voor koffie, bier en andere versnaperingen. En natuurlijk de Godenzonen van DESTO - ongeslagen kampioenen van de derde helft - want DESTO 6.....DAT IS GEZELLIGHEID!

Mijn vader en moeder hebben mij altijd de dingen laten doen die ik leuk vind. Ze oefenden nooit druk op me uit en altijd stonden ze voor me klaar : echte toppers! Nog zo'n zeldzame topper is Belinda. Vroeger kon je me al boeien met je spannende verhalen en nu - inmiddels samen met Case en Kristan - kom ik nog steeds ontzettend graag bij jullie langs.

Het is al gezegd, kleine dingen zijn belangrijk, maar één *klein ding* is écht het *meest* belangrijk, en dat is Mendely. De afgelopen zes jaren samen met jou waren één grote happening! Ik kan niet wachten om samen met jou naar Brabant te trekken (jawel, u hoort het goed) alwaar de provinciale huisdierenpopulatie een periode van grote bloei tegemoet kan zien wanneer jij als dierenarts je opwachting zal maken.





## CURRICULUM

## VITAE

---

De schrijver van dit proefschrift werd geboren op 19 augustus 1972 te Bennekom, in de gemeente Ede. In 1990 behaalde hij het VWO diploma aan “*Het Wagenings Lyceum*” te Wageningen om vervolgens aan een studie Scheikunde aan de Universiteit Utrecht te beginnen. In augustus 1991 werd het propedeutisch diploma behaald en in augustus 1995 het doctoraal diploma. De studie omvatte twee keuzepakketten, te weten *Fysica en Chemie van Materialen* en *Fysisch-Organische Chemie*. Het hoofdvak werd uitgevoerd bij de vakgroep Gecondenseerde Materie. Op 1 september 1995 trad hij als Onderzoeker in Opleiding (OiO) in dienst van NWO voor een promotie-onderzoek binnen de vakgroep Gecondenseerde Materie van de Universiteit Utrecht. Het grootste gedeelte van de behaalde resultaten zijn beschreven in dit proefschrift. Tijdens zijn promotieperiode werden resultaten van het onderzoek door de schrijver gepresenteerd op een drietal buitenlandse conferenties. In 1997 werd de Joint International Meeting of the Electrochemical Society (ECS) and the International Society of Electrochemistry (ISE) te Parijs bezocht, in 1998 de Meeting of the Electrochemical Society (ECS) te Boston en in 1999 de International Conference on Luminescence and Optical Spectroscopy of Condensed Matter (ICL) te Osaka. Naast het doen van wetenschappelijk onderzoek werden enkele onderwijstaken uitgevoerd. Dit betrof de begeleiding van de werkcolleges *Structuur en Binding 2A* en *Spectroscopie* en het practicum *Fysisch Chemisch Meten*. Vanaf 1 november 1999 zal de schrijver van dit proefschrift in dienst zijn als wetenschappelijk medewerker van het Philips Natuurkundig Laboratorium te Eindhoven.



